Imperial College London

Department of Physics

New Non-Ergodic Phenomena in Quantum Many-Body Systems

Author:
Hongzheng Zhao

Supervisors:
Prof. Johannes Knolle
Prof. Florian Mintert

A thesis submitted in fulfillment of the requirements for the degree of Doctor of Philosophy in physics

October 27, 2021

Abstract

The dynamics of generic closed many-body quantum systems is believed to be ergodic. A paradigmatic example is a quantum quench, which takes the system out of equilibrium. Local properties relax quickly and then approach the thermal equilibrium asymptotically, which can be sufficiently described via the eigenstate thermalization hypothesis (ETH). Alternatively, non-equilibrium dynamics can also be induced by time-dependent drives. In this setup, as energy conservation is absent, those systems normally keep absorbing energy and heat up to a featureless "infinite-temperature" state.

There has been great effort on the last decades to understand how to prevent many-body systems from thermalization. For time-independent systems, a prominent example is many-body localization (MBL) where all eigenstates deviate from the ETH prediction. The recent discovery of quantum many-body scars (QMBS) suggests that special ergodicity-breaking eigenstates can also appear in an otherwise thermalizing spectrum. Periodically driven or Floquet systems can also be non-ergodic. The driving induced heating can either be completely evaded via MBL, or significantly suppressed by using high frequency driving which can give rise to a transient but long-lived prethermal phenomenon.

This thesis introduces several new ergodicity-breaking phenomena in closed quantum many-body systems. First, an experimentally feasible protocol will be proposed to realize QMBS in optical lattices via Floquet engineering. Then I will show that QMBS in a fractionalized strongly correlated system can demonstrate the coexistence of persistent oscillations and the volume-law entanglement generation. Such a behavior is very counter-intuitive as within the ETH paradigm, volume-law scaling normally implies ergodic behavior. Similarly, in all previously identified models demonstrating persistent oscillations, the underlying QMBS only exhibits sub-extensive entanglement.

The fact that Hamiltonians governing these non-ergodic phenomena always have time translation symmetry (TTS) naturally raises the question: Can systems without TTS also exhibit interesting non-ergodic collective phenomenon? Those systems can be expected to exhibit far richer dynamics, yet are also challenging to study due to

the lack of Floquet theory. Nevertheless, I will provide affirmative answers to the above question by investigating both quasi-periodic and structured random drivings. For continuous quasi-periodic driving, the idea of the Floquet time spiral will be developed. This leads to a new non-equilibrium phase of matter — the discrete-time quasicrystal where quasi-TTS is spontaneously broken. I will finally introduce a new family of random driving protocols with a $n-$multipolar structure. Although the TTS is completely broken due to the temporal randomness, I will show that a prethermal phenomenon still exists for high frequency driving similar to Floquet systems. This provides a sufficiently long time window to host novel non-equilibrium phases, e.g. a prethermal random multipolar discrete time crystal.

Declaration of Authorship

I, Hongzheng Zhao, declare that this thesis titled, "New Non-Ergodic Phenomena in Quantum Many-Body Systems" and the work presented in it are my own. I confirm that:

- This work was done wholly or mainly while in candidature for a research degree at this University.
- Where I have quoted from the work of others, the source is always given. With the exception of such quotations, this thesis is entirely my own work.
- I have acknowledged all main sources of help.
- Where the thesis is based on work done by myself jointly with others, I have made clear exactly what was done by others and what I have contributed myself.

The core part of the thesis is based on the research appearing in:

[1] H. Zhao, J. Vovrosh, F. Mintert and J. Knolle. “Quantum many-body scars in optical lattices". Phys. Rev. Lett. 124, 160604 (2020).

Covering chapter 2

[2] H. Zhao, A. Smith, F. Mintert, J. Knolle. “Orthogonal quantum many-body scars". Phys. Rev. Lett. 127, 150601 (2021).

Covering chapter 3.

[3] H. Zhao, F. Mintert and J. Knolle. “Floquet time spirals and stable discrete-time quasicrystals in quasiperiodically driven quantum many-body systems". Phys. Rev. B 100, 134302 (2019).

Covering chapter 4

[4] H. Zhao, F. Mintert, R. Moessner and J. Knolle. “Random multipolar driving: tunably slow heating through spectral engineering". Phys. Rev. Lett. 126, 040601 (2021).

Covering chapter 5

[5] T. Mori, H. Zhao, F. Mintert, R. Moessner and J. Knolle. “Rigorous bounds on the heating rate in Thue-Morse quasiperiodically and randomly driven quantum many-body systems". Phys. Rev. Lett. 127, 050602 (2021).

Covering chapter 5

Other works published during my doctoral research not included in this thesis:

[6] H. Zhao, J. Knolle and F. Mintert. “Engineered nearest-neighbor interactions with doubly modulated optical lattices". Phys. Rev. A 100, 053610 (2019).

[7] J. Vovrosh, H. Zhao, J. Knolle, A. Bastianello. “Confinement induced impurity states in spin chains". arXiv:2108.03976. Submitted to Phys. Rev. Lett. (2021).

Hongzheng Zhao
October 27, 2021

Acknowledgements

First of all, I would like to thank my supervisors, Johannes Knolle and Florian Mintert, for their support during my PhD. I am always impressed by their wide knowledge in different fields and extraordinary insights to elaborate fundamental concepts via simple models. They have been always patient and available for suggestions for both physics and life, which benefited me a lot throughout my whole PhD. I am proud to have achieved many things that I would not be able to do without their help.

I would like to give special thanks my collaborator, Roderich Moessner, who can always give me enlightening suggestions. His physical insights were indispensable to the discovery of random multipolar driving that forms a crucial part of this thesis.

I have benefited from many other collaborators during my PhD and I am particularly grateful to Joseph Vovrosh. We together proposed many-body scars in optical lattices at Les Houches and later explored interesting confinement physics. I also thank him for proofreading parts of the thesis. I would like to give special thanks to my friend Andrea Pizzi, who is always energetic in both physics and life, for all the fascinating discussions about non-equilibrium phases, and for sharing memorable moments in Munich. Additionally, I have profited from collaborations with Takashi Mori, whose analytical skill deeply impressed me and provided great insights into driven systems. Furthermore, I give my thanks to Adam Smith for his ideas on lattice gauge models and fractionalization.

I have also benefited a lot from interacting with other great scientists, for instance, Anushya Chandran and Philip Crowley are always willing to share their exciting ideas on quasi-periodically driven systems. Particularly, I would like to acknowledge Monika Aidelsburger for our discussion on connecting theoretical models and experiments in optical lattices.

I would like to acknowledge support from the fellowship within the Doctoral Program of the German Academic Exchange Service (DAAD).

A huge thank you to everyone in the quantum theory group at Imperial College for creating an amazing atmosphere for research of quantum everything. In particular, I thank Frederic Sauvage for his valuable suggestions regarding numerical simulations. It is also great to share the office and write up our thesis together. I give special thanks to Hyukjoon Kwon for answering my many questions and for the interesting discussion about entanglement measures. I would also like to thank Rick Mukherjee for helping me with my DAAD fellowship application and for career advice. I also thank Myungshik Kim, Jake Lishman, Mahdi Sameti, Omar Raii, Yue Ma, Himadri Dhar, Yuxun Ling, Sean Greenaway, Simon Lieu and many others.

Moreover, I am grateful to the condensed matter theory group at TU Munich for hosting me for a long time. I would like to thank particularly my friends Josef Willsher, Yujie Liu, Pablo Sala, Huike Jin, Yanbai Zhang, Gibaik Sim, Alvise Bastianello, Valentin Leeb, Markus Drescher, Jonas Mayer, Oliver Franke for maintaining my basic social life in Munich, which was of great value during the COVID-19 pandemic. I would also like to mention Frank Pollmann, Michael Knap, Sergej Moroz, Ruben Verresen, Umberto Borla, ShengHsuan Lin, Johannes Feldmeier, and many other members of the group.

Most importantly, I thank my love, Jiawei, who made my life so enjoyable during the past years and shared my happiness. Finally, I am grateful to my parents who have always been encouraging me to be brave, to pursue my dreams, and to explore the world.

Contents

List of Figures

List of Abbreviations

ETH	**E**igenstate **T**hermalization **H**ypothesis
RMT	**R**andom **M**atrix **T**heory
GOE	**G**aussian **O**rthogonal **E**nsemble
POI	**Poi**sson Statistics
PGE	**P**eriodic **G**ibbs **E**nsemble
GGE	**G**neralized **G**ibbs **E**nsemble
MBL	**M**any **B**ody **L**ocalization
QMBS	**Q**uantum **M**any **B**ody **S**cars
TTS	**T**ime **T**ranslation **S**ymmetry
TTSB	**T**ime **T**ranslation **S**ymmetry **B**reaking
PD	**P**eriodically **D**riven
QPD	**Q**uasi**p**eriodically **D**riven
FTS	**F**loquet **T**ime **S**piral
QTTSB	**Q**uasi**p**eriodic **T**ime **T**ranslation **S**ymmetry **B**reaking
DTC	**D**iscrete **T**ime **C**rystal
SG	**S**pin **G**lass
DTQC	**D**iscrete **T**ime **Q**uasi**c**rystal
HSF	**H**ilbert **S**pace **F**ragmentation
BHM	**B**ose-**H**ubbard **M**odel
SF	**S**uper**f**luidity
MI	**M**ott **I**nsulator
BO	**B**loch **O**scillation
RMD	**R**andom **M**ultipolar **D**riving
FGR	**F**ermi's **G**olden **R**ule
OM	**O**rthogonal **M**etal
TFIM	**T**ransverse **F**ield **I**sing **M**odel

Chapter 1

Introduction

Understanding the rich behavior of quantum many-body systems is one of the biggest challenges of modern science. Although the underlying fundamental laws governing their dynamics can be simple, the macroscopically large number of degrees of freedom significantly increases their complexity [1]. Fortunately, many interesting features of interacting many-body systems in or close to thermal equilibrium, e.g. different phases of matter, are universal and their microscopic details are less important. Instead of analyzing the behavior of individual particles, we can describe these phenomena by only using a small number of thermodynamic quantities, such as temperature and magnetization. However, a true equilibrium phenomena can only be reached asymptotically and the vast majority of what we observe in our daily life, such as air cooling, oscillation of pendulums and chemical reactions, are far from equilibrium. In this thesis, I am particularly interested in the non-equilibrium phenomena of isolated quantum many-body systems.

Unlike the equilibrium scenario, fewer universal principles have been established in non-equilibrium settings and many studies can only target specific examples. Perhaps the most important question to understand is the following: How do closed many-body systems approach thermal equilibrium after they are taken far from it? For classical systems, the nonlinearity and chaoticity of the equations of motion provide a plausible answer. It is believed that all accessible regions, subjected to a few macroscopic constraints such as energy and particle number, of the phase space are equally likely to be explored in the long-time limit [2, 3]. This idea is known as the ergodicity hypothesis, which is pivotal to the current development of statistical mechanics [4]. However, the understanding for quantum systems is more subtle as their dynamics is governed by the linear Schrödinger equation, which by itself seems insufficient for chaos. Additionally, the uncertainty principle [5] indicates that a particle cannot have a well-defined trajectory in phase space as its position and momentum cannot be simultaneously determined.

A remarkable breakthrough bridging the gap between microscopic quantum dynamics and statistical mechanics was the proposal of the Eigenstate Thermalization Hypothesis (ETH) [6, 7]. Assuming many-body systems can act as their own bath, ETH states that each eigenstate of a static Hamiltonian is thermal. Those thermal eigenstates can be locally described by the microcanonical ensemble constrained by a set of macroscopic quantities, for instance, energy and particle number. Hence, generic initial states, which are normally superpositions of a plethora of eigenstates, will thermalize after a quench. Namely, the expectation values of local observables equilibrate to the thermal prediction after a sufficiently long time.

The advent of highly controllable experimental techniques permits us to modulate quantum many-body systems in a time-dependent fashion [8, 9]. The ensuing non-equilibrium phenomenon is rightfully expected to be richer than static quench, yet challenging to analyze. As a special case which preserves TTS, periodic driving has been widely employed to drastically modify properties of quantum systems which can be conveniently analyzed by the Floquet theory [10]. However, by Noether's theorem [11, 12], generic time-dependent quantum systems do not preserve energy. Therefore, they are expected to keep absorbing energy from the drive and eventually heat up indefinitely towards a so-called "infinite temperature state" without any interesting local features [13].

The exploration of ergodicity-breaking phenomena in closed quantum systems flourished in the past decades, which is the main focus of the thesis. Apart from the basic motivation of understanding different paths towards the thermal equilibrium, interest also comes from the fact that thermalization poses a serious limitation to the development of quantum technologies, for instance, quantum computers [14] or simulators [15, 16]. Prominent mechanisms of ergodicity-breaking include integrability and, more generically, many-body localization (MBL) when strong disorder is present. These systems have been shown to strongly violate ETH as all eigenstates are non-thermal, and the asymptotic states after a quantum quench maintain the local memory of the initial states. The recent discovery of quantum many-body scars (QMBS) significantly enriches this field. Here, ergodicity-breaking phenomenon only happens for some special eigenstates, which coexist with a sea of thermal eigenstates.

These ergodicity-breaking mechanisms also notably change the thermalization procedure in Floquet systems and can prohibit Floquet heating. The stability of MBL in Floquet systems furthermore enables a range of novel non-equilibrium phases of matter, for example, the discrete time crystals [17] and the anomalous Floquet-Anderson insulators [18]. Additionally, as a transient ergodicity-breaking phenomenon, prethermalization has been attracting great attention and extensively studied in Floquet systems. It appears when using high frequency drives and does not require MBL or integrability. Instead of monotonically heating up to a featureless state, the system first relaxes towards a quasi-steady state where the heating is exponentially suppressed [19]. Such prethermal states can be engineered to exhibit sought-after non-equilibrium properties which might not be obtainable in static systems [8], e.g. the matter-field couplings in a Z_2 lattice gauge model [8].

Besides quenching and Floquet driving, there are many other ways for taking a quantum system out-of-equilibrium which are yet to be fully explored, for instance by using a random drive where TTS is absent. A crucial question of broad interest is whether non-ergodic behaviors can still appear without TTS? If so, are there interesting collective phenomena which are long-lived and perhaps unobtainable in Floquet systems? The intuitive answer should be *No* as those driving protocols normally involve more complicated driving tones. These additional tones unavoidably open more resonance channels than Floquet systems which rapidly destabilize any non-trivial phenomena. Fortunately, it turns out that the absence of TTS does not completely exclude ergodicity-breaking behaviors. I will briefly review the recent insightful developments considering both continuous quasi-periodic and discrete drivings.

1.1 Thesis Outline

In the remainder of this Chapter, I will introduce the main concepts used throughout the thesis. In Sec. 1.2, I will elaborate quantum thermalization and ETH in both static and periodically driven systems. I also introduce a few commonly used methods to diagnose quantum thermalization. In Sec. 1.3, my focus will shift to ergodicity-breaking phenomena discovered in the past decades, ranging from integrable systems, MBL to QMBS. I will show that some or all eigenstates in these systems deviate from the ETH prediction, hence, their dynamics can be either slowly thermalizing or completely non-thermal. The transient prethermal phenomenon will be introduced in Sec. 1.4 with the particular focus on Floquet systems. I will also give an explicit example illustrating how to use Floquet engineering to realize quantum phase transitions. The final section of this chapter, Sec. 1.5, concerns the progress in understanding the dynamics with quasi-periodic drivings without TTS.

I will start introducing my own discoveries in Chapter. 2 where I propose an experimentally feasible model to realize QMBS via Floquet engineering in optical lattices. In Chapter 3, I investigate a fractionalized model where orthogonal QMBS appear with novel entanglement properties absent in all previously discovered QMBS. Next in Chapter 4, I propose the construction of Floquet time spirals in quasi-periodically driven (QPD) systems. This leads to the discovery of a new non-equilibrium phase of matter — the discrete time quasi-crystal (DTQC)— which does not have any counterpart in Floquet systems. In Chapter 5, I introduce a new family of driving protocols without TTS, named as random multipolar drivings, and show that they give rise to a prethermal regime with the notably suppressed heating. Finally, in Chapter 6, I close this thesis by summarizing my findings and discussing open questions worth exploring in the future.

1.2 Quantum Thermalization

Let us first define the precise meaning of quantum thermalization by considering a quench from an initial state $|\psi(0)\rangle$ by a generic local Hamiltonian H in a lattice. Normally, we consider the initial state as a simple product state as this is most relevant for experiments, but the following arguments would still be valid for general initial states that are not eigenstates of H. One can decompose the initial state over the

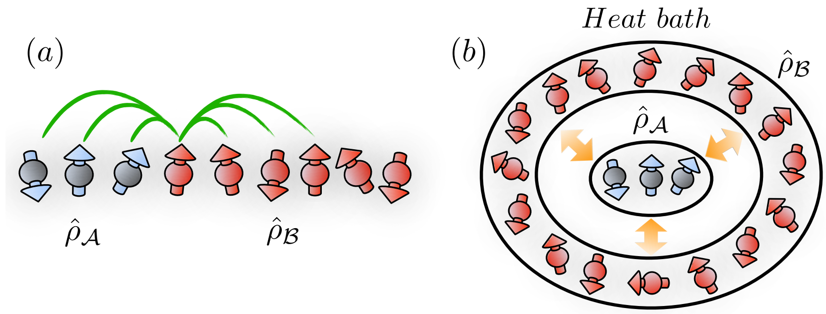

FIGURE 1.1: Schematic diagram of generic interacting many-body systems. (a) Blue spins denote the subsystem $\mathcal{A}$ of interest and the rest system represent subsystem $\mathcal{B}$ described by the reduced density matrix $\hat{\rho}_{\mathcal{A}}$ and $\hat{\rho}_{\mathcal{B}}$ respectively. (b) Subsystem $\mathcal{B}$ acts as a heat bath of $\hat{\rho}_{\mathcal{A}}$ which thermalizes after a sufficiently long time.

eigenbasis $|\alpha\rangle$, as

$$|\psi(0)\rangle = \sum_{\alpha} A_{\alpha} |\alpha\rangle \,, \tag{1.1}$$

where the coefficient is defined via $A_{\alpha} = \langle \alpha \, |\psi(0)\rangle$. Each eigenstate acquires a phase factor during time-evolution as

$$|\psi(t)\rangle = e^{-i\hat{H}t}|\psi(0)\rangle = \sum_{\alpha} A_{\alpha} e^{-iE_{\alpha}t}|\alpha\rangle, \tag{1.2}$$

where E_{α} denotes the corresponding eigenenergy. I am interested in properties of a subsystem $\mathcal{A}$ of size $L_{\mathcal{A}}$ which is normally small compared with the whole system size L. Such a subsystem can be described by a reduced density matrix

$$\hat{\rho}_{\mathcal{A}}(t) \equiv \mathrm{Tr}_{\mathcal{B}}(|\psi\rangle\langle\psi|), \tag{1.3}$$

and exchanges energy and information with the rest of the system $\mathcal{B}$ in the presence of generic many-body interactions. The subsystem $\mathcal{B}$ can be effectively treated as a heat bath, sketched in Fig. 1.1, and quantum thermalization occurs as $\hat{\rho}_{\mathcal{A}}$ evolves towards the thermal canonical ensemble [20]

$$\lim_{t\to\infty} \hat{\rho}_{\mathcal{A}}(t) = \mathrm{Tr}_{\mathcal{B}}(\hat{\rho}_{\mathrm{G}}), \tag{1.4}$$

where the corresponding density matrix is defined by

$$\hat{\rho}_G = \frac{1}{Z} e^{-\beta \hat{H}}, \tag{1.5}$$

where Z is the partition function and β denotes for the inverse temperature associated with the energy of the initial state. Correspondingly, the expectation value of any physical observable $\hat{O}$, which normally takes the form of a product of local operators, also approaches its thermal prediction as [20]

$$\lim_{t\to\infty} O(t) \equiv \lim_{t\to\infty} \langle\psi(t)|\hat{O}|\psi(t)\rangle = \mathrm{Tr}\left[\hat{\rho}_{\mathrm{G}}\hat{O}\right]. \tag{1.6}$$

1.2.1 Eigenstate Thermalization Hypothesis (ETH)

According to Eq. (1.2), the time-dependent expectation value of $\hat{O}$ can also be formally expanded in the eigenbasis as

$$O(t) = \sum_{\alpha} |A_\alpha|^2 O_{\alpha\alpha} + \sum_{\alpha\neq\beta} A^*_\alpha A_\beta O_{\alpha\beta} e^{i\left(E_\alpha - E_\beta\right)t}, \tag{1.7}$$

where $O_{\alpha\beta} = \langle\alpha|\hat{O}|\beta\rangle$. Its long time behavior converges to the infinite-time average of the expectation value $O(t)$ as [20]

$$\langle\hat{O}\rangle_\infty = \lim_{T\to\infty} \frac{1}{T}\int_0^T O(t)dt = \sum_\alpha p_\alpha O_{\alpha\alpha}, \tag{1.8}$$

where nondegeneracy of the eigenvalues is assumed. $p_\alpha = |A_\alpha|^2$ defines the probability distribution of finding an eigenstate for a given initial state, and the off-diagonal contributions in Eq. (1.7) oscillate with irregular frequencies hence average out for large T.

The assumption of non-degenerate spectrum is indeed reasonable for generic many-body systems once all symmetries of the Hamiltonian are resolved [2]. Degenerated eigenstates lead to time-independent off-diagonal contributions in Eq. 1.7, which will not be averaged out even for a large T. However, in the thermodynamic limit, as long as there are not extensively many degeneracies, diagonal contributions still dominate the dynamics, hence, Eq. 1.8 still gives a good approximation to the expectation value $\langle\hat{O}\rangle_\infty$.

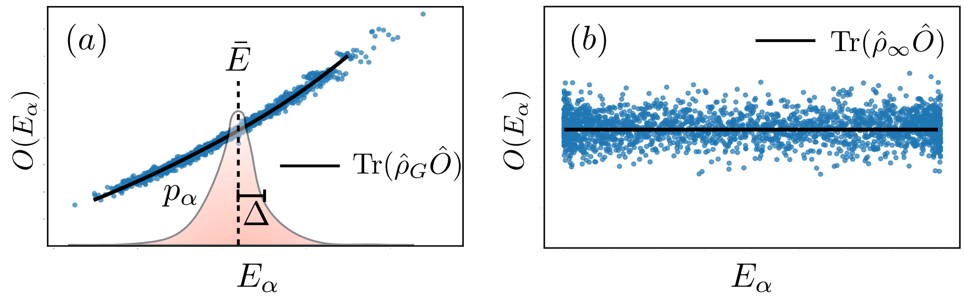

FIGURE 1.2: Distribution of expectation values of local observables for eigenstates $O(E_\alpha) \equiv \langle\alpha|\hat{O}|\alpha\rangle$ as a function of sorted eigenenergies. According to ETH, such a distribution matches well with the prediction (black line) by Gibbs density matrix. (a) For a generic non-integrable system, $O(E_\alpha)$ is a continuous function of energy in the thermodynamic limit. The distribution p_α defines the weight of eigenstates for a given initial state, which is normally narrow. (b) $O(E_\alpha)$ becomes independent of energy for Floquet-ETH (see Sec. 1.2.3) as all eigenstates locally cannot be distinguished from infinite-temperature state $\hat{\rho}_\infty$.

As the distribution of p_α versus eigenenergy is normally narrow [20] (sketched as shaded area in Fig. 1.2 (a)), the natural way to ensure $\langle\hat{O}\rangle_\infty$ reaches its thermal value for any generic initial state is by assuming that each eigenstate $|\alpha\rangle$ is thermalizing which forms the central idea of ETH [6, 7]. Therefore, illustrated as a black line in Fig. 1.2 (a), local expectation values for individual eigenstate follow the canonical prediction

$$\langle\alpha|\hat{O}|\alpha\rangle = \frac{1}{Z}\,\mathrm{Tr}\left(\hat{O}e^{-\beta_\alpha\hat{H}}\right), \tag{1.9}$$

where β_α defines the inverse temperature for each eigenstate $|\alpha\rangle$. By inserting $\hat{O} = \hat{H}$ in Eq. (1.9), one can determine the inverse temperature β_α for each eigenstate $|\alpha\rangle$ via the relation

$$E_\alpha = \frac{\sum_\gamma E_\gamma e^{-\beta_\alpha E_\gamma}}{\sum_\gamma e^{-\beta_\alpha E_\gamma}}. \tag{1.10}$$

Therefore, according to Eq. (1.9), the expectation value of the local observable $\langle\alpha|\hat{O}|\alpha\rangle$ solely depends on the inverse temperature β_α or its energy E_α, rather than the local details of each eigenstate.

More precisely, consider a distribution p_α centered around the energy

$$\bar{E} \equiv \langle\psi(0)|\,\hat{H}\,|\psi(0)\rangle\,,$$

with a small energy variance $\Delta \equiv \sqrt{\left\langle \psi(0) \left| \hat{H}^2 \right| \psi(0) \right\rangle - \bar{E}^2}$ in the thermodynamic limit. As long as the thermal expectation $O(E_\alpha) \equiv \langle \alpha | \hat{O} | \alpha \rangle$ is a continuous function and can be approximated as linearly varying within a small energy shell $[\bar{E}-\Delta, \bar{E}+\Delta]$ [1] with $N(\bar{E}, \Delta)$ number of eigenstates as shown in Fig. 1.2 (a), the late time expectation can be well approximated as [2]

$$\lim_{t\to\infty} O(t) = \sum_\alpha p_\alpha O_{\alpha\alpha} \approx \frac{1}{N(\bar{E}, \Delta)} \sum_{E_\alpha = \bar{E}-\Delta}^{\bar{E}+\Delta} O_{\alpha\alpha} \approx O(\bar{E}). \tag{1.11}$$

This is independent of the details of the initial state but only a function of the mean energy.

For a better understanding of the approach to thermal equilibrium, the following formal ansatz for operator $\hat{O}$ is introduced in Ref. [21]

$$\langle \alpha | \hat{O} | \beta \rangle = O(E_\alpha) \delta_{\alpha\beta} + e^{-S(E)/2} R_{\alpha\beta} f(\omega, E), \tag{1.12}$$

where $E = (E_\alpha + E_\beta)/2$, $\omega = E_\alpha - E_\beta$ denotes the energy average and difference respectively, $R_{\alpha\beta}$ is a random number with zero mean and unit variance, $O(E_\alpha)$ is the thermal expectation value as defined in Eq. (1.9), and $f(\omega, E)$ represents a spectral function (both $O(E_\alpha)$ and $f(\omega, E)$ are smooth function) and $S(E)$ is the thermodynamic entropy at energy E which scales as $\log D$ for eigenstates in the middle of the spectrum with D the Hilbert space dimension. Hence, Eq. (1.12) implies that the width of the distribution of the expectation values of operator $\hat{O}$ decreases for larger Hilbert space as $1/\sqrt{D}$, which serves as a standard measure to diagnose ETH [2]. In addition, Eq. 1.12 also leads to the equation

$$\lim_{T\to\infty} \frac{1}{T} \int_0^T dt \left(O(t) - O(\bar{E}) \right)^2 = \mathcal{O}\left(e^{-S(E)} \right) = \mathcal{O}\left(D^{-1} \right), \tag{1.13}$$

which bounds the temporal fluctuation at late time which is exponentially suppressed in system sizes [2].

[1] We are interested in states which are experimentally accessible and these states normally have a narrow energy variance Δ. In principle for the initial state, one can also consider a superposition of two eigenstates with a large energy difference. This state has a large Δ and $O(E_\alpha)$ might not vary linearly within the energy shell $[\bar{E}-\Delta, \bar{E}+\Delta]$. Thus, the diagonal contribution does not match with the microcanonical prediction. However, such an initial state is normally long-range correlated and difficult to prepare in experiments.

1.2.2 Diagnostics of Thermalization

Apart from the fact that the width of the distribution of $\langle\alpha|\hat{O}|\alpha\rangle$ decreases for larger system sizes as a result of ETH, there are some other diagnostics for quantum thermalization which will be briefly reviewed in the following.

Entanglement

Bipartite entanglement, normally quantified via the von Neumann entropy, serves as a good measure for quantum thermalization and has been extensively studied in quantum information research [22, 23]. The entanglement entropy between a subsystem $\mathcal{A}$ and the rest of the system is defined as [22]

$$S_{\text{ent}}(\mathcal{A}) = -\operatorname{tr}\hat{\rho}_{\mathcal{A}}\log\hat{\rho}_{\mathcal{A}} = -\sum_i \lambda_i \ln\lambda_i, \tag{1.14}$$

where λ_i are eigenvalues of the reduced density matrix $\hat{\rho}_{\mathcal{A}}$.

For the ground state of a gapped local quantum many-body system, it is well-known that the entanglement entropy exhibits an "area-law", namely $S_{\text{ent}} \sim L^{d-1}$ where d denotes the physical dimension and L represents the linear system size [24]. Intuitively, one can understand this behavior as quantum correlations in the ground state can only be established via local interactions with a finite number of neighbors at the boundary of the subsystem $\mathcal{A}$. As a special case for $d = 1$, this boundary does not increase with the subsystem size, hence, S_{ent} remains as a constant [25].

As a comparison, for highly excited eigenstates of generic non-integrable systems, any local observables are thermal and ETH applies. Hence, S_{ent} is equal to the extensive thermodynamic entropy at the corresponding temperature of the subsystem $\rho_{\mathcal{A}}$ [26]. Therefore, the entanglement entropy obeys an "volume-law", i.e. scales linearly with system volume as $S_{\text{ent}} \sim L^d$. In a quench setup, starting from a initial product state, S_{ent} normally increases linearly with time before the finite-size saturation occurs [27, 169].

It is worth noting that although thermal eigenstates necessarily have volume-law entanglement, it is not always true the other way around. Exceptions include integrable systems where the usual ETH fails, as detailed in Sec. 1.3.1, in which excited eigenstates might also have volume-law entanglement but the prefactor of the scaling exhibits a dependence on a fraction of the subsystem [28]. Additionally, in Chapter 3, I introduce a new form of ergodicity-breaking behavior showing that eigenstates can exist with volume-law entanglement but nevertheless result in non-thermal persistent oscillations [29].

Level Statistics

The statistical properties of the distribution of eigenenergies are also insightful to predict whether quantum thermalization happens. Remarkable results have been made from Wigner [30], Dyson [31] and others for understanding the spectrum of complicated atomic nuclei. Thereafter those results have been further developed to describe quantum chaos, and nowadays are known as random matrix theory (RMT) [32].

As quantum chaos is tightly related to ETH [2], some of the results predicted from RMT will also be valid in systems where ETH applies. One important conclusion obtained from RMT is that, in a given symmetry sector, neighboring energy levels of generic interacting systems repel each other. More precisely, I focus on the probability distribution $P(s_n)$ of neighboring energy gaps s_n defined as

$$s_n = (E_{n+1} - E_n)\,, \tag{1.15}$$

where E_n denotes the ordered eigenenergies. It has been numerically verified that $P(s_n)$ drops to zero (level-repulsion) for $s_n \to 0$ in a number of thermalizing many-body systems [33]. On the contrary, s_n demonstrates a Poisson distribution for ergodicity-breaking systems where ETH fails. Predominant examples for the latter include integrable and many-body localized systems which will be further illustrated in Sec. 1.3.

Alternatively, one can also use the probability distribution $P(r)$ of the ratio between consecutive energy gaps defined as [34]

$$r = \frac{\min(s_n, s_{n+1})}{\max(s_n, s_{n+1})}, \tag{1.16}$$

with $r \in [0, 1]$. According to the RMT prediction [35, 36], for a non-integrable Hamiltonian with real symmetric elements, the distribution $P(r)$ matches well with the

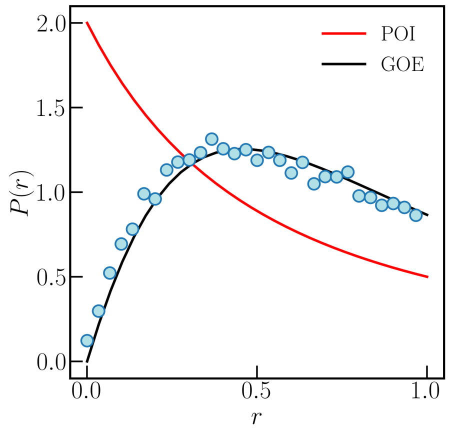

FIGURE 1.3: Level statistics for a non-integrable spin model which follows the Gaussian orthogonal ensemble (GOE) prediction exhibiting level repulsion. The ratio between adjacent energy gaps is defined in Eq. (1.16).

Gaussian orthogonal ensemble (GOE) prediction

$$P_{\mathrm{GOE}}(r) = \frac{27}{4} \frac{r + r^2}{(1 + r + r^2)^{5/2}}, \tag{1.17}$$

with the average value $\langle r \rangle_{\mathrm{GOE}} \approx 0.535898$ [35]. Whereas for integrable systems, it follows Poisson statistics (POI)

$$P_{\mathrm{POI}}(r) = \frac{2}{(1 + r)^2}, \tag{1.18}$$

with average $\langle r \rangle_{\mathrm{POI}} \approx 0.386294$ [35].

1.2.3 Periodically Driven Systems and Floquet-ETH

Periodically driven systems, or Floquet systems, are receiving growing interest and tremendous progress has been made during the last decades. For instance, discrete time crystal (see Sec. 1.3.2) and anomalous Floquet-Anderson insulators [18] are novel non-equilibrium phases of matter absent in undriven systems [37]. The vast developments in accurate control of quantum simulators also stimulate studies of Floquet engineering [38] which will be later elaborated in Sec. 1.4.3. However, time-dependence of the Hamiltonian also implies that the system does not conserve energy. Therefore, generic Floquet systems can absorb energy from the drive and are expected to keep heating to a featureless infinite temperature state.

To understand such a heating phenomenon more rigorously, let us consider a temporally periodic Hamiltonian, $\hat{H}(t) = \hat{H}(t+T)$, where T defines the period of the driving. In addition, I also assume that the Hamiltonian $\hat{H}(t)$ is local at each time t. The time evolution operator over a period from $t = 0$ to $t = T$ is captured by the Floquet operator $\hat{U}_F$ defined as

$$\hat{U}_{\mathrm{F}} = \mathcal{T} e^{-i\int_0^T dt \hat{H}(t)}, \tag{1.19}$$

where $\mathcal{T}$ denotes time ordering. $\hat{U}_F$ is now time independent and one can formally define the time-independent Floquet Hamiltonian $\hat{H}_F$ via the relation

$$\hat{U}_{\mathrm{F}} = e^{-i\hat{H}_{\mathrm{F}}T}. \tag{1.20}$$

Therefore, as long as we are interested in the dynamics at stroboscopic times $t = nT$, the dynamics is governed by the Floquet Hamiltonian as

$$\hat{U}_{\mathrm{F}}^n = e^{-i\hat{H}_{\mathrm{F}}nT}. \tag{1.21}$$

The thermalization processes for Floquet systems can then be understood in a similar way as for the static systems discussed in Sec. 1.2 by analyzing properties of eigenstates and eigenenergies of $\hat{H}_F$ [36].

However, the determination of the Floquet Hamiltonian is a highly-nontrivial task, and only few results are known in a closed form, for instance a two-level system subject to special driving fields [39, 40]. For generic many-body systems, one can instead construct $\hat{H}_F$ perturbatively if the system is in the rapid driving regime, i.e. the driving frequency $\omega = 2\pi/T$ is the dominant energy scale. Following Ref. [41], let me expand the Floquet Hamiltonian as

$$\hat{H}_{\mathrm{F}} = \sum_{n=0}^{\infty} T^n \hat{\Omega}_n, \tag{1.22}$$

with a small driving period T. The contribution to each order can be obtained via a Floquet-Magnus expansion as [2]

$$\begin{aligned}\hat{\Omega}_n = \sum_{\sigma} \frac{(-1)^{n-\theta[\sigma]}\theta[\sigma]!(n-\theta[\sigma])!}{i^n(n+1)^2 n! T^{n+1}} \int_0^T dt_{n+1} \int_0^{t_{n+1}} dt_n \cdots \int_0^{t_2} dt_1 \\ \times \left[\hat{H}\left(t_{\sigma(n+1)}\right), \left[\hat{H}\left(t_{\sigma(n)}\right), \ldots \left[\hat{H}\left(t_{\sigma(2)}\right), \hat{H}\left(t_{\sigma(1)}\right)\right] \ldots\right]\right],\end{aligned} \tag{1.23}$$

where σ denotes one permutation of $\{1, 2, \ldots, n+1\}$ and $\theta[\sigma] = \sum_{i=1}^{n} \theta(\sigma(i+1) - \sigma(i))$ with the unit step function $\theta(\cdot)$ [41]. All possible permutations will be summed over in the above equation. The lowest order contribution is simply the temporal average as $\hat{\Omega}_0 = \int_0^T dt \hat{H}(t)$. Suppose the Floquet-Magnus expansion converges, due to the locality of $\hat{H}(t)$, the Floquet Hamiltonian $\hat{H}_F$ becomes quasi-local[3] which can be sufficiently approximated via a few lowest orders of the expansion. Consequently, the Floquet dynamics thermalizes similar to a static system governed by the quasi-local Hamiltonian $\hat{H}_F$, and its local properties of which can be predicted by the corresponding microcanonical ensemble.

For generic interacting many-body systems, it is believed that the Floquet-Magnus expansion diverges. To see this, the following upper bound of the operator norm $||T^n \hat{\Omega}_n||$ can be calculated [13]

$$||T^n \hat{\Omega}_n|| \leq \left(\frac{1}{\xi} \int_0^T ||H(t)|| dt\right)^n, \tag{1.24}$$

where ξ is a universal constant. The norm of the Hamiltonian $||H(t)||$ increases with the system size and diverges in the thermodynamic limit. Therefore, the convergence condition of the Floquet-Magnus expansion, $\int_0^T ||H(t)|| dt \leq \xi$, cannot be satisfied unless the driving period T also scales with the system size. The Floquet Hamiltonian $\hat{H}_F$ now contains highly non-local many-body operators. The dynamics is not restricted to any energy shell and it is then suggested that any subsystem $\mathcal{A}$ for all eigenstates $|\alpha\rangle_F$ of $\hat{H}_F$, can be treated as an infinite-temperature density matrix $\hat{\rho}_\infty = \hat{1}/D$ with D the Hilbert space dimension. As shown in Fig. 1.2 (b), the local

[2] Note, other perturbation expansions of the Floquet Hamiltonian have also been proposed, see details in Ref. [42–45].

[3] "Quasi-local" here means that a term in the Hamiltonian can involve local operators distant in space but the associated amplitude rapidly decays in space.

expectation value for each eigenstate also becomes trivial, given by [46]

$$\langle\alpha|\hat{O}|\alpha\rangle_F = \frac{1}{Z}\operatorname{Tr}\left(\hat{O}\hat{\rho}_\infty\right) = \frac{1}{D}\operatorname{Tr}\hat{O}. \tag{1.25}$$

Such a behavior is also named Floquet-ETH which has been verified numerically [36, 46] and also experimentally [47] in many systems. It is thus implied that for a generic interacting Floquet many-body system, initial states will eventually approach the same infinite-temperature state and lose all interesting local features. The entanglement entropy also reaches the average value S_∞ of a random state in the Hilbert space [48], which, for a spin$-\frac{1}{2}$ chain of length L reads

$$S_\infty = \frac{L\log 2 - 1}{2}. \tag{1.26}$$

1.3 Violation of ETH

Now I start introducing non-ergodic systems where all or some eigenstates violate the canonical ETH prediction. These systems can thus maintain the memory of local properties of the initial states either permanently or for an exceptionally long time.

1.3.1 Integrable Systems

As the first example, I focus on integrable systems. Although a precise definition is still under debate, here by "integrable systems" I mean there exists an extensive number of local integrals of motion $\hat{I}_k$ which commute with each other as well as the Hamiltonian. Note that the projector $|\alpha\rangle\langle\alpha|$ on each eigenstate $|\alpha\rangle$, also commute with the Hamiltonian $\hat{H}$, however, they are normally highly non-local hence do not imply integrability. The statistics of the level spacing is thus expected to follow Poisson distribution due to the presence of degeneracy in the spectrum induced by $\hat{I}_k$ [33].

As the $\hat{I}_k$ commute with the Hamiltonian, their expectation values at any given time are fixed by the initial state $|\psi_0\rangle$, hence, deviate from the canonical ensemble prediction as reviewed in Sec. 1.2. Therefore, apart from the regular energy or momentum conservation, these new conserved quantities impose additional constraints on the thermal equilibration. To capture the thermal relaxation of local observables for integrable systems, the generalized Gibbs ensemble (GGE) was proposed [49] and its density matrix reads

$$\hat{\rho}_{\mathrm{GGE}} = \frac{\exp\left(-\sum_k \lambda_k \hat{I}_k\right)}{\mathrm{Tr}\left[\exp\left(-\sum_k \lambda_k \hat{I}_k\right)\right]}, \tag{1.27}$$

which maximizes the entropy $S = k_{\mathrm{B}}\,\mathrm{Tr}\,[\hat{\rho}\ln(1/\hat{\rho})]$ subject to the additional constraints. The values of the Lagrange multipliers are determined by requiring

$$\mathrm{Tr}\left[\hat{\rho}_{\mathrm{GGE}}\hat{I}_k\right] = \langle\psi_0|\,\hat{I}_k\,|\psi_0\rangle\,. \tag{1.28}$$

The validity of the GGE has been verified in many integrable models, for instance hard-core bosons [50] and transverse field Ising models [51].

Floquet Systems Integrability significantly changes the heating behavior for Floquet systems. Instead of heating to the infinite temperature, it is shown that after a sufficiently long time, a steady state is obtained which can be described by the periodic Gibbs ensemble (PGE) proposed in Ref. [52] as

$$\hat{\rho}_{\mathrm{PGE}}(t) = Z^{-1}\exp\left(-\sum_k \lambda_k \hat{I}_k(t)\right), \tag{1.29}$$

where Z is the time-independent normalization factor. The operators

$$\hat{I}_k(t) = \hat{U}(t)\hat{I}_k\hat{U}^{\dagger}(t),$$

where $\hat{U}(t)$ denotes the time evolution operator for Floquet systems at time t, are temporally periodic integrals of motion, the expectation value of which defines time independent conserved quantities [52]. Therefore, the PGE ensemble is also periodic, hence, the expectation values of local observables synchronize with the drive.

1.3.2 Many-Body Localization

Another important mechanism to evade quantum thermalization is many-body localization (MBL) [53–55]. It is a generalization of Anderson localization [56] by including many-body interactions. The XXZ spin model serves as a paradigmatic model for

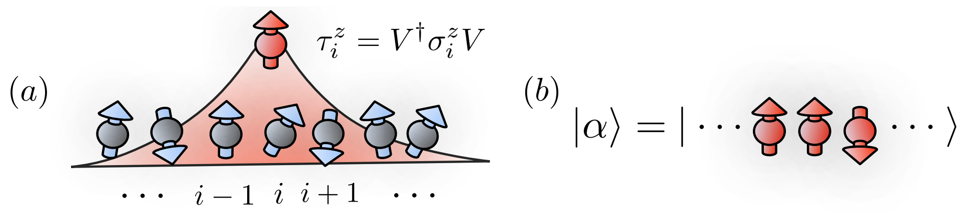

FIGURE 1.4: (a) Local integrals of motion $l-$bits τ_i can be transformed from physical qubits σ_i via a local unitary transformation V. Support of τ_i decays exponentially away from site i. (b) Eigenstates $|\alpha\rangle$ of a MBL Hamiltonian are products of the eigenstate of τ_i^z.

MBL captured by the Hamiltonian [57, 58]

$$\hat{H}_{\mathrm{MBL}} = \sum_{i=1} J\left(\sigma_i^x \sigma_{i+1}^x + \sigma_i^y \sigma_{i+1}^y\right) + J_z \sigma_i^z \sigma_{i+1}^z + h_i \sigma_i^z, \tag{1.30}$$

where σ_i^α represents pauli operators for spin-$\frac{1}{2}$ operators at site i, J and J_z denotes interaction strength and h_i defines a random field on each site. Via the Jordan-Wigner transformation [59], the XXZ model can be mapped to a fermionic model as

$$\hat{H}_{\mathrm{MBL}} = \sum_i 2J\left(\hat{c}_i^\dagger \hat{c}_{i+1} + \mathrm{H.c.}\right) + J_z\left(2\hat{n}_i - 1\right)\left(2\hat{n}_{i+1} - 1\right) + \sum_i h_i\left(2\hat{n}_i - 1\right), \tag{1.31}$$

where $\hat{c}_i^\dagger$ defines standard fermionic creation operator at site i and $\hat{n}_i = \hat{c}_i^\dagger \hat{c}_i$ denotes the occupation number. For a vanishing interaction $J_z = 0$, Eq. (1.31) describes the Anderson localized model where all single-particle eigenstates become localized for any nonzero disorder potential. Such localization generalizes to MBL in the presence of weak interaction $J_z \neq 0$ as long as the disorder strength is sufficiently strong.

Many properties of MBL in spin systems can be understood via the phenomenological degrees of freedom (d.o.f.) τ_i as illustrated in Fig. 1.4 (a) [60]. They are known as $l-$bits, which can be transformed from the physical qubit of σ via a local transformation V as $\tau_i = V^\dagger \sigma_i V$. Crucially, they commute with other $l-$bits as $[\tau_i, \tau_j] = 0$ [61]. In the localized phase, the original Hamiltonian take the general form

$$\hat{H}_{\mathrm{MBL}} = \sum_i \tilde{h}_i \tau_i^z + \sum_{ij} J_{ij} \tau_i^z \tau_j^z + \sum_{ijk} J_{ijk} \tau_i^z \tau_j^z \tau_k^z + \cdots, \tag{1.32}$$

where $\tilde{h}_i$ denotes an effective random field, and J_{ij} and J_{ijk} characterize interaction between $l-$bits which decays exponentially with distance $|i-j|$. As the Hamiltonian is purely diagonal in the new basis, all $l-$bits commute with the Hamiltonian

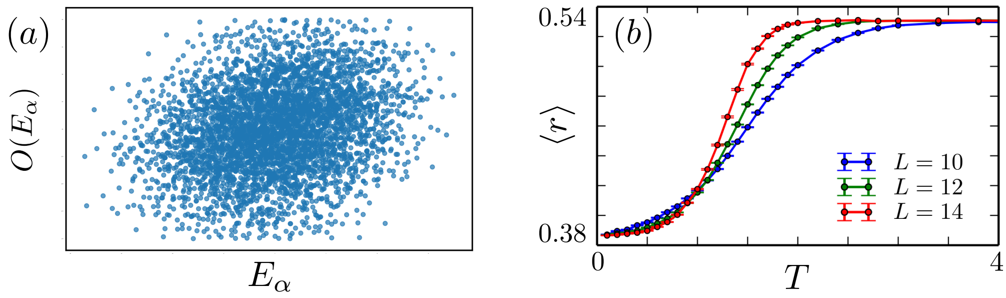

FIGURE 1.5: (a) Local expectation values for (Floquet-)MBL eigenstates fluctuate chaotically. (b) Level statistics of a Floquet model with disorder. The average value of the ratio of consecutive quasi-energy gaps detects the Floquet-MBL to thermal phase transition, which occurs for a large driving period T. Figure is adapted from Ref. [62]

$[\tau_i, \hat{H}_{\text{MBL}}] = 0$ and they are regarded as emergent local integrals of motion, which makes the system similar to an integrable model. The level statistics therefore obeys POI distribution stemming from the lack of level repulsion, which has also been employed as a signature to probe the MBL-thermal phase transition [58].

All eigenstates of MBL are simply products of τ_i, as shown in Fig. 1.4 (b), which maintain locality even when transformed back to the physical d.o.f. It results in the area-law scaling of the entanglement entropy as localized bits cannot establish correlations throughout the whole system [58], in sharp contrast to the volume-law scaling expected for ETH-obeying excited eigenstates. Likewise, the system cannot act as its own thermal bath. Hence, eigenstates are not thermal and their local properties fluctuate chaotically even for eigenstates close in energy as shown in Fig. 1.5 (a). In a quench setup, the expectation values of each $l-$bit are determined by the initial condition and remain conserved during the time evolution. Therefore, the memory of initial states is preserved for an infinitely long time [63] as verified in recent cold atoms experiments [64, 65].

Floquet MBL

MBL has also been shown to evade heating when the system is subject to a periodic drive [66], which again can be intuitively understood via the $l-$bits representation [62]. Without loss of generality, here I consider a generic MBL system driven by a local field $\hat{D}$ which oscillates monochromatically as

$$\hat{H}(t) = \hat{H}_{\text{MBL}} + \hat{D}\cos(\omega t), \tag{1.33}$$

where ω determines the driving frequency. As the eigenstates of $\hat{H}_{\mathrm{MBL}}$ are products of $l-$bits, a local drive can only modify a group of $l-$bits in a finite spatial region. These $l-$bits span a typical local energy bandwidth W. In the rapid driving regime, as long as $\omega \gg W$, there are no transition channels between different many-body eigenstates to absorb an energy quanta ω. Therefore, MBL remains stable in Floquet systems (Floquet-MBL) [62]. Formally, although there is no rigorous proof, such a non-thermal behavior suggests that the Floquet-Magnus expansion introduced in Eq. (1.23) converges for sufficiently rapid driving and strong disorders [67]. The resulting Floquet Hamiltonian $\hat{H}_F$ defined in Eq. (1.22) is also many-body localized associated with a new set of dressed $l-$bits different from the ones for the undriven Hamiltonian $\hat{H}_{\mathrm{MBL}}$. The late time relaxation in such a system will be similar to the Floquet integrable systems discussed in Sec. 1.3.1, namely synchronizing with the driving and the stroboscopic time evolution is purely captured by $\hat{H}_F$.

When the driving frequency is reduced, a transition from Floquet-MBL to the thermal phase happens, illustrated in Fig. 1.5 (b), as energy absorption via many-body resonances is restored for $\omega \lesssim W$. In other words, higher order contributions obtained from the Floquet-Magnus expansion become dominant for smaller driving frequency. These highly non-local processes eventually destabilize MBL and heat up the system.

Floquet Time Crystals

The stability of MBL in Floquet systems permits the existence of non-equilibrium phases of matter without any counterpart in static systems. There are many of them [18, 37, 68], but here I focus on discrete time crystals (DTC) which have attracted great attention in recent years. As discussed in previous sections, the late-time steady state $\hat{\rho}(t)$ of a Floquet many-body system either synchronizes with the periodic drive for integrable models or completely thermalizes. These two types of steady states are both periodic in time with the same frequency as the driven Hamiltonian[4], hence preserving the discrete time translation symmetry (TTS). A natural question

[4]Infinite temperature state is indeed time-independent but can still be regarded as periodic in time

arises, namely is it possible to realize a time crystal with spontaneous time translation symmetry breaking (TTSB) in a similar way to the spatial symmetry breaking in crystals? To be precise, for a simple initial state subject to a driving $\hat{H}(t)$ of period T, is it possible that the expectation value of at least one local observable $O(t)$ of the steady state exhibits persistent regular dynamics? For instance, periodic oscillations as $O(t+T') = O(t)$ where T' is different from T hence breaking TTS of the original Hamiltonian.

There are lots of models identified to demonstrate TTSB and the so-called $\pi-$ spin glass (SG) serves as an exemplary one with period-doubling time crystalline dynamics [69], i.e. the observable oscillates with a doubled period $T' = 2T$. I first focus on the soluble limit where the driving protocol consists of two steps captured by the Floquet operator

$$\hat{U}_F = e^{-i\hat{H}_x} e^{-i\hat{H}_z}, \tag{1.34}$$

where $\hat{H}_x = \sum_i^L g_i \sigma_i^x$ and $\hat{H}_z = \sum_i^L J_i \sigma_i^z \sigma_{i+1}^z$, here L is the system size. Both of them commute with a global Z_2 Ising symmetry generated by the operator $P_x = \prod_i \sigma_i^x$. The coupling strength J_i is randomly chosen and results in a spin glass phase, see details in [17, 69]. For $g_i = \pi/2$, the second driving step reduces to

$$\exp\left[-i\frac{\pi}{2}\sum_j \sigma_j^x\right] = (-i)^L \prod_j \sigma_j^x, \tag{1.35}$$

which is proportional to the Ising symmetry operator P_x up to a phase.

Time crystalline behavior appears for any Ising symmetry broken state. For instance, after the first half of the drive, the state $|\uparrow\uparrow\downarrow\ldots\uparrow\downarrow\rangle$ only gains an additional phase induced by H_z as such the spin configuration remains invariant. The Ising symmetry operator then performs a spin flip on all of the sites, thus, after a single period one obtains

$$\hat{U}_F \left|\uparrow\uparrow\downarrow\ldots\uparrow\downarrow\right\rangle \propto \left|\downarrow\downarrow\uparrow\ldots\downarrow\uparrow\right\rangle. \tag{1.36}$$

The initial spin configuration can be restored after two periods hence the magnetization exhibits period-doubling behavior as $\langle\sigma_i\rangle(t+2T) = \langle\sigma_i\rangle(t)$. Likewise, the Floquet Hamiltonian of the Floquet operator for two periods reads

$$\hat{U}_F^{2n} = \left[(-i)^L P_x e^{-iH_z}\right]^{2n} = e^{-i2n\hat{H}_z}, \tag{1.37}$$

suggesting the dynamics after even periods is fully governed by $\hat{H}_z$.

Surprisingly, thanks to the stability of Floquet-MBL, the period-doubling behavior described above is not merely a fine-tuned phenomenon, but rather defines a non-equilibrium $n-$DTC phase of matter with $n = 2$. It remains infinitely long lived with a period rigidly locked at $2T$ even when deviating from the soluble limit [70], for instance, in the presence of rotation imperfections during the spin flip, or perturbations which break the Ising symmetry of $\hat{H}_z$ as long as the perturbation strengths are small.

Nowadays the zoo of DTCs keeps growing and developments include, for instance, the ones with higher ($n = 4$) [71] or fractional ($n = 8/3$) orders [72] and also in higher dimensions [73]. I am particularly interested in time crystalline dynamics in time-dependent systems which cannot be simply captured by the Floquet framework. For instance in Chapter 4 and 5, I will show the TTSB can also appear in systems driven by quasi-periodic and structured random drivings.

1.3.3 Quantum Many-Body Scars

Both the integrability and MBL strongly violate ETH as all eigenstates are non-thermal. An interesting phenomenon observed experimentally on a Rydberg atom platform as seen in Fig. 1.6 (a) [74] suggested that ergodicity-breaking can also happen in non-integrable systems in a weak manner [75–79]. Persistent coherent oscillations appeared only for certain special initial states, while most of the other generic initial states rapidly thermalize. It turns out that a special band of non-thermal eigenstates, named quantum many-body scars (QMBS) as seen in Fig. 1.6 (b), play a key role in the appearance of the non-ergodic dynamics. QMBS have dominant support in a small portion of Fock space and are decoupled (either approximately or exactly) from the sea of thermalizing eigenstates obeying ETH. Therefore, any initial states with a large overlap with QMBS display non-ergodic behavior that manifests itself through

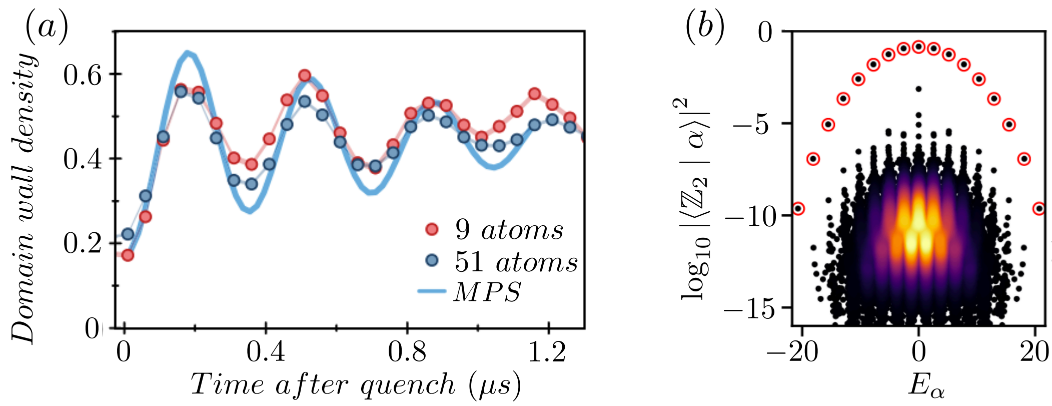

FIGURE 1.6: (a) Coherent oscillations of the domain wall density observed when Rydberg-atoms are quenched from the $|\mathbb{Z}_2\rangle$ initial state. The exceptionally slow thermalization persist in large systems of 51 atoms, and the dynamics can be captured using matrix product state (MPS) simulation. Figure is adapted from Ref. [74]. (b) Overlap between the initial states and eigenstates proposed in Ref. [75]. The slowly thermalizing dynamics in (a) is attributed to a band of non-thermal eigenstates, namely the quantum many-body scars which weakly break the ergodicity. The color scheme represents the density of eigenstates. This figure is adapted from Ref. [75]

persistent coherent oscillations. A key characteristic of QMBS is their sub-volume entanglement entropy [80, 81] whereas other ETH-obeying eigenstates are volume-law entangled. This property is also commonly used for the diagnosis of QMBS as entropy-outliers which clearly separates them from other thermal eigenstates in the bulk of the spectrum as shown in Fig. 1.7 (a).

Many different mechanisms have been discovered so far to realize the decoupling between the scared subspace with the thermal ones [82], for instance, spectrum-generating algebra [83], projector embedding [84] and Hilbert space fragmentation (HSF) [77, 79, 85] which will be covered in Chapters 2 and 3 of the thesis. For a Hamiltonian $\hat{H}$ and some arbitrary state in the Hilbert space $|\psi_0\rangle$, one can define the Krylov subspace $\mathcal{K}$ by repeatedly applying the Hamiltonian on the state as [82] $\mathcal{K} = \text{span}\left\{|\psi_0\rangle, \hat{H}|\psi_0\rangle, \hat{H}^2|\psi_0\rangle, \ldots \hat{H}^n|\psi_0\rangle \ldots\right\}$. For a given system size, HSF happens when the Krylov subspace stops growing for larger n and its dimension is much smaller than the total Hilbert space. I also restrict the state $|\phi_0\rangle$ in a given symmetry sector to ensure the disconnection of different Krylov subspaces is not due to obvious symmetry reasons as sketched in Fig. 1.7 (b). For instance, $\mathcal{K}$ does not involve states with different particle numbers if the starting state $|\phi_0\rangle$ and the Hamiltonian $\hat{H}$ both preserve the particle number.

The dimension of $\mathcal{K}$ has a strong dependence both on the Hamiltonian $\hat{H}$ and

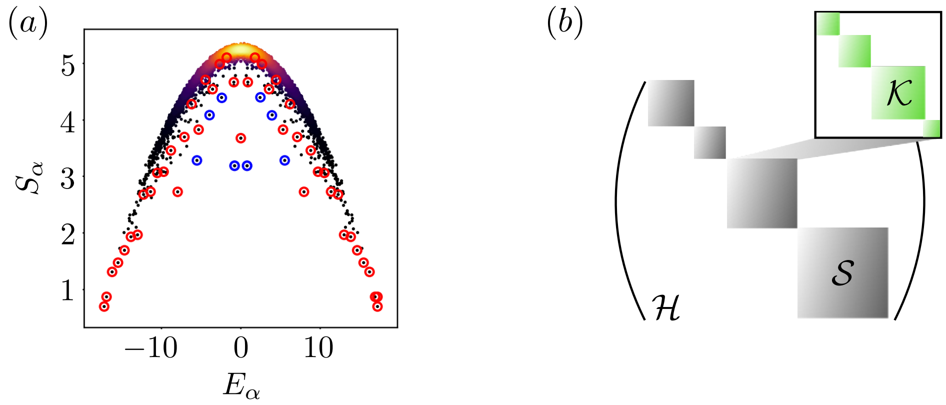

FIGURE 1.7: (a) Entanglement entropy S_α for all eigenstates versus eigenvalues E_α [86]. QMBS manifest themselves as entropy-outliers highlighted via blue or red circles whereas others are mostly volume-law entangled. Figure is adapted from Ref. [86]. (b) Schematic diagram for Hilbert space fragmentation. The Hilbert space is block-diagonalized due to symmetry reasons (gray), but can be furthermore fragmented into isolated Krylov subspaces $\mathcal{K}$ (green).

the starting state $|\phi_0\rangle$. It can scale exponentially versus system size or even remain constant [77]. Special subspaces $\mathcal{K}$ may have a small dimension that is insufficient for thermalization hence hosting QMBS and violate ETH. Time evolution of a state within a small $\mathcal{K}$ will always remain in the same subspace and exhibit coherent oscillations.

HSF has been proposed in systems with strong kinetic constraints induced by, for instance, higher momentum conservation laws [77, 87] and a strong tilt in optical lattices [88]. In Chapter 2, I will employ the idea of Floquet engineering (see details in Sec. 1.4.3) for the realization of QMBS in optical lattices. By periodically modulating the on-site interaction of the Bose-Hubbard model, I show that the so-called density-assisted tunneling emerges. This can be tuned to significantly constrain the dynamics of cold atoms. These kinetic constraints induce QMBS, and they will be further verified via the spectrum properties of the Floquet operator and the long-lasting coherent oscillations for special initial states.

In Chapter 3, I will address the intriguing question of whether long-lived coherent oscillations can coexist with rapid volume-law entanglement generation in a standard quench setup. I confirm its existence by imposing kinetic constraints to a multi-component strongly correlated system, which naturally hosts two fractionalized d.o.f. It turns out that the kinetic constraints result in HSF in one component, hence, persistent oscillations appear and break the ergodicity. However, the other emergent d.o.f. is thermal and generates volume-law entanglement.

1.4 Prethermalization

Instead of focusing on the asymptotic long-time behavior of a quantum system, I am also interested in a transient non-ergodic phenomenon, dubbed as prethermalization. When there are several well-separated time scales in a many-body system, the state might first relax to a prethermal quasi-steady state of a finite lifetime instead of thermalizing monotonically towards the eventual equilibrium. This behavior has been identified in both static or Floquet systems as elaborated in this section.

1.4.1 Static Systems

Consider a time-independent Hamiltonian consisting of two parts

$$\hat{H} = \hat{H}_0 + \lambda \hat{V}, \tag{1.38}$$

where λ is dimensionless and controls the separation of different time scales. If λ is very small, the short time evolution is thus mainly governed by $\hat{H}_0$. Hence, the system quickly relaxes to a prethermal state at some timescale which we call τ_{rel}. According to ETH as reviewed in Sec. 1.2, its local expectation values of operator $\hat{O}$ can be predicted as $\text{Tr}\left[\hat{\rho}_{\text{pre}}\hat{O}\right]$, where the density matrix $\hat{\rho}_{\text{pre}}$ corresponds to the microcanonical ensemble for Hamiltonian $\hat{H}_0$. However, such a prethermal state is not stable as $\hat{V}$ will introduce slow processes which, in many cases, become notable at a time scale $\tau_{\text{pre}} = \mathcal{O}\left(\lambda^{-2}\right)$. Thereafter the prethermal state evolves towards the final steady state [41] captured by the microcanonical ensemble $\hat{\rho}$ for $\hat{H}$.

However, for generic non-integrable systems and a small λ, the density matrix $\hat{\rho}_{\text{pre}}$ is similar to the $\hat{\rho}$. Hence, distinguishing the prethermal value $\text{Tr}\left[\hat{\rho}_{\text{pre}}\hat{O}\right]$ and the asymptotic value $\text{Tr}\left[\hat{\rho}\hat{O}\right]$ can be difficult and prethermalization might be invisible. For this reason, prethermalization in static systems normally happens when the Hamiltonian $\hat{H}_0$ preserves a number of conserved quantities until the time scale τ_{pre}. Then the perturbation $\hat{V}$ breaks one of these conservation laws and leads to eventual thermalization [89–91].

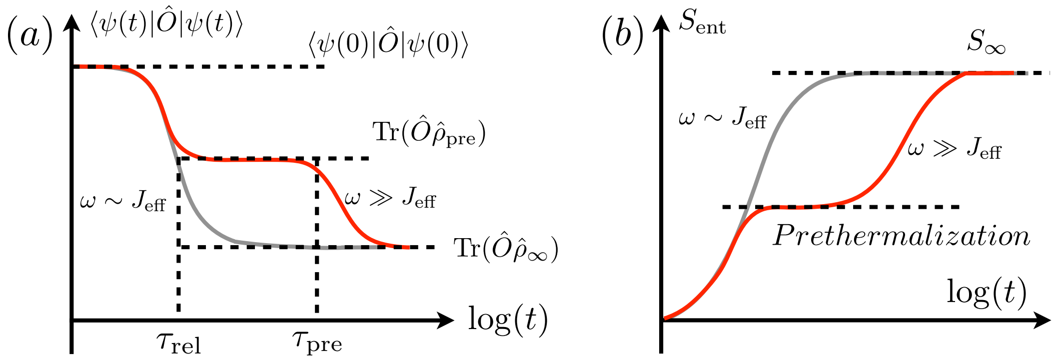

FIGURE 1.8: Thermalization of the state $|\psi(t)\rangle$ in Floquet systems with rapid driving (red) or relatively slow driving (gray). (a) For $\omega \gg J_{\mathrm{eff}}$, after a transient period, expectation of a local observable $\hat{O}$ first saturates to a prethermal plateau before heating to infinite temperature state $\hat{\rho}_{\infty}$. Whereas for slower driving, the state evolves to $\hat{\rho}_{\infty}$ rapidly. (b) Likewise the dynamics of entanglement entropy S_{ent} also exhibits prethermal plateau before reaching the maximum value S_{∞}. For a spin-$\frac{1}{2}$ chain of length L it reads $S_{\infty} = (L\log 2 - 1)/2$ [48].

1.4.2 Floquet Systems

As discussed in Sec. 1.2.3, a generic interacting many-body system heats indefinitely to infinite temperature unless the system is integrable or exhibits MBL. Here I show that prethermalization also appears in Floquet systems for high frequency drivings, which can be treated as a generic method to suppress drive induced heating in non-integrable systems. When the driving frequency ω is much larger than the local bandwidth J_{eff} of the effective Hamiltonian governing prethermal dynamics, energy absorption can only happen via many-body resonances. For instance, simultaneous flips of multiple spins, the number of which scales as $n_{\mathrm{flip}} = \omega/J_{\mathrm{eff}}$. The probability for such an event to happen is exponentially small in n_{flip}, hence, resulting in an exponentially long lifetime of prethermalization as illustrated in Fig. 1.8. Such an intuition has been verified in many setups both numerically [92] and experimentally [47, 93]. In fact, it can also be rigorously proved via bounding the heating rate [19, 94] obtained by the Floquet-Magnus expansion introduced in Sec. 1.2.3.

Let us consider a non-integrable system described by the time-dependent Hamiltonian $\hat{H}(t) = \hat{H}(t+T)$. The stroboscopic dynamics after each period is governed by the time-independent Floquet Hamiltonian $\hat{H}_F$ which can be perturbatively determined by the Floquet-Magnus expansion [Eq. (1.23)]. One can then define an effective

Hamiltonian by truncating the expansion up to a finite order n as

$$\hat{H}_{\mathrm{F}}^{(n)} = \sum_{m=0}^{n} T^m \hat{\Omega}_m, \tag{1.39}$$

which remains local if the original driven Hamiltonian $\hat{H}(t)$ is local, hence, does not obey Floquet-ETH introduced in Sec. 1.2.3. Instead, the effective Hamiltonian $\hat{H}_{\mathrm{F}}^{(n)}$ obeys the usual ETH, thus, the system approaches the prethermal state captured by the microcanonical ensemble $\hat{\rho}_{\mathrm{pre}} = e^{-\beta \hat{H}_{\mathrm{F}}^{(n)}}$ as shown in Fig. 1.8.

For a short-ranged interacting system, rigorous results have been established in Ref. [19, 41]. The upper bound for the distance between a local operator $\hat{O}$ propagated either by the Floquet Hamiltonian or the effective Hamiltonian at stroboscopic time t is given by [41]

$$\left\| e^{i\hat{H}_{\mathrm{F}}t}\hat{O}e^{-i\hat{H}_{\mathrm{F}}t} - e^{i\hat{H}_{\mathrm{F}}^{(n_0)}t}\hat{O}e^{-i\hat{H}_{\mathrm{F}}^{(n_0)}t} \right\| \leq t\|\hat{O}\| v_l k g e^{-\mathcal{O}(1/(kgT))}, \tag{1.40}$$

where $\|\cdot\|$ denotes the operator norm, n_0 defines the optimal order beyond which the Floquet-Magnus expansion starts to diverge. The optimal order scales linearly in frequency as $n_0 \sim \mathcal{O}(1/(kgT))$, where k measures the maximum interacting range of $\hat{H}(t)$ and the absolute energy per site is bounded above by g. The above inequality indicates that the local property of the Floquet dynamics can be well-approximated by the truncated Hamiltonian up to the prethermal time scale $\tau_{\mathrm{pre}} \sim e^{\mathcal{O}(1/(kgT))}$. One can further show that the effective Hamiltonian can be regarded as a conserved quantity during prethermalization by inserting $\hat{O} = \hat{H}_{\mathrm{F}}^{(n)}$ in Eq. (1.40) for $0 \leq n \leq n_0$ as

$$\frac{1}{V}\left\| e^{i\hat{H}_{\mathrm{F}}t}\hat{H}_{\mathrm{F}}^{(n)}e^{-i\hat{H}_{\mathrm{F}}t} - \hat{H}_{F}^{(n)} \right\| \leq tkg^2 e^{-\mathcal{O}(1/(kgT))} + \mathcal{O}\left(T^{n+1}\right), \tag{1.41}$$

where V denotes the system size and $\mathcal{O}\left(T^{n+1}\right)$ measures the fluctuation which is time independent. The expectation value of $\hat{H}_{\mathrm{F}}^{(0)}$ is normally interpreted as the mean energy of the state, which remains conserved up to an exponentially long time as suggested by Eq. (1.41) for $n = 0$. Therefore, the heating rate of the system, whose energy grows towards the infinite-temperature value $\mathrm{Tr}\left(\hat{H}_{\mathrm{F}}^{(0)}\hat{\rho}_{\infty}\right)$, is exponentially small in frequency. Hence, the change in the energy only becomes notable after an exponentially long time.

1.4.3 Floquet Engineering

Floquet driving allows us to drastically modify the dynamical properties of quantum many-body systems and create effective physical processes which are otherwise difficult to obtain. Although for generic non-integrable systems these driving induced effects ultimately disappear, prethermalization allows us to observe them in a sufficiently long time window. Such an idea is also called Floquet engineering [38], which is broadly applied not only in cold atoms in optical lattices [95, 96], but also in electronic systems [38]. However, according to the rigorous results of the last section, Floquet heating is only well controlled when the driving frequency is the dominating energy scale of the system and crucially the driving amplitude should not be too strong. As such, the resulting effective Hamiltonian $\hat{H}_F^{(n)}$ can be well approximated as $\hat{H}_F^{(n)} \approx \hat{\Omega}_0$ because higher order corrections are negligible. It indeed poses a strong limitation to Floquet engineering as the induced dynamics remain close to the undriven ones trivially generated by $\hat{\Omega}_0$. One exception happens when $\hat{\Omega}_0$ vanishes, in which the effective Hamiltonian is dominated by the first order process

$$\hat{H}_{\mathrm{F}}^{(n)} \approx T\hat{\Omega}_1, \tag{1.42}$$

this can be very non-trivial as presented in Ref. [97].

Alternatively, strong driving is commonly used to significantly modify the Hamiltonian by using a driving amplitude comparable to, or even much larger than, the driving frequency. Although the standard Floquet-Magnus expansion becomes invalid, one might find a properly defined rotating frame in which the driving amplitude does not contribute to the amplitude of the Hamiltonian. Therefore, the driving frequency is still the largest energy scale permitting a perturbative expansion in the new frame.

For concreteness, I will illustrate the idea of Floquet engineering through the periodically driven 1D Bose-Hubbard system described by the Hamiltonian

$$\hat{H}(t) = \sum_{\langle pq \rangle} \hat{c}_p^\dagger J_{pq} \hat{c}_q + \frac{U}{2} \sum_p \hat{n}_p(\hat{n}_p - 1) + F(t) \sum_p \epsilon_p \hat{n}_p, \tag{1.43}$$

where $\hat{c}_p(\hat{c}_p^\dagger)$ annihilates (creates) a boson at site p, and $\hat{n}_p = \hat{c}_p^\dagger \hat{c}_p$ is the occupation number operator. This Hamiltonian has been discussed in Ref. [98] and describes a system of spinless bosons in the lowest band of 1D driven optical lattices. The first term on the right hand side indicates that particles can hop to its neighboring sites with the bare hopping rate $J_{pq} = -J$. The second term represents the on-site interaction with the amplitude U, tunable by modulating a magnetic field inducing a Feshbach resonance [99]. The sign of U can be either positive or negative, generating repulsive or attractive forces between particles if more than two of them are occupying the same site. The final term defines a tilted potential with $\epsilon_p = -p$, and its amplitude $F(t)$ is a temporally periodic function with a period T. Experimentally, the time dependence can be achieved via a periodic tilt or acceleration of the lattice [100].

For the static system with $F(t) = 0$ and positive U, the dimensionless quantity U/J drastically changes the groundstate property [101]. For $U/J \ll 1$, where hopping dominates, the groundstate features superfluidity (SF) where all particles are free to move. On the contrary for $U/J \gg 1$, the system enters a Mott insulator (MI) phase where particles fix their position on each lattice site to avoid on-site repulsion. The SF to MI phase transition has been realized experimentally in optical lattices by increasing the lattice depth [102, 103].

The SF-MI phase transition can also be realized by periodically shaking the lattice with a continuous driving profile, e.g. $F(t) = F_1 \cos(\omega t)$, with a large amplitude i.e. $F_1 \gtrsim \omega$. In this case, the lowest order contribution to the effective Hamiltonian $\hat{\Omega}_0$ is the time average of $\hat{H}(t)$ which trivially gives the static Bose-Hubbard model, and the higher-order expansion of the Hamiltonian quickly diverges. To resolve this, the time dependent unitary transformation $R(t)$ was employed in Ref. [98] as

$$R(t) = \exp\left[i \sum_p \theta_p(t) \hat{n}_p\right], \tag{1.44}$$

where $\theta_p(t) = \epsilon_p \int_0^t d\tau F(\tau)$. The Hamiltonian $\tilde{H}(t) = R\hat{H}(t)R^\dagger - iR\dot{R}^\dagger$ in the rotating frame reduces to

$$\tilde{H}(t) = \sum_{\langle pq \rangle} \hat{c}_p^\dagger \hat{A}_{pq}(t) \hat{c}_q + \frac{U}{2} \sum_p \hat{n}_p(\hat{n}_p - 1), \tag{1.45}$$

where the hopping term is modified to

$$\hat{A}_{pq}(t) = J_{pq} e^{i(\theta_p(t) - \theta_q(t))}, \tag{1.46}$$

and the driving profile $F(t)$ contributes a time-dependent phase factor. The Hamiltonian in the rotating frame now permits a perturbative expansion in the rapid driving regime, i.e. $\omega \gg J, U$, and the lowest order contribution reduces to

$$\hat{\Omega}_0 = -J_{\text{eff}} \sum_{\langle pq \rangle} \hat{c}_p^\dagger \hat{c}_q + \frac{U}{2} \sum_p \hat{n}_p(\hat{n}_p - 1), \tag{1.47}$$

where the hopping rate is now renormalized as $J_{\text{eff}} = J\mathcal{B}_0(F_1/\omega)$, here $\mathcal{B}_0(x)$ denotes the zero-th order Bessel function [98]. Consequently, the ratio between the renormalized hopping and the on-site interaction J_{eff}/U can be tuned in a wide range by varying F_1/ω, enabling the SF-MI phase transition [98].

There has been a vast amount of research on Floquet engineering and many theoretical proposals have already been experimentally realized [38]. Besides the above-mentioned renormalization of hopping rates [100], artificial gauge fields [95, 96] and a basic Z_2 lattice gauge model [8] have been simulated by Floquet engineering. In Chapter 2, I will further modulate the on-site interaction of the Bose-Hubbard model [Eq. (1.43)] and investigate the interaction induced process - the density-assisted tunneling. For special driving profiles, this process constrains the dynamics notably and results in QMBS.

1.5 Quasi-Periodically Driven Systems

By now I have discussed non-ergodic systems exhibiting either non-thermal or slowly thermalizing dynamics caused by a static quench or Floquet driving. Hamiltonians in both situations possess TTS, thus both the eigenstates and eigenvalues of either the time-independent Hamiltonians or Floquet operators are well-defined. Based on ETH, properties of these eigenstates provide useful information to infer whether the quantum system thermalizes, and if so, how they approach thermal equilibrium.

However, there are many other ways for taking a quantum system out-of-equilibrium which are yet to be fully explored, for instance, by applying driving fields following quasi-periodic (or aperiodic) sequences. Quasi-periodic drives (QPD) are deterministic and structured in time whereas TTS is absent, hence, such setups interpolate between perfectly periodic and purely random protocols. As those systems are not restricted by TTS, it is expected that they can give us more flexibility and controllability to engineer exotic physical processes or new non-equilibrium phases of matter [104–106]. On the other hand, the absence of TTS also implies that Floquet theory fundamentally does not work which makes both the numerical simulations and analytical investigations of these non-equilibrium phenomena very difficult.

Although there is not yet a well-established universal theoretical framework for studying aperiodically driven systems, interesting properties have been proposed for special types of drivings. I will first briefly review the up-to-date findings in the following section and later introduce my new discoveries of non-equilibrium phases of matter and prethermalization in aperiodically driven systems in Chapters 4 and 5.

1.5.1 Continuous Driving

There are two commonly used approaches to achieve a quasi-periodic driving, either in a continuous or a discrete manner. I first consider the Hamiltonian of a continuous QPD system with a finite number of driving frequencies defined via a Fourier expansion [107–109]

$$\hat{H}(t) = \sum_{\vec{n}} \hat{H}_{\vec{n}} e^{i\vec{n}\cdot\vec{\theta}_t}, \tag{1.48}$$

with $\vec{n} = (n_1, n_2, n_3, \dots) \subseteq \mathbb{Z}^N$ and $\theta_{t,i} = \omega_i t$. The system is QPD if all or a subset of the N frequencies ω_i are incommensurate, i.e. their mutual ratios are irrational. Indeed, investigations of QPD systems actually started decades ago focusing on simple two level systems. For instance in Ref. [110], it was shown that even a two-level system driven by two incommensurate frequencies can exhibit quantum chaos.

Recently there is a resurgence of interest in studying such QPD systems and an elegant generalization of Floquet theory facilitates the investigation. There, the system is transformed into a higher-dimensional synthetic Floquet lattice where the time-dependent QPD Hamiltonian now becomes static. The dimension of the Floquet lattice equals the incommensurate quasi-periodic tones [108, 111]. For some special

QPD protocols, one can then treat the spatial and synthetic dimensions on equal footing, which has been further applied to realize higher dimensional topological phases in QPD low-dimensional systems [112, 113].

Although the idea of a Floquet lattice is in principle valid for any QPD system with a finite number of incommensurate tones, simulations of the dynamics quickly become unfeasible for interacting many-body systems. Indeed, most of the recent findings [112–115] are mainly focusing on two-level systems or one dimensional tight-binding models.

Compared with Floquet systems, many-body QPD systems are also expected to suffer from a more drastic heating issue. To see this, let us consider a bichromatic driving with incommensurate frequencies ω_1 and ω_2. A generic many-body system can absorb the amount of energy $\Delta E = |n_1\omega_1 \pm n_2\omega_2|$ for an arbitrary integer photon number $n_{1/2}$ via multi-photon events. It has been shown that ΔE can be arbitrarily small if the photon number is sufficiently large [104]. Such a property makes QPD systems manifestly different from Floquet systems where ΔE is strictly bounded from below. Therefore, simply increasing the driving frequency does not necessarily suppress heating as it can still happen via multi-photon events instead of many-body resonances which is the main reason for Floquet heating as introduced in Sec. 1.4.2. It is thus expected that heating in generic QPD many-body systems is inevitable and, non-equilibrium phases like MBL cannot be stable for an infinitely long lifetime. Very recently, it has been proposed that heating can still be controlled by suppressing the probability of multi-photon events [104]. Consequently a transient but long-lived prethermal regime can appear if the QPD protocols satisfy some restrictive conditions [104].

Despite the lack of a generic framework to investigate QPD systems, in Chapter 4, I will show a specific example, e.g. the Floquet time spiral (FTS), which can be mapped to Floquet system via a time-dependent unitary transformation. Hence, a FTS can be efficiently treatable within the known Floquet framework. A QPD two-level system is first studied as a pedagogical example, followed by a generalization to a disordered many-body system. It further leads to the discovery of a new non-equilibrium phase of matter, the discrete time quasi-crystal, which remains stable even when the equivalence to its Floquet counterpart is absent.

1.5.2 Discrete Driving

Another approach to induce quasi-periodic driving is by stepwise protocols following aperiodic sequences generated by recursive relations [116–119]. For instance, the aperiodic Thue-Morse sequence involving an infinite sequence of $s_i = \pm 1$ can be obtained as follows: One first starts from the element $s_1 = -1$, then sequentially appends a sequence containing all elements in the previously obtained sequence but with the opposite sign, e.g. $s_1, s_2 = -1, -(s_1) = -1, +1$. One can repeat this procedure and get the following sequence recursively

$$\begin{aligned}
&s_1, s_2, s_3, s_4 = -1, +1, +1, -1, \\
&s_1, \ldots\ldots, s_8 = -1, +1, +1, -1, +1, -1, -1, +1, \\
&s_1, \ldots\ldots, s_{16} = -1, +1, +1, -1, +1, -1, -1, +1, +1, -1, -1, +1, -1, +1, +1, -1.
\end{aligned} \tag{1.49}$$

To perform the corresponding driving protocol, one can define two operators U_+ and U_- and apply them to an initial state according to the sequence above. Compared to the continuous quasi-periodic functions [Eq. (1.48)] whose Fourier decomposition is a simple collection of delta functions, these aperiodic sequences can have a more complicated and perhaps continuous frequency spectrum [120]. A large number of frequency components also implies that the above-mentioned Floquet lattice has an infinite dimension, thus cannot provide useful insights for the understanding of the resulting dynamics.

The recursive relation used for the generation of Eq. 1.49 indeed permits us to efficiently simulate the time evolution of a quantum system [117]. Starting by defining the matrices

$$U_0 = U_+, \; \tilde{U}_0 = U_-, \tag{1.50}$$

one can construct the time evolution operator U_n after exactly 2^n drives recursively as

$$U_n = \tilde{U}_{n-1} U_{n-1}, \quad \tilde{U}_n = U_{n-1} \tilde{U}_{n-1}, \tag{1.51}$$

with an integer n. For instance, after 2 steps, the time evolution operator is $U_1 =$

$\tilde{U}_0 U_0$, and after 4 steps, $U_2 = \tilde{U}_1 U_1 = U_0 \tilde{U}_0 \tilde{U}_0 U_0$. It is worth noting that only a linearly increasing number $\mathcal{O}(n)$ of matrix multiplication is needed to simulate exponentially long times $\mathcal{O}(2^n)$. Similar ideas have been employed to analyze the slow relaxation or non-thermal behavior in some integrable or MBL systems subject to aperiodic drives [105, 117–119, 121].

In Chapter 5, I propose a family of discrete driving protocols, the nth order random multipolar driving (RMD), to further investigate the effect of the quasi-periodicity in heating suppression for generic non-integrable systems. For $n \to \infty$, $n-$RMD corresponds to the quasi-periodic Thue-Morse driving. The non-negative integer n quantifies the temporal correlation in the protocol which leads to a polynomially suppressed low frequency spectrum. For $n \geq 1$, prethermalization appears and its lifetime follows a surprisingly simple algebraic scaling versus the driving rate with exponent $2n+1$. A simple theory based on Fermi's golden rule is sufficient to explain this behavior. In spite of its eventual heat death, I will demonstrate that the time crystalline behavior can exist even the driving protocol does not have TTS.

Chapter 2

Floquet Engineering of Quantum Many-body Scars

QMBS have been recently discovered as a novel mechanism to weakly break ergodicity. These special eigenstates violate ETH and have sub-extensive entanglement whereas most of other eigenstates are thermal. Any initial state with a dominant overlap with QMBS exhibits non-thermal coherent oscillations and low entanglement generation. By now, QMBS have been identified in several theoretical proposals, mostly in spin models [75–78, 122–130] and fermionic models [88, 131]. One common feature of these models is the finite local Hilbert space dimension. A crucial question I want to address is whether QMBS can also occur in experimentally realizable settings with bosons.

In this Chapter, by periodically modulating the on-site energy and interaction, I propose an experimentally feasible driving protocol to engineer the density-assisted tunneling for bosonic atoms trapped in an optical lattice. As shown in Sec. 2.1 and Sec. 2.2, this tunneling process appears as a dominant effective process of the modulated BHM for high frequency drivings. Hence, the rate for a particle to tunnel depends on the number of particles on its local site and neighboring sites. By tuning the driving amplitudes and frequencies, these hopping rates also change accordingly. I find the optimal driving parameters such that some tunneling channels are suppressed to zero between Fock states that are connected without the driving. Consequently, HSF happens for the effective model even though the local Hilbert space for bosons can be infinitely large. In Sec. 2.3, I confirm the appearance of QMBS in the rapid driving regime by analyzing the properties of the Floquet operator. In Sec. 2.4, I further demonstrate that QMBS can be experimentally probed by preparing selected initial states and detecting the long-lived coherent oscillations. Later in Sec. 2.5, I compare these coherent oscillations with Bloch oscillations that can appear without the need of driving. Finally, potential experimental realizations and open questions will be discussed.

2.1 Bose-Hubbard Model with Doubly Modulation

Let me focus on a system of spinless bosons occupying the lowest band in the 1D optical lattice described by the BHM,

$$\hat{H}(t) = \sum_{\langle pq \rangle} \hat{c}_p^\dagger J_{pq} \hat{c}_q + \frac{U(t)}{2} \sum_p \hat{n}_p(\hat{n}_p - 1) + F(t) \sum_p \epsilon_p \hat{n}_p \, , \tag{2.1}$$

$\epsilon_p = -p$ represents the tilt potential, $F(t)$ is the shaking amplitude, $U(t)$ is the amplitude of the on-site interaction, and $J_{pq} = -J$ is the bare tunneling rate between adjacent sites. The same model with a static on-site interaction has been discussed in Sec. 1.4.3 where the hopping rates can be dynamically suppressed by tuning the shaking profile $F(t)$. Here, I also periodically drive the on-site interaction $U(t)$ and its time dependence can be experimentally achieved via modulating the magnetic field which induces a Feshbach resonance [99, 132].

Let me now show that this driving can lead to density-assisted tunneling which does not exist in the bare Hamiltonian. For a suitably chosen set of driving parameters, such tunneling processes can effectively introduce kinetic constraints to the system, hence, breaking the ergodicity of the dynamics. A monochromatically varying on-site interaction $U(t) = U_d \cos(\omega t)$ and a bichromatic shaking $F(t) = F_2 \cos(2\omega t) + F_4 \cos(4\omega t)$ are sufficient for my purpose. In the following, I introduce the dimensionless quantities $\tilde{U}_d = U_d/\omega$, $\tilde{F}_2 = F_2/2\omega$ and $\tilde{F}_4 = F_4/4\omega$ for simplification.

2.2 Floquet Engineering of Density-Assisted Tunneling

Following the discussion in Sec. 1.4.3, I employ a strong driving in both the interaction and the shaking to dramatically modify the dynamics, namely $\tilde{U}_d, \tilde{F}_2$ and $\tilde{F}_4$ are not necessarily small. Therefore, I first need to perform a time-dependent unitary transformation, such that in the rotating frame, the strong driving amplitude does not contribute to the amplitude of the Hamiltonian. For the model in Eq. 2.1, I consider a unitary transformation which has been previously used in Refs. [133, 134]

$$R(t) = \exp\left[i\left(\sum_p \theta_p(t)\hat{n}_p + \frac{\Gamma(t)}{2}\sum_p \hat{n}_p\left(\hat{n}_p - 1\right)\right)\right], \tag{2.2}$$

where $\Gamma(t) = \int_0^t d\tau U(\tau)$ and $\theta_p(t) = \epsilon_p \int_0^t d\tau F(\tau)$. The Hamiltonian $\tilde{H}(t) = R\hat{H}(t)R^\dagger - iR\dot{R}^\dagger$ in the rotating frame reduces to

$$\tilde{H}(t) = \sum_{\langle pq\rangle} \hat{c}_p^\dagger \hat{A}_{pq}(t)\hat{c}_q, \tag{2.3}$$

where the hopping term modifies to

$$\hat{A}_{pq}(t) = J_{pq} e^{i(\theta_p(t)-\theta_q(t))} e^{i\Gamma(t)(\hat{n}_p - \hat{n}_q)}. \tag{2.4}$$

The detailed derivation is illustrated in the Appendix. A. The fact that strong driving amplitudes now only contribute to the time-dependent phase factor permits us to derive an effective Hamiltonian to approximate the dynamics. Importantly, modulation of the interaction leads to a phases which depends on particle number $\hat{n}_p$. The lowest order contribution to the high-frequency expansion (Eq. (1.23)) is the time average $\hat{H}^0_{\text{eff}} = \frac{1}{T}\int_0^T dt\tilde{H}(t)$, which reduces to the so-called density assisted tunneling [133]

$$\hat{H}^0_{\text{eff}} = \sum_{pq} \hat{c}_p^\dagger \hat{A}^0_{pq}(\hat{n}_p, \hat{n}_q)\hat{c}_q. \tag{2.5}$$

The hopping process now depends on the occupation number, which is contained in the operator

$$\hat{A}^0_{pq}(\hat{n}_p, \hat{n}_q) = -J\mathcal{J}_0\Big(\tilde{U}_d(\hat{n}_p - \hat{n}_q), \tilde{F}_2(p-q), \tilde{F}_4(p-q)\Big), \tag{2.6}$$

in terms of the zeroth order three-dimensional Bessel function $\mathcal{J}_0$, see details in Appendix. A. The existence of the term $\hat{n}_p - \hat{n}_q$ in the operator $\hat{A}^0_{pq}$ suggests that the hopping rates explicitly depend on the occupation number difference of specific initial and final states. More concretely, I consider the one-dimensional Fock state

$|\psi_i\rangle = |n_1 \dots n_N\rangle$ as initial state and obtain

$$\hat{c}_p^\dagger \hat{A}^0_{p,p+1} \hat{c}_{p+1} |\psi_i\rangle = h^L_{n_p,n_{p+1}} \hat{c}_p^\dagger \hat{c}_{p+1} |\psi_i\rangle \ , \tag{2.7}$$

where the prefactor is in the form of the Bessel function

$$h^L_{n_p,n_{p+1}} = -J\mathcal{J}_0(\tilde{U}_d(-n_p + n_{p+1} - 1), \tilde{F}_2, \tilde{F}_4) \ . \tag{2.8}$$

It can be regarded as the tunneling rate for a particle to transit from site $p+1$ to p, or in order words, to the left. Similarly for a particle to tunnel to the right from site p to $p+1$, the rate reads

$$h^R_{n_p,n_{p+1}} = -J\mathcal{J}_0(\tilde{U}_d(-n_p + n_{p+1} + 1), \tilde{F}_2, \tilde{F}_4) \ , \tag{2.9}$$

and explicitly depends on the occupation number difference on neighboring sites. Here I will mainly focus on systems with a low particle density because they are experimentally most relevant and can be sufficiently simulated via exact diagonalization. More interesting features can appear at a larger filling which will be further explored in the future. At a low filling, the following rates for different hopping channels become particularly relevant

$$\begin{aligned}
h^L_{(0,1)} = h^R_{(1,0)} = h^R_{(2,1)} = h^L_{(1,2)} &= -J\mathcal{J}_0(0, \tilde{F}_2, \tilde{F}_4) \ , \\
h^{L/R}_{(1,1)} = h^R_{(2,0)} = h^L_{(0,2)} &= -J\mathcal{J}_0(\tilde{U}_d, \tilde{F}_2, \tilde{F}_4) \ , \\
h^L_{(2,1)} = h^R_{(1,2)} = h^L_{(0,3)} = h^R_{(3,0)} &= -J\mathcal{J}_0(2\tilde{U}_d, \tilde{F}_2, \tilde{F}_4) \ ,
\end{aligned} \tag{2.10}$$

which are crucial for the formation of Hilbert space fragmentation and QMBS.

2.2.1 Hilbert Space Fragmentation

Specific choices of the hopping rates in Eq. (2.10) can result in different connectivity of the Hilbert space. To understand how Hilbert space fragmentation happens, I start from the following insightful example of three lattice sites with periodic boundary condition as illustrated in Fig. 2.1. Fock states are connected via solid and dashed lines, which represents different hopping channels, and processes that occur with the

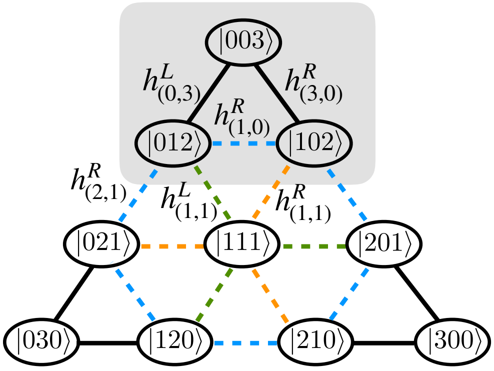

FIGURE 2.1: Fragments for a system of 3 sites. Connections are assigned with hopping rates. If all dashed ones are forbidden for conditions in Eq. (2.11), four blocks of states appear. For clarity one of these is shadowed in gray.

same rate are depicted with the same color.

Suppose that the all rates of processes depicted with dashed line are suppressed to zero, the Hilbert space is being separated into four fragments – one involving three states $|012\rangle$, $|102\rangle$, $|003\rangle$, two blocks containing their cyclic permutations, and the one-dimensional fragment $|111\rangle$. Such fragmentation happens if hopping channels specified in Eq. (2.10) fulfill the conditions

$$h^R_{(2,0)} = h^L_{(0,2)} = h^{L/R}_{(1,1)} = 0 \ , \ h^L_{(1,2)} = h^R_{(2,1)} = 0 \ . \tag{2.11}$$

In practice, these rates do not need to vanish exactly. Notable deviation from ETH as a signature of ergodicity breaking can also be observed when small but finite values of these hopping rates are present, which can be thought of as *leaking channels*.

Fragmentation also arises in large systems of any number of sites and filling factor via combing elementary building blocks of few sites. The simplest ones for unit filling would be the Mott state $|111\dots1\rangle$ as well as the density wave state $|2020\dots20\rangle$, which are generated from the building block $|1\rangle$ and $|20\rangle$ respectively. Since no dynamics are permitted for these two states, they are also the eigenstates of the effective Hamiltonian.

I am more interested in building blocks where dynamics are allowed. One example containing the Fock states $|n_1n_2n_3n_4n_5n_6\rangle$ for a system of six sites at unit-filling is illustrated in Fig. 2.2, where the dashed line connects the mirror symmetric states. Notice that the n_2 and n_5 always has a particle number smaller than or equal to 2, hence according to the condition in Eq. (2.11), no particle is permitted to move to

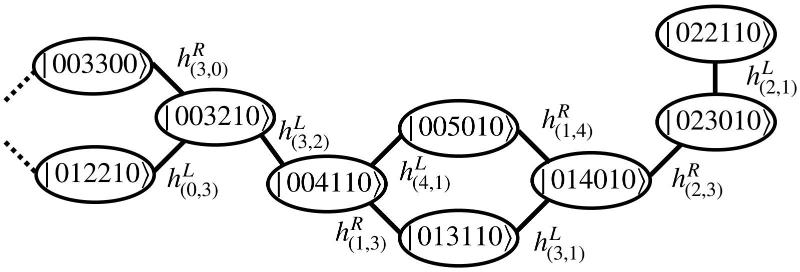

FIGURE 2.2: Fragments for a system of 6 sites where both ends are empty. Connections are assigned with hopping rates and doted lines connect mirror symmetric states.

the boundary sites. Therefore, starting from any initial state within this fragment, the vanishing occupation on sites 1 and 6 is conserved throughout time evolution. Additionally, a product form of such 6-site states also retains, simply because no particles can hop across different blocks. As such, it generates a fragment which has a much smaller dimension than the total Hilbert space. This product form also implies that only area-law entanglement can be established as a typical behavior of QMBS. There are many other building blocks resulting in a substantial number of QMBS in large systems.

2.2.2 Optimal Control

To achieve the Hilbert space fragmentation experimentally, the driving parameters need to be chosen such that

$$\mathcal{J}_0(\tilde{U}_d, \tilde{F}_2, \tilde{F}_4) = 0 \ , \quad \mathcal{J}_0(0, \tilde{F}_2, \tilde{F}_4) = 0 \ , \tag{2.12}$$

to satisfy the conditions given in Eq. (2.11).

In general, according to Eq. (2.10), a large ratio of U_d/ω is needed for a notable difference between hopping rates with different occupation numbers. For concreteness, from now on I fix the parameters $U_d/J = 12$, $\omega/J = 6$. I will use the ratio between dominant leaking rates and the leading hopping rate within the fragment

$$r = \frac{|h^L_{(0,1)}| + |h^L_{1,1}|}{|h^L_{(2,1)}|},$$

to measure how well the fragmented subspace can be disconnected with others. Physically, it serves as a suitable quantity to indicate the existence of long-lived coherent

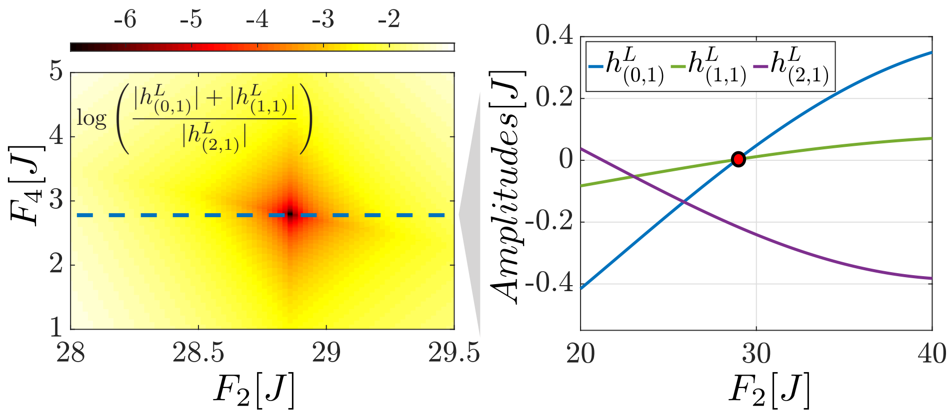

FIGURE 2.3: Left: Figure of merit for the appearance of quantum many-body scars given by the ratio (log scale) of leaking and hopping channels for a Hilbert space fragment. The red region labels the best parameter space with ratios lower than 10^{-4}. Right: Hopping rate as a function of F_2. Two leaking channels cross zero at the same time.

oscillations because its inverse indicates the time scale for the leaking effects to become notable. In the left panel of Fig. 2.3, I plot the ratio r as a function of the shaking amplitude F_2, F_4 . A sweet spot in black can be identified around $(28.8, 2.8)$ with the ratio $r < 10^{-6}$. The right panel illustrates the rates for a fixed shaking amplitude $F_4 = 2.8J$, where two leaking rates cross zero at the same point. As such these two leaking channels can be suppressed to strictly zero where perfect fragmented subspaces appear.

So far our discussion focus on the conditions for fragmentation of the Hilbert space of the effective Hamiltonian $\hat{H}^0_{\text{eff}}$, which significantly modifies the stroboscopic dynamics for rapid driving, but higher order processes of magnitude $O(1/\omega)$ will play an increasing role for smaller frequencies. Therefore, leaking channels will inevitably exist for any finite frequency and the transition to an ergodic system without scars is expected. In the following, I use exact diagonalization implemented via the Quspin package [135] to analyse higher order effects through the spectrum of the Floquet operator, $\hat{U}(T) = \mathcal{T}\int_0^T \exp\left(-i\hat{H}(t)dt\right)$. The ratio between the driving amplitude U_d, F_2, F_4 and frequency ω is fixed to the optimal point determined in this section.

2.3 ETH Violation in Spectrum

Unlike the smooth dependence of expectation values of local observables versus eigenenergies for ETH-obeying eigenstates as reviewed in Sec. 1.2.1, QMBS typically lead to

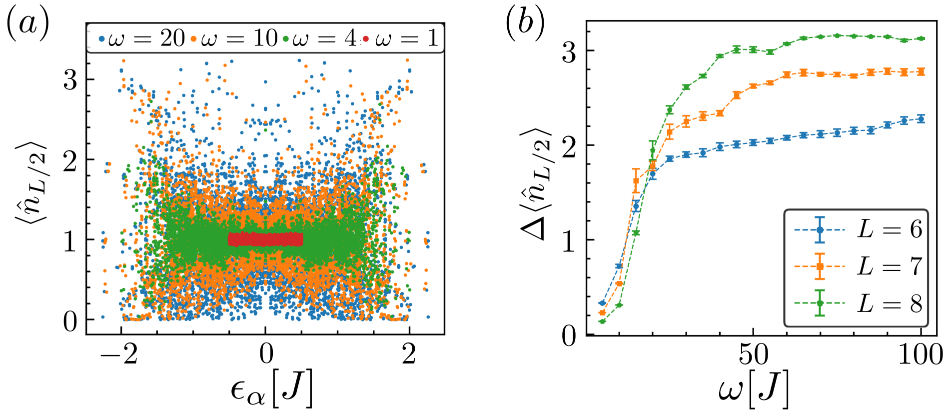

FIGURE 2.4: Violation of ETH as a function of driving frequency in units of J. (a) Expectation value of the local particle number operator, with respect to eigenstates of the Floquet operator as function of the quasienergy for system size $L = 8$. (b) Width of the distribution of $\langle \hat{n}_{L/2} \rangle$ as a function of frequency for different system sizes .

very different values even for states close in energy. Fig. 2.4 (a) illustrate the expectation value of the local particle number $\langle \hat{n}_{L/2} \rangle$ for eigenstates of the Floquet operator versus quasienergy ϵ_α. For slow driving (red), the local particle number is close to one for all values of quasienergy. As a comparison, for faster driving (blue), the local expectation fluctuates notably from one eigenstate to the next. The range of the quasienergies also indicates the formation of scared states in fast driving regime: the full interval $[-\omega/2, \omega/2)$ is occupied outside the fast driving regime ($\omega/J = 1$), whereas the occupied interval hardly increases with larger ω for $\omega/J \geq 4$.

The width of the distribution of local particle numbers can be characterized via the difference between the largest and smallest values. Fig. 2.4 (b) depicts the width $\Delta\langle \hat{n}_{L/2} \rangle = \langle \hat{n}_{L/2} \rangle_{\max} - \langle \hat{n}_{L/2} \rangle_{\min}$, where $\langle \hat{n}_{L/2} \rangle_{\max/\min}$ is the average over the 20 largest/lowest local particle numbers. The error bars are estimated from the variances of these averages. The dependence of $\Delta\langle \hat{n}_{L/2} \rangle$ on the driving frequency ω shows a well-pronounced increase suggesting the formation of scared states on the transition to the high-frequency regime.

After confirming the existence of scared eigenstates in the spectrum, I will concentrate on the crucial question: how to experimentally realize and detect them from the dynamics?

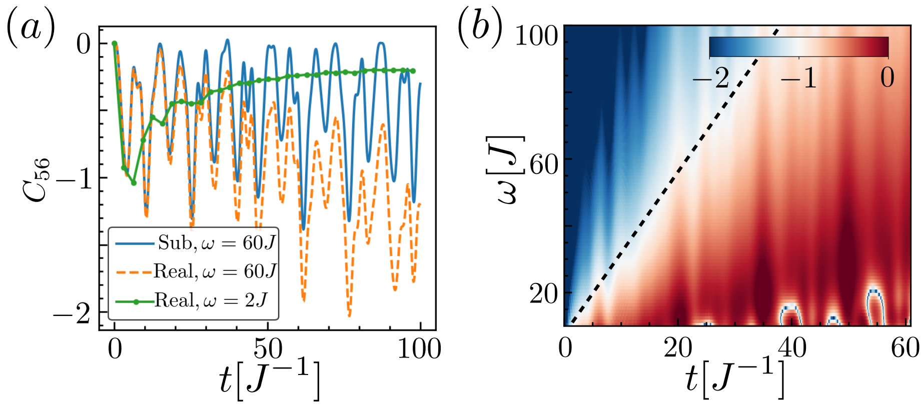

FIGURE 2.5: (a) Dynamics of correlation function for optimal driving parameters. Coherent oscillation with fast driving (orange) can be well approximated via subsystem dynamics (blue), suggesting the existence of scared states. As a comparison, correlation rapidly saturates in the ergodic case with $\omega = 2J$ where higher order effects induce deleterious leaking. (b) Deviation between real dynamics and subspace approximation $\log_{10}(R(t))$ [Eq. (2.13)] for different driving frequencies. Some blue spots appear within the red region at longer times because of the accidental similarity between $C_{\text{real}}(t)$ and $C_{\text{sub}}(t)$.

2.4 Coherent Oscillation

For the optimal driving parameters and in the high-frequency limit, a properly selected initial state can always remain within a perfectly isolated subspace. If the subspace has a small enough dimension such that ETH does not apply, persistent oscillations will appear and the system does not thermalize. For a finite but sufficiently large driving frequency, the leaking rates will be non-zero but can be tuned to be much smaller than the tunneling rates within the subspace. In this case, coherent oscillation will persist for a finite but long lifetime with an overall damping before the eventual thermalization.

Many initial states can be used to demonstrate the coherent oscillations. For concreteness, I consider the initial Fock state $|1100330011\rangle$ of ten sites with periodic boundary condition and simulate their stroboscopic dynamics. This state is a composition of the Mott state $|1111\rangle$ and a state of six sites $|003300\rangle$ where the oscillating dynamics is permitted on the middle two sites. As shown in Fig. 2.5 (a), I use the two-point correlation function, $C_{56}(t) = \langle \hat{n}_5(t)\hat{n}_6(t)\rangle - \langle \hat{n}_5(t)\rangle\langle \hat{n}_6(t)\rangle$, of the two central sites which exhibits coherent oscillations. The actual system dynamics $C_{\text{real}}(t)$ obtained by the Floquet operator are depicted in orange and compared to the dynamics $C_{\text{sub}}(t)$ generated by the subsystem Hamiltonian where all leaking channels are suppressed to zero. For slow driving (green), driving induced higher order effects are notable even at early times, hence, the dynamics is ergodic with the correlation saturating rapidly on a time-scale $t \sim O(1/J)$. Although the deviation between the real dynamics and the effective subsystem dynamics indicates the inevitable leakage, the lifetime of the coherent oscillation still clearly exceeds the time-scale of thermalization $O(1/J)$.

To quantify the lifetime of the coherent oscillations, I define the difference between the two correlation functions

$$R(t) = |C_{\text{real}}(t) - C_{\text{sub}}(t)|, \tag{2.13}$$

comparing the actual dynamics and the effective subsystem dynamics. Fig. 2.5 (b) depicts the difference $R(t)$ in log scale versus time t and driving frequency ω. Clearly, at a fixed driving frequency, in the blue region, the difference remains small for short times with $R(t)$ smaller than 0.1. However, for longer times the deviation notably increases as seen in the red area. As suggested by a dashed black line, the transition between these two areas happens at a time which grows linearly with ω. It further permits us to define the lifetime for QMBS, which thus become increasingly stable by increasing the driving frequency.

2.5 Comparison to Bloch Oscillation

The long-lived coherent oscillation can also appear in the form of Bloch oscillations (BO) as a non-interacting effect. It normally appears after quenching the bosonic gases with a static tilted lattice instead of using periodic driving [136, 137]. Here I discuss several crucial differences between BO and the coherent oscillation induced by QMBS, such that one can experimentally distinguish these two phenomenon.

First, in contrast to BO, coherent oscillation observed in the previous section only happens for properly prepared initial states, *e.g.* Fock states constructed with building blocks of small dimension. The dimension also needs to be larger than one otherwise the Fock state itself becomes an eigenstate such as the Mott state. However, the superfluid state as a counter example, will thermalize very quickly. Moreover, the oscillating frequency of BO is fixed by the tilted potential [136], while for the scared dynamics, it can differ for different initial states.

Second, in the presence of additional density-density interactions (of energy scale U comparable to bare tunneling J), BO are very sensitive to interaction-induced dephasing and instabilities thus decay rapidly [137]. However, this is not true for scar dynamics. The unitary transformation to the rotating frame as defined in Eq. 2.2 commutes with density-density interaction, which can thus be simply introduced to the lowest order effective Hamiltonian (Eq. 2.5) in the same form. Therefore, the density assisted tunneling will not be impacted and resulting fragmented Hilbert space structure remains untouched. Even for a finite driving frequency, our previous work [133] suggested that only negligible ($1/\omega^2$) interaction-induced effects appear, therefore the coherent oscillation will still have a long lifetime for fast driving before thermalization.

Third, the correlation between different building blocks serves as a good measure since no tunnelling is permitted in-between in the effective Hamiltonian. As an example, for the initial state $|1100330011\rangle$, the correlation function $C_{15}(t) = \langle \hat{n}_1(t)\hat{n}_5(t)\rangle - \langle \hat{n}_1(t)\rangle\langle \hat{n}_5(t)\rangle$ remains zero for a sufficiently long time with fast driving. On the contrary, BO will build up such a spatial correlation after a short period.

All these three aspects exploit the many-body character of the density assisted tunneling which does not have a counterpart in non-interacting systems. Importantly, they are experimentally verifiable via local occupation number or two-point correlation functions as discussed in the last section.

2.6 Experimental Realization

The doubly modulated Hubbard system in cold atomic gases and the required initial states can be constructed via existing experimental techniques. The driving can be realized via a periodically modulating external magnetic field in the vicinity of Feshbach resonances [99] and lattice shaking [138]. Indeed, density assisted tunneling has already been successfully realized by Floquet engineering in 2016 [139] but they are not sufficiently fine-tuned to impose kinetic constraints. Therefore, it has been experimentally demonstrated that bosonic systems can be modulated up to 0.2s, corresponding to around 5 tunneling times, which is enough to observe a complete coherent oscillation as seen in Fig. 2.5. During the last years, the tunneling time scale has been significantly increased; for instance, Refs. [9] and [140] show that systems of fermionic cold atoms remain stable with Floquet driving up to 1s, i.e. several hundreds of tunneling times. Even though experimental achievements with fermions do not directly verify feasibility with bosons, these results give good reasons for confidence that the coherent dynamics in my proposal can persist for more than 30 tunneling times in the near future. Such a time scale allows one to show at least five coherent oscillations as in Fig. 2.5 and to explore the more subtle higher-order effects, i.e. the coupling between blocks, by scanning driving frequencies.

An additional, typically harmonic trapping potential will be involved in experiments. However, as it commutes with the driving term in the Hamiltonian [Eq. (2.1)], Hilbert space fragmentation happens in the same manner although the oscillating frequency might change.

The remaining challenge is thus to prepare fine tuned initial states. The easiest states to verify fragmentation and violation of ETH are the Mott insulator state and the density wave state with two particles on every second site. Both of them are eigenstates of the effective Hamiltonian, therefore, they will be frozen for a long time in the high frequency regime until higher order leaking effects become notable. For more interesting cases discussed in Sec. 2.4, one can first prepare Mott states with three bosons per site [141] and then apply the single-spin addressing scheme [142] to remove unwanted particles on selected sites to obtain, for instance $|\ldots 003300003300\ldots\rangle$. Such a state will result in coherent oscillations with an exceptionally long lifetime before reaching the final thermal death.

2.7 Discussion

The proposal permits the experimental realization of QMBS in a bosonic system, enabling the investigation of quantum thermalization and lack thereof in systems unreachable by classical means of numerical simulation. The emergent density-assisted tunnelings by Floquet engineering are realizable independently of the dimensionality and geometry. Therefore, it paves the way for further investigations of different thermalization approaches in higher dimensional systems with different lattice geometries. It is also interesting to explore the topological properties of QMBS in bosonic systems in higher dimensions [143].

The suppression of leaking channels, as well as the density assisted hopping in general, is not limited to realize QMBS. It can also be potentially useful to control Floquet heating as discussed in Secs. 1.2.3 and 1.4.2 which impedes the development of quantum simulation with driven cold atomic gases. Furthermore, the controlability of the hopping channels between selected Fock states also provides new insights for the states preparation. For instance, one can use it for the accurate creation of coherent superposition of multiple Fock states [144] as required *e.g.* for precision sensing.

By now, all of the QMBS discovered are sub-extensively entangled, i.e. the entanglement entropy scales as an area- or subvolume- law. It is also clear that the fragmented Hilbert space considered in Sec. 2.2.1 are spanned by products of building blocks of small finite sizes, hence, cannot host eigenstates with volume-law. In the next chapter, I will construct a minimal model demonstrating QMBS with volume-law entanglement which are still non-thermal and violate ETH.

Chapter 3

Orthogonal Quantum Many-body Scars

QMBS generally exhibit an area-law or sub-volume law entanglement scaling. Such a characteristic low entanglement behavior has also been employed routinely to detect QMBS in the spectrum [82]. In this chapter, I propose a clean non-integrable many-body system exhibiting QMBS with a volume-law entanglement scaling. They lead to the intriguing phenomenon of the coexistence of long-lived coherent oscillations and rapid volume-law entanglement generation after quenching a simple initial state. Such a counter-intuitive behavior has never been proposed because within the ETH (or generalized ETH for integrable systems) paradigm volume-law entanglement of eigenstates normally goes hand-in-hand with ergodic dynamics. Likewise, the fact that persistent oscillations always appear together with an area-law scaling of entanglement has been thought to be governed by a much more fundamental principle of quantum thermalization. This novel phenomenon is also in sharp contrast to non-ergodic MBL systems, where the volume-law entanglement can be generated after a quench but no coherent oscillations persist after averaging over disorder. However, strongly correlated multi-component systems can violate ETH in unexpected ways. Here, I construct a concrete counter-example exhibiting the surprising form of ergodicity-breaking dynamics.

It has been suggested that multi-component systems can evade or slow down thermalization via the inter-component interactions, for instance in the heavy-light particle mixtures [145–147]. There, quenched disorder is not present yet the slow heavy particles in thermal equilibrium effectively generate the disordered background. Light particles can localize on this disordered background for a long time, thus slow down thermalization. Thereafter, quantum disentangled liquids (QDLs) were proposed as an ergodicity-breaking phase of matter [148], where certain d.o.f. exhibit a volume-law while others show an area-law scaling of entanglement. By now, QDL-like behavior has been identified in a number of strongly correlated systems, such as the Hubbard model at half-filling [149], lattice gauge models [150–155] and frustrated quantum magnets [156, 157]. However, none provide the intriguing phenomenon that I want to achieve.

I will present a basic construction of a QDL where infinitely long-lived persistent oscillations and rapid volume-law entanglement generation can coexist. The starting point is the Orthogonal Metal (OM) model which was initially introduced in Ref. [158] as a particularly simple example of a non-Fermi liquid. The original physical d.o.f. of OMs can be decomposed into fractionalized d.o.f. which are decoupled, each carrying fractions of the original quantum numbers. OMs were named *orthogonal* because the physical charge carriers can be insulating despite of the presence of a well defined Fermi sea. In the following, I will first follow Ref. [158] to briefly review the basic solvable OM model in Sec. 3.1. Then I will elaborate how to impose kinetic constraints to the OM for the realization of *orthogonal* QMBS in Sec. 3.2 which leads to the sought-after coexistence of extensive entanglement and persistent oscillations. These oscillations turn out to have a finite but long lifetime in the presence of generic perturbations as verified at the end of this chapter.

3.1 The Orthogonal Metal

I first review the one-dimensional model containing two types of particles as proposed in Ref. [158]:

$$H_{OM} = -\sum_i \left(h\sigma^x_{i-1,i}\sigma^x_{i,i+1}(-1)^{\hat{n}_i} + J\sigma^z_{i,i+1} \right) - t\sum_i \left(c_i^\dagger \sigma^z_{i,i+1} c_{i+1} + \text{H.c.} \right), \quad (3.1)$$

The $c_i^\dagger$ operators create physical spinless fermion d.o.f. at site i and $\hat{n}_i = c_i^\dagger c_i$ denotes the occupation number. Note, the notation $\hat{n}$ is used to distinguish it with the integer number n. The $\sigma_{i,i+1}$ operators represent a spin-$\frac{1}{2}$ background field, and the subscripts

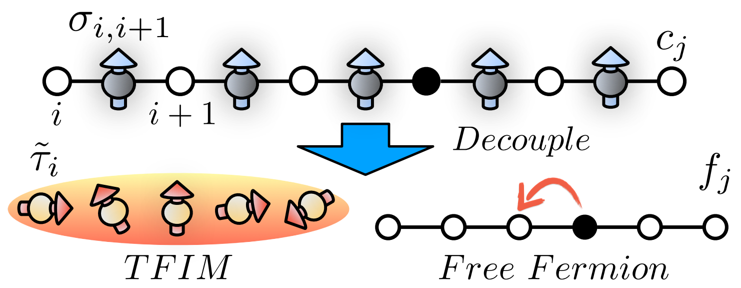

FIGURE 3.1: Schematic picture of the multi-component model, with $\sigma-$spins positioned on the bonds between $c-$fermions. Occupied fermionic site is represented by the filled black circle. This model can be decomposed into mutually commuting dual $\tilde{\tau}-$spins and $f-$fermion. Dynamics in each sector is described by the transverse field Ising model (TFIM) and the free fermion Hamiltonian respectively.

$\{i, i+1\}$ indicates that these spin d.o.f. are positioned on the links between site i and $i+1$ of a one dimensional lattice as sketched in Fig. 3.1. Unlike models with a single component of particles, here I also have inter-component interactions, for instance the first term $\sigma^x_{i-1,i}\sigma^x_{i,i+1}(-1)^{\hat{n}_i}$ where the coupling rate between adjacent spins has an explicit dependence on the parity of the middle fermionic site. Similarly, the hopping processes of $c-$fermions also couple to the background spin via $c^\dagger_i\sigma^z_{i,i+1}c_{i+1}$.

3.1.1 Duality Mapping of the Hamiltonian

Although the original d.o.f. are strongly coupled, as illustrated in Fig. 3.1, here I demonstrate explicitly how the different sectors emerge to simplify the model. First, a duality transformation [159, 160] maps the link-spins σ to a site-spin τ as

$$\tau^z_i = \sigma^x_{i-1,i}\sigma^x_{i,i+1},\ \tau^x_i\tau^x_{i+1} = \sigma^z_{i,i+1}, \tag{3.2}$$

such that the Hamiltonian reduces to

$$H = -\sum_i \left(J\tau^x_i\tau^x_{i+1} + h\tau^z_i(-1)^{\hat{n}_i}\right) - t\sum_i \left(c^\dagger_i\tau^x_i\tau^x_{i+1}c_{i+1} + \text{H.c.}\right). \tag{3.3}$$

Next, I introduce new d.o.f. for fermions $f_i = \tau^x_i c_i$ and dual spins

$$\tilde{\tau}^z_i = \tau^z_i(-1)^{f^\dagger_i f_i},\quad \tilde{\tau}^x_i = \tau^x_i. \tag{3.4}$$

Note, both of them are compositions of the physical spins and fermions. Finally, in the new variables the Hamiltonian separates into two components $H = H_{\tilde{\tau}} + H_f$

$$H_{\tilde{\tau}} = -\sum_i J\tilde{\tau}_i^x\tilde{\tau}_{i+1}^x + h\tilde{\tau}_i^z, \quad H_f = -t\sum_i f_i^\dagger f_{i+1} + \text{H.c.}\ . \tag{3.5}$$

Most importantly, these two fractionalized d.o.f. commute with each other as $[\tilde{\tau}_i^\alpha, f_i^{(\dagger)}] = 0$ for $\alpha = x, y, z$, thus, the original model is now completely decoupled. This separability can remain in the presence of certain types of interactions, for instance, the density-density interaction between fermions can be introduced without influencing the $\tilde{\tau}$ d.o.f. However, I will first focus on the simplest model which already provides useful physical insights before involving more complicated interaction.

It is worth noting that the $\tilde{\tau}-$spin is now described by the transverse field Ising Hamiltonian [161] meanwhile the fermionic sector becomes a simple free-fermion model. This is in sharp contrast to some other models hosting emergent d.o.f, e.g. the Kiteav honeycomb model [162] or lattice gauge models demonstrating disorder-free localization [150] where the gauge d.o.f. is static. Both sectors are exactly solvable and the $f-$fermion is clearly in a metallic phase and conducting [163]. For the $\tilde{\tau}-$spin, one can perform the well-known Jordan-Wigner transformations [164] to analyze the ground state phase transition between the ordered (anti-)ferromagnetic with $\langle\tilde{\tau}_i^x\rangle \neq 0$ to disordered paramagnetic phase with $\langle\tilde{\tau}_i^x\rangle = 0$ by tuning the ratio J/h, as well as their non-equilibrium properties induced by a quench [165] or periodic drivings [166]. To bridge the gap between these solvable properties of the emergent components and the physically detectable phenomenon, I further illustrate the transformations of initial states and observables in different representations.

3.1.2 Transformation of Observables

Dynamics of the physical variables is a combination of these separate sectors [158]. For instance, consider simple product states as initial states, the physical correlation function and magnetization for the background $\sigma-$spin can be obtained according to Eqs. (3.2) and (3.4) as

$$\langle\sigma_{i-1,i}^x\sigma_{i,i+1}^x\rangle = \langle\tilde{\tau}_i^z\rangle(1 - 2\langle n_i\rangle), \quad \langle\sigma_{i,i+1}^z\rangle = \langle\tilde{\tau}_i^x\tilde{\tau}_{i+1}^x\rangle. \tag{3.6}$$

Similarly, the correlation function of the physical $c-$fermions is a product of correlation functions of the two emergent sectors

$$\langle c_i^\dagger c_j \rangle = \langle f_i^\dagger f_j \rangle \langle \tilde{\tau}_i^x \tilde{\tau}_j^x \rangle, \tag{3.7}$$

where I use $c_i = \tilde{\tau}_i^x f_i$. The $f-$fermions are governed by the free theory as in Eq. (3.5), therefore, they are obviously in a metallic phase with a power law decaying correlation $\langle f_i^\dagger f_j \rangle$. However, the correlation function $\langle c_i^\dagger c_j \rangle$ of the physical charge carrier $c-$fermions can vanish which strongly depends on the $\tilde{\tau}-$spins. In the ordered phase of $\tilde{\tau}$ where $\langle \tilde{\tau}_i^x \tilde{\tau}_j^x \rangle \neq 0$, $f-$fermions have a non-zero overlap with the physical fermions, hence the groundstate of which is also conducting and corresponds to a Fermi liquid. In contrast, in the disordered phase with $\langle \tilde{\tau}_i^x \tilde{\tau}_j^x \rangle$ vanishing exponentially in distance $|i-j|$, $f-$ and $c-$fermions are orthogonal to each other, thus, the system enters the so-called orthogonal metal as a simple non-Fermi liquid. Its transition to the Fermi liquid phase is determined by the Ising transition of $\tilde{\tau}$. More discussion regarding OMs and non-Fermi liquid can be found in Refs. [158, 167].

Lastly, as a special case, by setting $i = j$, the local density for $c-$ and $f-$ fermions are identical as $(\tilde{\tau}_i^x)^2 = 1$.

3.1.3 Transformation of States

I will mainly consider the initial state in the product form $|0\rangle = |\psi\rangle_c \otimes |S\rangle_\sigma$ with periodic boundary condition, where $|S\rangle_\sigma$ denotes the state for $\sigma-$spin and $|\psi\rangle_c$ represents the fermionic Fock state as $|\psi\rangle_c = c_i^\dagger c_j^\dagger c_k^\dagger \dots |0\rangle$, which takes the same form in the new fermionic basis as $f_i^\dagger f_i = c_i^\dagger c_i$.

Global constraint In order to identify the transformation between two spin d.o.f., it is crucial to realize the global constraint imposed by the duality transformation in Eq. (3.2)

$$\prod_i \tau_i^z = \prod_i \sigma_{i-1,i}^x \sigma_{i.i+1}^x = \mathbb{1}, \tag{3.8}$$

which trivially works for $\sigma-$spin as the $\sigma_{i,j}^x$ operator on each bond appears twice for system with periodical boundary condition and the product of which automatically gives identity. However, such a constraint becomes non-trivial for $\tau-$spin as well as $\tilde{\tau}-$spin as

$$\prod_i \tau_i^z = \prod_i \tilde{\tau}_i^z (-1)^{f_i^\dagger f_i} = (-1)^{N_f} \prod_i \tilde{\tau}_i^z = \mathbb{1}, \tag{3.9}$$

where $N_f = \sum_i \hat{n}_i$ represents the total fermionic number. Thus, the product of $\tilde{\tau}_i^z$ depends on the fermionic parity as

$$\prod_{\text{all } i} \tilde{\tau}_i^z = (-1)^{N_f}. \tag{3.10}$$

I will consider the spin state polarized in z direction as $|S\rangle_\sigma = |\uparrow\uparrow \ldots \uparrow\rangle_\sigma$. According to the duality transformation [Eq. (3.2)], the definition of dual spin [Eq. (3.4)] and the global constraint [Eq. (3.10)], I derive the set of conditions

$$\tilde{\tau}_i^x \tilde{\tau}_{i+1}^x | \uparrow\uparrow\uparrow \cdots\rangle_\sigma = | \uparrow\uparrow\uparrow \cdots\rangle_\sigma, \quad \prod_{\text{all } i} \tilde{\tau}_i^z | \uparrow\uparrow\uparrow \cdots\rangle_\sigma = (-1)^{N_f} | \uparrow\uparrow\uparrow \cdots\rangle_\sigma. \tag{3.11}$$

The left set of conditions leads to the parameterized state $| \uparrow\uparrow\uparrow \cdots\rangle_\sigma = \alpha| \rightarrow\rightarrow \cdots\rangle_{\tilde{\tau}} + \beta| \leftarrow\leftarrow \cdots\rangle_{\tilde{\tau}}$, and the right set of condition fixes the state up to a global phase as

$$| \uparrow\uparrow\uparrow \cdots\rangle_\sigma = \frac{1}{\sqrt{2}} \left(| \rightarrow\rightarrow \cdots\rangle_{\tilde{\tau}} + (-1)^{N_f} | \leftarrow\leftarrow \cdots\rangle_{\tilde{\tau}}\right). \tag{3.12}$$

In the following discussions, for my purpose, different initial states for $\sigma-$spins yield qualitatively the same results hence I will fix the initial state as $|\uparrow\uparrow \ldots \uparrow\rangle_\sigma$ without loss of generality. On the contrary, the dynamics of the composite system strongly depends on the initial fermionic states as elaborated in detail later.

3.2 Kinetically Constrained Orthogonal Metal

The exactly solvable model becomes non-integrable once generic perturbations are introduced. I would first consider perturbations which breaks the integrability but preserve the separability of the model, therefore, the previous discussion of the transformation of states and operators are still valid. Consequently, in each emergent sector, the state will follow ETH's prediction and thermalize quickly meanwhile generating extensive entanglement, but cannot exhibit any persist oscillations [168, 169].

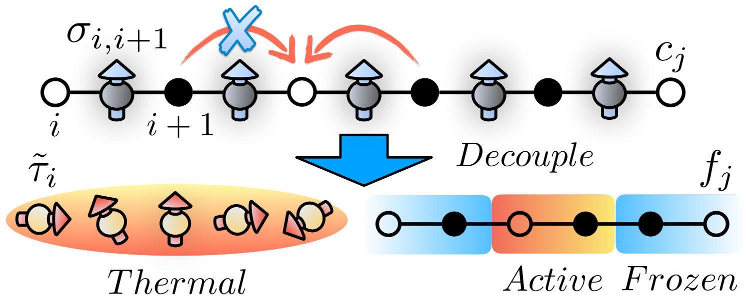

FIGURE 3.2: Schematic picture of the multi-component model with kinetic constraints, with $\sigma-$spins positioned on the bonds between $c-$fermions. Occupied fermionic site is represented by the filled black circle. In the emergent sectors, dynamics is governed by a non-integrable spin Hamiltonian and a kinetically constrained fermionic model respectively. Fermionic dynamics strongly depends on the configuration of initial states, and in the current case dynamics is only permitted on the central two active sites.

To resolve this, I further introduce kinetic constraints to the physical fermions which eventually lead to the coexistence of persistent oscillation and volume-law entanglement.

3.2.1 The Model

Let me introduce density-dependence to the hopping

$$\begin{aligned} H = &-\sum_i \left(h\sigma^x_{i-1,i}\sigma^x_{i,i+1}(-1)^{\hat{n}_i} + g_z\sigma^z_{i,i+1}\sigma^z_{i+1,i+2} + J\sigma^z_{i,i+1}\right) \\ &- t\sum_i \left(\hat{n}_{i-1}c^\dagger_i\sigma^z_{i,i+1}c_{i+1}\hat{n}_{i+2} + \text{H.c.}\right). \end{aligned} \tag{3.13}$$

I also consider the interaction $g_z\sigma^z_{i,i+1}\sigma^z_{i+1,i+2}$ between adjacent spins which preserves the separability of the model but breaks the integrability. This model is sketched in Fig. 3.2.

Using the same mapping employed in the last section, the full Hamiltonian can be decomposed as $H = H_{\tilde{\tau}} + H_f$ where

$$\begin{aligned} H_{\tilde{\tau}} &= -\sum_i \left(J\tilde{\tau}^x_i\tilde{\tau}^x_{i+1} + h\tilde{\tau}^z_i + g_z\tilde{\tau}^x_i\tilde{\tau}^x_{i+2}\right), \\ H_f &= -t\sum_i \left(\hat{n}_{i-1}f^\dagger_i f_{i+1}\hat{n}_{i+2} + \text{H.c.}\right). \end{aligned} \tag{3.14}$$

The newly introduced spin interaction $\sigma^z_{i,i+1}\sigma^z_{i+1,i+2}$ was shown to only enter the $\tilde{\tau}$ d.o.f. via using $\sigma^z_{i,i+1} = \tilde{\tau}^x_i\tilde{\tau}^x_{i+1}$ and break the integrability of TFIM. The hopping process for $f-$fermion now depends on the local fermionic particle number $\hat{n}_i$. This operator has the same form in both $c-$ and $f-$representations as $f_i^\dagger f_i = c_i^\dagger c_i (\tau_i^x)^2 = c_i^\dagger c_i$.

3.2.2 Hilbert Space Fragmentation in Fermionic Sector

The density-dependent hopping processes in H_f significantly restrict the dynamics of f-fermions, i.e. hopping is only permitted when two sites are both surrounded by occupied ones. For example, applying one term of H_f on the Fock state $|\psi\rangle_f = |n_1, \dots, n_N\rangle_f$, one obtains

$$-t\hat{n}_{i-1} f_i^\dagger f_{i+1} \hat{n}_{i+2} |\psi\rangle = -t n_{i-1} n_{i+2} f_i^\dagger f_{i+1} |n_1, \dots, n_N\rangle_f \,, \tag{3.15}$$

which gives non-zero value only when the sites $i-1, i+2$ are both filled. More concretely, I consider the Fock state of six fermionic sites $|010110\rangle_f$ with periodic boundary condition as depicted in Fig. 3.2. The middle two sites are active where hopping is permitted

$$H_f^2 |010110\rangle_f = -H_f t |011010\rangle_f = t^2 |010110\rangle_f \ . \tag{3.16}$$

Other sites are frozen and the two ends always remain empty since particle on site 2 or 5 is forbidden to move due to the density-dependence in the hopping. As such, I obtain a fragmented Hilbert space of dimension 2. Following the ideas developed in Sec. 2.2.1, one can treat this state as an elementary building block to construct states of large sizes, e.g. the product of the same state $\dots |010110\rangle_f \otimes |010110\rangle_f \dots$ at a finite fermion density. As there is no hopping events permitted between different blocks, the tensor product form is retained during time evolution. The dimension of the reduced subspace, $2^{L/6}$ for a chain of length L which is a multiple of 6, becomes substantially smaller than the total Hilbert space [80, 170]. Therefore, quenching this initial state by the constrained model H_f only results in dynamics in a small isolated subspace, where persistent oscillations appear[1]. As discussed in Sec. 3.1.2, the local density for $c-$ and $f-$ fermions are identical thus the movement for the physical fermion is also highly restricted. On the contrary, for a non-vanishing g_z, the spin Hamiltonian $H_{\tilde{\tau}}$

[1] In Appendix B, I show that for properly chosen initial states, the dynamics still persist in the presence of fermionic density-density interaction. I also give one example with non-integrable fermionic subspaces where the fermionic dynamics rapidly thermalizes.

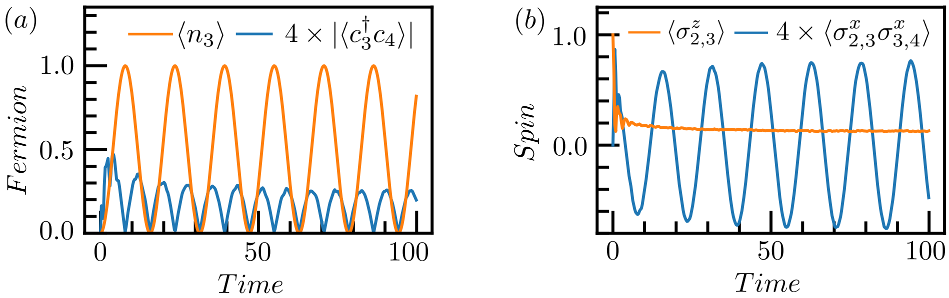

FIGURE 3.3: Dynamics of local observables (orange) and nearest neighbor correlation (blue) after a quench for physical $c-$fermions and $\sigma-$spins in panel (a) and (b) respectively ($L = 20, h = 1, J = 0.7, t = 0.2, g_z = -0.4$).

is non-integrable and the dynamics is ergodic. In this case, local observable quickly saturates to its thermal equilibrium and volume-law entanglement is established [171].

In the following, I will support the analysis via numerical calculation by exact diagonalization, confirming the coexistence of persistent oscillations and volume-law entanglement in the physical d.o.f..

3.3 Coherent Dynamics with Volume-Law Entanglement

The initial state $|0\rangle$ is a tensor-product of $c-$fermions and $\sigma-$spins as $|0\rangle = |\psi\rangle_c \otimes |S\rangle_\sigma$, where $|S\rangle_\sigma = |\uparrow\uparrow\ldots\uparrow\rangle_\sigma$ and $|\psi\rangle_c$ represents the fermionic Fock state. For simplicity, I focus on a chain of length L with three fermions, and the initial state involves one building block $|010110\rangle_c$ and empty sites $|0\ldots0\rangle_c$ of length $L-6$, i.e., $|\psi\rangle_c = |0101100\ldots0\rangle$ with periodic boundary conditions. For a finite density of fermion, as long as the the kinetic constraints result in small isolated active regions, e.g. here sites 3 and 4, which are separated by frozen segments, the qualitative behavior remains the same.

In Fig. 3.3, I depict the dynamics of local observables (orange) and nearest neighbor correlations (blue) for physical $c-$fermions and $\sigma-$spins in panel (a) and (b), respectively. Note that the separability of the model enables us to simulate the dynamics of a large system size,

By construction, coherent oscillation of the fermionic occupation $\langle n_i \rangle$ appears only for $i = 3, 4$, while no dynamics is observed on other sites. Let me project the Hamiltonian H_f to the reduced basis $|01\rangle_f, |10\rangle_f$ where only the active sites are involved. The effective Hamiltonian can be easily obtained as $H_f = -t(f_3^\dagger f_4 + f_4^\dagger f_3)$.

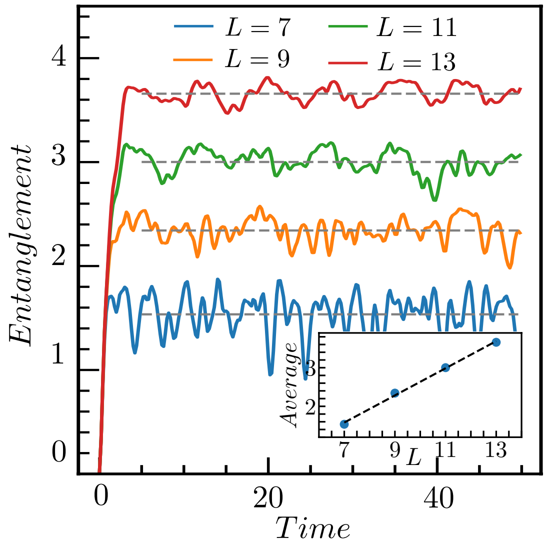

FIGURE 3.4: Dynamics of the half-system entanglement entropy which rapidly saturates to a volume-law plateau. (inset) Average entropy for the plateau for varying system sizes. $h = 1, J = 0.7, t = 0.2, g_z = -0.4$

The initial state $|01\rangle_f$ hence starts evolving coherently within the isolated subspace, resulting in the time-periodic occupation $\langle n_3\rangle(s) = \sin^2(ts)$ where s stands for time with frequency $2t$. The nearest-neighbor correlation function $\langle c_3^\dagger c_4\rangle$ oscillates as well because my choice of quench parameters leads to $\langle\tilde{\tau}_3^x\tilde{\tau}_4^x\rangle \neq 0$.

In Fig. 3.3 (b), the local magnetization (orange) rapidly saturates, but surprisingly the correlation (blue) between adjacent spins $\langle\sigma_{2,3}^x\sigma_{3,4}^x\rangle$ exhibits persistent oscillations. Indeed, according to Eq. (3.6), it synchronizes with the local fermionic occupation if $\langle\tilde{\tau}_i^z\rangle$ equilibrates at a non-vanishing value, which normally happens for quenches within the disordered phase of $H_{\tilde{\tau}}$.

The entanglement behavior of the composite model strongly depends on the choice of partition of the system. In Fig. 3.4, I depict the half-system entanglement $S_{L/2} = -\mathrm{Tr}\left[\hat{\rho}_{L/2}\log\hat{\rho}_{L/2}\right]$ where $\hat{\rho}_{L/2}$ is the reduced density matrix for the whole system defined by the physical d.o.f. of $c-$fermions and $\sigma-$spins. Entanglement quickly grows before equilibrating around a plateau, the value of which is depicted as a grey dashed line. As seen in the inset of the figure, this averaged entropy scales linearly with system size, confirming the volume-law behavior of the entanglement. Note, this volume-law entanglement is much smaller than the thermal value as only one component thermalizes: In terms of the separable d.o.f., the non-intergrable $\tilde{\tau}-$spins are also volume-law entangled, whereas the $f-$fermions are only area-law entangled

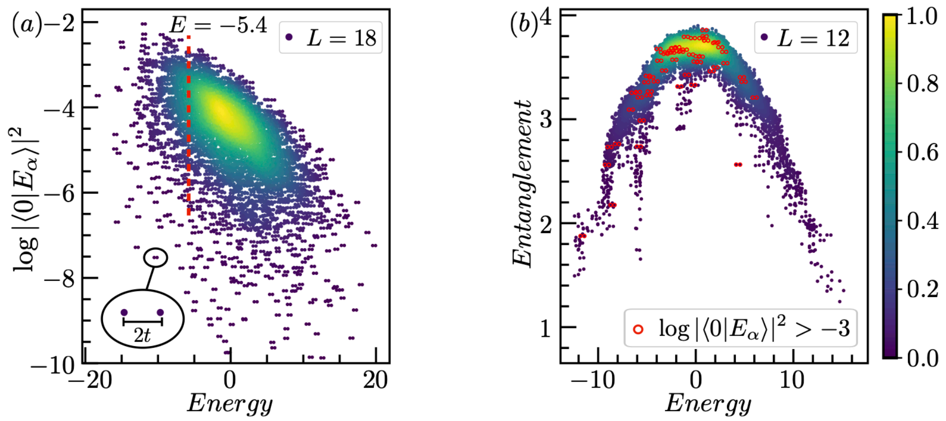

FIGURE 3.5: (a) Overlap between the initial state and eigenstates for $L = 18$. Eigenstate pairing with energy difference $2t$ are visible for all eigenstates. The red dashed line denotes the energy of the initial state. (b) Half-system entanglement entropy for each eigenstate for $L = 12$. Eigenstates with a large overlap with initial state are highlighted in red. Compared with panel (a), the width of the distribution of energy reduces since a smaller system size is used for exact diagonalization. $(h = 1, J = 0.7, t = 0.2, g_z = -0.4)$.

as the spreading of correlation is prohibited by frozen sites. Indeed, the active and frozen regions also retain for the physical $c-$fermions, thus for which only area-law entanglement can be established. Such an exotic behavior of entanglement between different species of particles is precisely the defining characteristic of the QDLs. Here on top of that, persistent oscillations also appear owing to the kinetic constraints.

3.4 Eigenstate Pairing in Spectrum

In this section I discuss the peculiar features of *orthogonal* quantum many-body scars via analysing the overlap $F_\alpha = |\langle 0|E_\alpha\rangle|^2$ between the initial state $|0\rangle$ and eigenstates $|E_\alpha\rangle$. According to the separability of the model, one can decompose the eigenstate as $|E_\alpha\rangle = |E_f\rangle \otimes |E_{\tilde{\tau}}\rangle$ and the eigenenergy reads

$$E_\alpha = E_{\tilde{\tau}} + E_f \tag{3.17}$$

where $E_{\tilde{\tau}/f}$ denotes eigenvalues for $\tilde{\tau}-$spins and $f-$fermions respectively [2]. The quantity F_α can be obtained by products of the overlap between initial state and

[2]Note, eigenstates $|E_{\tilde{\tau}}\rangle$ of Hamiltonian for $\tilde{\tau}-$spins [Eq. (3.5)] does not automatically preserve the global constraint [Eq. (3.10)]. However, eigenstates with proper global constraint can be selected out by requiring F_α is non-zero, where the initial state has a well-defined global constraint as in Eq. (3.19).

eigenstates in each sector as

$$F_\alpha = |\langle\psi_c| \otimes \langle S_\sigma|E_f\rangle \otimes |E_{\tilde{\tau}}\rangle|^2 = |\langle\psi_c|E_f\rangle|^2 |\langle S_\sigma|E_{\tilde{\tau}}\rangle|^2, \tag{3.18}$$

to compute which one needs to follow the rules as explained in Sec. 3.1.3 to transform the initial state into the emergent d.o.f. as

$$\begin{aligned} |\psi\rangle_c \otimes |S\rangle_\sigma &= |0101100\dots0\rangle_c \otimes |\uparrow\uparrow\dots\uparrow\rangle_\sigma \\ &= |0101100\dots0\rangle_f \otimes \frac{1}{\sqrt{2}}\left(|\rightarrow\rightarrow\cdots\rangle_{\tilde{\tau}} - |\leftarrow\leftarrow\cdots\rangle_{\tilde{\tau}}\right), \end{aligned} \tag{3.19}$$

where I used $N_f = 3$ to determine the fermionic parity required in Eq. (3.12).

The numerical results for the overlap is depicted in Fig. 3.5 panel (a) on a log scale versus the eigenenergy E_α, and the color indicates the density of eigenstates. Unlike the previous work about QMBS where the initial state has dominate overlap with a few number of scared eigenstates as seen in Fig. 1.6 (b), here the initial state overlaps with an extensive number of eigenstates. The initial state energy can be obtained as $E = \langle 0|H|0\rangle = -5.4$ locating at the bulk of the spectrum as indicated via the red dashed line in panel (a). Therefore, generic thermalizing behavior would be expect if the kinetic constraints are absent. However, as seen in Fig. 3.3 thermalization does not occur, thus indicating the violation of ETH which can be understood by the decomposition as in Eq. (3.17). In the reduced subspace, eigenenergy for the emergent $f-$fermion E_f only takes value $\pm t$, thus all eigenstates shown in Fig. 3.5 (a) are paired with another one with the same overlap but with energy separation $2t$. These eigenstate pairs have different expectation values for the fermion number and the energy separation $2t$ is directly related to the frequency of persistent oscillations.

Although ETH is strongly violated, entanglement can still be largely generated for most of the eigenstates through the background spins. Fig. 3.5 (b) depicts the entanglement entropy for the half-system $S_{L/2}$ for all eigenstates in the reduced Hilbert space[3], which increases towards the bulk of the spectrum. Note that the distribution of energies is different from Fig. 3.5 (a) due to a smaller system size, but in both

[3] Due to kinetic constraints, for the initial state in Eq. (3.19), two active sites contribute to the dynamics, hence only two fermionic Fock state are needed for exact diagonalization $|\psi\rangle_c = |0101100\dots0\rangle$ and $|\psi\rangle_c = |0110100\dots0\rangle$. One can use such reduced basis even in the presence of separability breaking perturbation, as long as the kinetic constraint remains unperturbed.

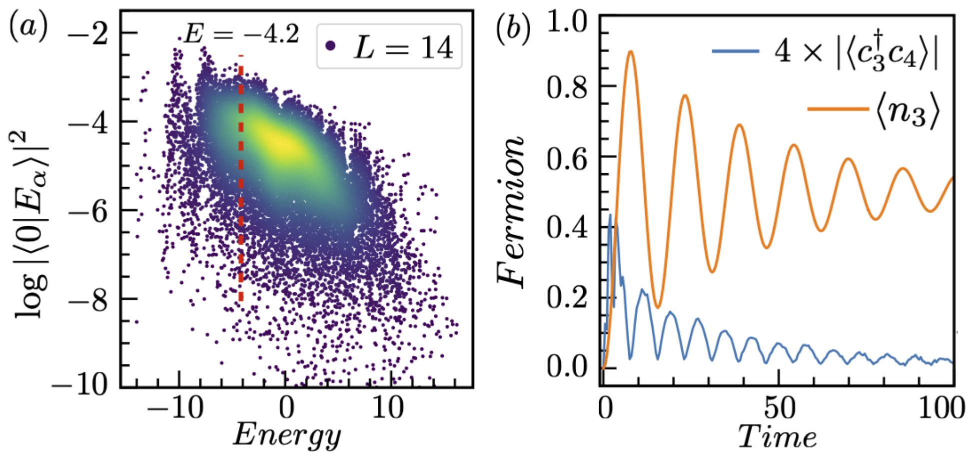

FIGURE 3.6: (a) Overlap between the initial state and eigenstates E_α. (b) Damping of the local dynamics and correlation function. Parameters are chosen as $L = 14, J = 0.7, h = 1, t = 0.2, g_z = -0.4$ with an additional interaction $g_x = 0.1$ which breaks the fine-tuned construction and separability into to independent sectors.

cases the energy of initial state locates in the bulk of the spectrum. The states with dominant overlap with the initial state ($\log|\langle 0|E_\alpha\rangle|^2 > -3$) are highlighted in red, and most of them are highly entangled with $S_{L/2} \gtrsim 3.5$. This is in sharp contrast to known quantum many-body scars, which normally exhibit exceptionally low entropy in accordance with their non-ergodic dynamical behavior.

3.5 Thermalization through Separability Breaking

The long-lived oscillation and volume-law entanglement generation also appear in the presence of generic perturbations which break the separability of the Hamiltonian into separate terms H_f and $H_{\tilde{\tau}}$. This can be demonstrated with the example of the perturbation $g_x \sum_i \sigma^x_{i-1,i}\sigma^x_{i,i+1}$ without the coupling to fermion $(-1)^{c_i^\dagger c_i}$ as in the original model Eq. (3.13). As such, although the mobility of $c-$fermions remains restricted to two active sites, their dynamics cannot be decoupled from the background $\sigma-$spins. These spins can then act as a thermal bath for the fermions.

In Fig. 3.6 (a), I depict the overlap between initial states and eigenstates $|\langle 0|E_\alpha\rangle|^2$, and the mean energy $E = -4.2$ (red dashed line) still locates in the bulk of the spectrum. The typical eigenstate pairing as seen in Fig. 3.5 is absent as the perturbation violates the separability. The dynamics of local observables (orange) and correlation functions (blue) of $c-$fermions is illustrated in Fig. 3.6 (b) for a finite perturbation

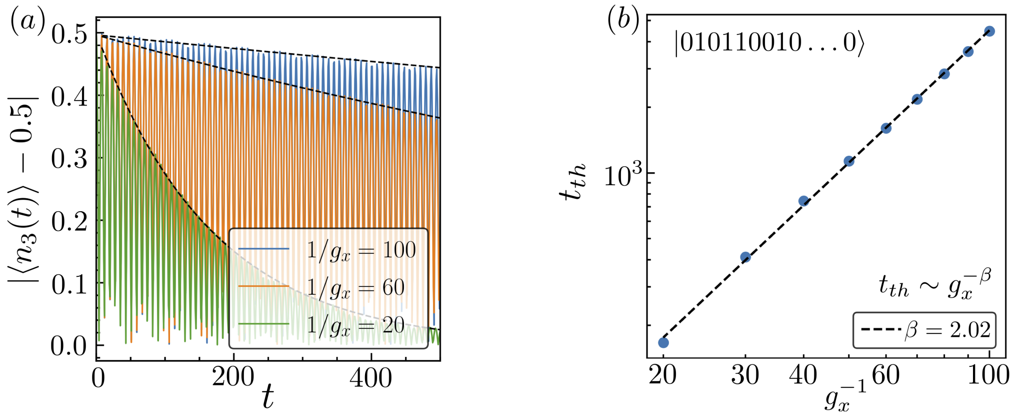

FIGURE 3.7: (a) Damped oscillations of the local fermionic dynamics. Parameters are chosen as $h = 1, J = 0.7, t = 0.2, g_z = -0.4$. (b) Lifetime t_{th} of the oscillation versus the separability breaking perturbation g_x, which fits well with $t_{th} \sim g^{-2}$.

strength $g_x = 0.1$. The oscillations of the fermionic occupation is not infinitely long-lived but decays with a finite lifetime eventually saturating to the thermal average 0.5.

To quantify the dependence of the lifetime t_{th} on the perturbation strength g_x, in panel (a) of Fig. 3.7, I depict the deviation between the occupation number on site 3 and its thermal equilibration 0.5 starting from the initial state $|\uparrow\uparrow\ldots\uparrow\rangle \otimes |010110010\ldots0\rangle$ for $L = 14$. Similar as in Fig. 3.6, the oscillation is damping and I fit the envelop as an exponential function $0.5e^{-t/t_{th}}$ as indicated as the black dashed curve. In panel (b), the lifetime t_{th} is plotted versus the inverse of the separability breaking perturbation g_x^{-1} which scales approximately as $t_{th} \sim g_x^{-2}$ as predicted by the Fermi's Golden rule [172].

The same behavior also appears for correlation functions, which decay towards zero at long times. Therefore, in the presence of generic perturbations, the *perfect* orthogonal QMBS turn into orthogonal scars demonstrating long-lived but not persistent oscillations.

3.6 Discussion

By combining kinetic constraints with the fractionaliztion mechanism of the OM, I propose a simple model of orthogonal QMBS demonstrating the sought-after ergodicity-breaking dynamics with the coexistence of persistent oscillations and extensive entanglement generation after a quench.

This work motivates many future directions to explore and perhaps the obvious one would be whether the orthogonal QMBS can appear in other correlated multi-component systems. For example, one can consider introducing kinetic constraints to the multi-orbital Hubbard systems which can host the OM as a low energy feature captured by slave-particle descriptions [158]. Furthermore, the current one-dimensional example can be generalized to higher dimensions where both the conventional OM and the kinetic constraints still exist [173]. Properties of the models in higher dimensions are considerably richer because the background spin sector can be topologically ordered [158]. Alternatively, another possible direction for future study is to explore the interplay between kinetic constraints and local gauge symmetry. For example, combining the disorder-free localization mechanism [150–155] with kinetic constraints could potentially result in ergodicity-breaking dynamics of the gauge d.o.f..

The key elements of my model are potentially realizable on controllable quantum simulators. The experimental tool boxes in development for lattice gauge theory simulations permits the coupling between the spin background and the fermions [8, 16, 174, 175]. The density-assisted tunneling for fermions can appear in the presence of dominant nearest-neighbor density-density interactions [176]. Alternatively, it also appears in cold atomic gases via periodic drives as previously illustrated in Chapter 2.

Up to now I have introduced several new non-ergodic behaviors related to QMBS in both static and periodically driven systems. Hamiltonian in static systems is manifestly time translation invariant as there is no time-dependence in the protocol after the quenching. For Floquet systems, the Hamiltonian also has a discrete form of TTS since the driving protocol repeats itself after a complete period. The existence of TTS is essential for the definition of eigenstates and eigenvalues of the static Hamiltonian or Floquet operators. They further allow us to determine whether and how many-body systems thermalize according to different well-established measures, such as the existence of QMBS, the level statistics of the spectrum or entanglement entropy of eigenstates.

There are naturally many questions regarding the precise role of TTS in isolated quantum systems: Does thermalization always occur asymptotically when TTS is absent, for instance in a QPD system? Is TTS a prerequisite condition for the appearance of stable non-equilibrium phases of matter in driven systems? Are there any transient many-body phenomenon exhibiting interesting universal features in the absence of TTS? Understanding these questions is not only for the theoretical interest but also experimentally relevant. For instance, highly accurate temporal control which does not preserve TTS can be readily implemented on superconducting qubits [115] and nitrogen-vacancy center in diamond [114]. The remainder of the thesis will focus on these questions and provide concrete examples demonstrating either stable non-equilibrium phases or transient prethermalization of a long lifetime.

Chapter 4

Floquet Time Spiral in Quasi-Periodically Driven Systems

For quantum systems with TTS, whether they thermalize or not in the long-time limit can be diagnosed by properties of eigenvalues or eigenstates. These properties can be numerically obtained via diagonalizing the static Hamiltonians or the Floquet operators. Here I will address the following question: Can many-body systems driven by protocols without TTS evade thermalization and demonstrate nontrivial steady states, for instance, the time crystalline behavior? As reviewed in Sec. 1.5, the general expectation is that non-integrable systems without TTS generically heat up to featureless infinite-temperature states owing to the seemingly inevitable multi-photon processes.

Although theoretically interesting and experimentally relevant, this question is indeed generically difficult to answer. One obvious reason is that the lack of Floquet theory significantly increases the numerical cost for the simulation of the dynamics. It is also challenging because no well-defined eigenstates or eigenenergies can be used to verify if ETH applies. In this chapter, I provide an affirmative answer to the above question by considering a class of QPD systems that can be efficiently analyzed within the Floquet framework. These systems can exhibit time-crystalline behavior for special fine-tuned parameters. Its stability to generic perturbations is further numerically investigated via exact diagonalization.

The main idea is that for special cases of QPD systems, the Hamiltonian $H(t)$ can be mapped exactly to a periodic counterpart $\tilde{H}(t)$ in a rotating frame by performing a time-dependent unitary transformation $U(t)$ as

$$\tilde{H}(t) = \hat{U}\hat{H}(t)\hat{U}^\dagger - i\hat{U}\partial_t\hat{U}^\dagger. \tag{4.1}$$

The dynamics in the rotating frame can be efficiently solved by the Floquet theory, then the inverse of the unitary maps the time-evolution back to the physical frame. The basic idea originates from the study of spiral magnetism in doped Hubbard models [177–180], although in that case *site*-dependent rather than *time*-dependent unitary transformations have been used. For co-planar spirals, by properly rotating the local spin axis, the Hubbard model becomes translationally invariant. Therefore, the system can be efficiently analysed via Bloch's theorem even if spirals are incommensurate. I will elaborate this idea in Sec. 4.1 and translate it to the time domain for the study of QPD systems, resulting in the construction of FTSs.

For pedagogical reasons, in Sec. 4.2 I will first demonstrate a FTS via a simple two level system in the presence of two incommensurate driving tones. Thereafter in Sec. 4.3, this idea is generalized to many-body systems. I construct a minimal model showing a DTQC which exhibits a generalized version of TTSB. Most importantly, in Sec. 4.4, it will be shown that the appearance of DTQC is not limited to models equivalent to a Floquet problem. Instead, the many-body localized system can still demonstrate the DTQC behavior even when this equivalence is absent when generic perturbations are present. Therefore, the exactly solvable models constructed based on FTS enable us to gain important lessons which are more fundamental than these special fine-tuning cases.

4.1 Mapping Quasi-Periodic to Periodic Systems

The basic idea of mapping quasi-periodic to periodic systems from the studies of magnetic phases in Mott-Hubbard insulators, where incommensurate spiral magnetic states can be induced by doping [177–179]. To describe the spin-symmetry broken phases within the single band Hubbard model, one convenient approach is by using site-dependent unitary transformations to locally rotate the spin quantisation axis, e.g. a unitary transformation

$$\mathcal{R}(\Omega_i) = e^{-i(\phi_i/2)\sigma_z} e^{-i(\theta_i/2)\sigma_y}$$

with the spherical angles ϕ_i, θ_i for each fermionic operator $d^\dagger_{i\eta} = \sum_\sigma [\mathcal{R}(\Omega_i)]_{\eta\sigma} c^\dagger_{i\sigma}$ (with the standard fermionic operator $c^\dagger_{i\sigma}$ to create a particle at site $\mathbf{r}_i$ with spin σ). In the rotating frame, the Hamiltonian (with nearest neighbor tunneling t, chemical potential μ and onsite interaction U) has a new form as

$$\begin{aligned}\tilde{H} = -t \sum_{<ij>,\sigma_1\sigma_2} & \left\{ d^\dagger_{i,\sigma_1} [\mathcal{R}^\dagger(\Omega_i)\mathcal{R}(\Omega_j)]_{\sigma_1\sigma_2} d_{j,\sigma_2} + h.c. \right\} \\ & + U \sum_i d^\dagger_{i,\uparrow} d_{i,\uparrow} d^\dagger_{i,\downarrow} d_{i,\downarrow} + \mu \sum_{i,\sigma} d^\dagger_\sigma d_\sigma .\end{aligned} \tag{4.2}$$

Under the spin rotation, the Hubbard interaction and chemical potential remain invariant. The important question here is whether I can still use Bloch's theorem and momentum as a good quantum number despite the site-dependent unitary transformation? It turns out that one can still efficiently describe the homogeneous co-planar spirals. Their oscillatory spiral spin order can be written as $\langle \mathbf{S}_i \rangle = m(\sin\theta_i, 0, \cos\theta_i)$, with $\theta_i = \mathbf{Q}\cdot\mathbf{r}_i$ defining the spiral wave number $\mathbf{Q}$ and m representing the magnetization. For incommensurate spirals, the ratio $(Q_x, Q_y)/(2\pi)$ is irrational hence resulting in a infinitely large unit cell. By choosing $\phi_i = 0$ and $\theta_i = \mathbf{Q}\cdot\mathbf{r}_i$ in Eq. (4.2), the spin axis becomes aligned with the spiral after the rotation and the kinetic term

$$\mathcal{R}^\dagger(\Omega_i)\mathcal{R}(\Omega_j) = e^{-i\mathbf{Q}\cdot(\mathbf{r}_i - \mathbf{r}_j)\sigma_y/2}$$

now only depend on the relative displacement $\mathbf{r}_i - \mathbf{r}_j$ and not on $\mathbf{r}_i, \mathbf{r}_j$ independently. Hence, as indicated in Fig. 4.1 (a), the co-planar spiral maps to a ferromagnet (FM) in the rotating frame. Importantly, the new Hamiltonian $\tilde{H}$ becomes translationally invariant thus momentum serves as a good quantum number. The system can then be conveniently analyzed, e.g. in a mean-field treatment of the interaction [178].

I generalize the same idea to the time domain: There are instances of Hamiltonians $\hat{H}(t)$ which are temporally *aperiodic* such that $\hat{H}(t) \neq \hat{H}(t+T)$ for any T, but the time evolution of states $|\tilde{\phi}(t)\rangle = \hat{U}(t)|\phi(t)\rangle$, which, in a rotating frame defined via

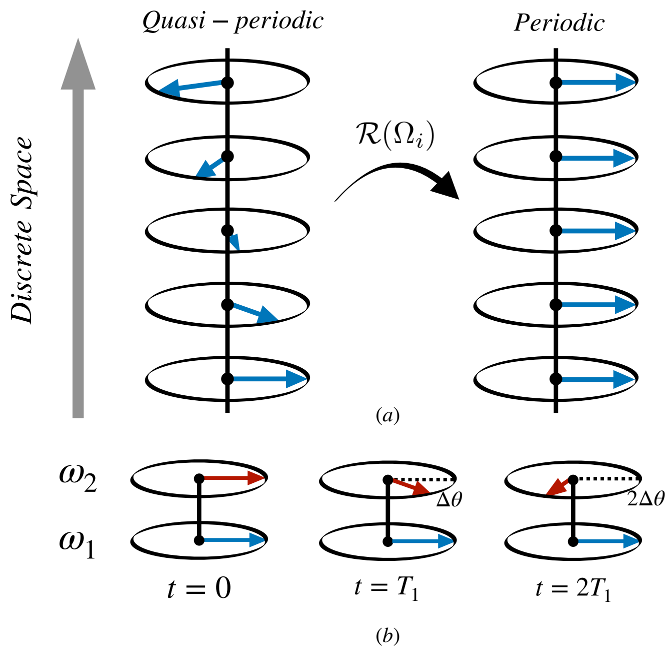

FIGURE 4.1: (a) Incommensurate magnetic spiral can be mapped to a periodic ferromagnet via a site-dependent rotation. (b)Two components of the QPD Hamiltonian are sketched on the Bloch sphere. Two driving fields in opposite directions with distinct frequencies $\omega_{1/2}$ are illustrated by two vectors. At stroboscopic times nT_1, the blue vector returns back to the original configuration. However, the red vector with frequency ω_2 never comes back with the mismatched angle $n\Delta\theta$.

a time-dependent unitary transformation $\hat{U}(t)$, is governed by a new Hamiltonian *periodic* in time with $\tilde{H}(t) = \tilde{H}(t+T)$. Here the wavefunction $|\phi(t)\rangle$ is the solution of the Schrödinger equation in the lab frame and the rotated Hamiltonian $\tilde{H}$ can be determined via Eq. (4.1) [181].

Practically, starting from a generic quasi-periodic Hamiltonian and identifying the proper mapping to a Floquet Hamiltonian is very difficult. Therefore in the following, I will construct the model in reverse such that any Floquet Hamiltonian helps to define specific instances of aperiodic Hamiltonian through a time-dependent unitary transformation, and to understand their dynamics. Importantly, these specific instances result in exotic non-equilibrium phenomenon persisting even in the absence of a perfect mapping between periodic and quasi-periodic systems. Consequently, Floquet theory can still provide valuable physical insights for systems to which Floquet theory fundamentally does not apply.

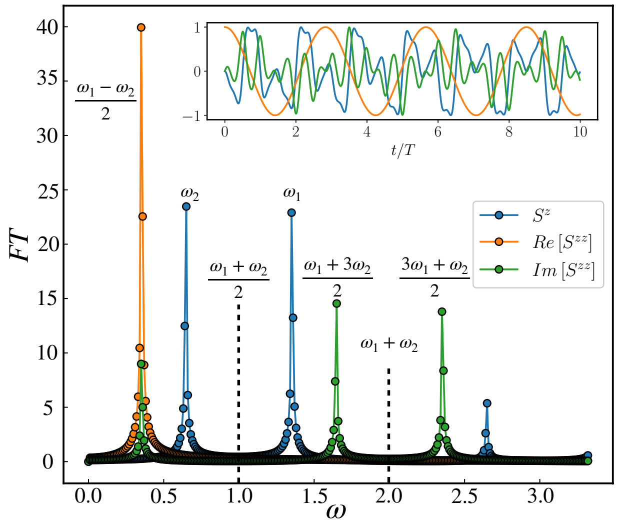

FIGURE 4.2: Fourier transform(FT) of the dynamics of observables computed for the QPD two-level system with parameters $A = 1, \omega = 1, \Omega = \sqrt{2}/4$. Fourier peaks of $S^z(t)$ appearing at $k\omega \pm \Omega$ for odd integer k suggests that the system synchronizes with the external drive. Frequencies of observables in the rotating frame are labels as black dashed lines. The inset depicts the real time behavior.

4.2 Floquet Time Spiral of a Two-Level System

The simplest example to demonstrate FTS would be a QPD two-level system with two frequencies ω_1, ω_2. I focus on the time-dependent Hamiltonian with two circular drivings , $\hat{H}(t) = \hat{H}_1(t) + \hat{H}_2(t)$ as

$$\begin{aligned}\hat{H}_1(t) &= -\frac{A}{2}\cos(\omega_1 t)\sigma_z + \frac{A}{2}\sin(\omega_1 t)\sigma_y,\\ \hat{H}_2(t) &= -\frac{A}{2}\cos(\omega_2 t)\sigma_z - \frac{A}{2}\sin(\omega_2 t)\sigma_y + \frac{\Omega}{2}\sigma_x,\end{aligned} \tag{4.3}$$

with Pauli matrices σ_α for $\alpha = x, y, z$ and the last term of $\hat{H}_2$ represents a constant field in x direction of strength $\Omega/2$. As illustrated intuitively in Fig. 4.1 (b), these two time-dependent components of the Hamiltonian behave as two conversely rotating vectors on the Bloch sphere. The driving component with ω_1 is chosen to determine a discrete time coordinate (blue) which now plays the role of a lattice. If the ratio between the two frequencies is irrational, the other rotating vector (red) with frequency ω_2 in Fig. 4.1 is aperiodic with a mismatched phase angle $n\Delta\theta = n\frac{\omega_2}{\omega_1}2\pi$ at discrete times nT_1. Based on the definition given in Eq. (1.48), the Hamiltonian is certainly quasi-periodic hence Floquet theory in principle does not apply. By employing the following time-dependent unitary transformation

$$\hat{U}(t) = e^{i(\omega_1-\omega_2)t\sigma_x/4}, \tag{4.4}$$

one can rotate the system around the x-axis, and according to Eq. (4.1), the Hamiltonian in the rotating frame reads

$$\tilde{H}(t) = -A\cos(\omega t)\sigma_z + (\frac{\Omega}{2} - \frac{\omega_1-\omega_2}{4})\sigma_x. \tag{4.5}$$

This Hamiltonian now describe a periodically driven two-level system with frequency $\omega = (\omega_1+\omega_2)/2$, which has been well-studied within the Floquet framework [39, 40]. For simplicity, I use $\Omega = (\omega_1-\omega_2)/2$ such that the static field vanishes. One can exactly solve the time evolution operator as

$$\hat{V}(t) = \mathcal{T}\exp\left[-i\int_0^t ds\tilde{H}(s)\right] = \exp\left[i\frac{A}{\omega}\sin(\omega t)\sigma_z\right], \tag{4.6}$$

and further more derive the time-dependent wavefunction as

$$|\tilde{\phi}(t)\rangle = \sum_\sigma c_\sigma(t=0)\exp\left[i\mathrm{sgn}[\sigma]\frac{A}{\omega}\sin(\omega t)\right]|\sigma\rangle, \tag{4.7}$$

where $\sigma =\uparrow,\downarrow$ and sgn$[\sigma]$ gives $+,-$ respectively. Consider an initial state with $c_\sigma(t=0) = 1/\sqrt{2}$, the magnetization in the z direction thus reads

$$\begin{aligned} S^z(t) &= \langle\phi(t)|\sigma^z|\phi(t)\rangle = \langle\tilde{\phi}(t)|\hat{U}(t)\sigma^z\hat{U}^\dagger(t)|\tilde{\phi}(t)\rangle \\ &= -\sin(\Omega t)\sin\left[\frac{2A}{\omega}\sin(\omega t)\right], \end{aligned} \tag{4.8}$$

where two independent frequencies appear in the time evolution, as indicated in the inset of Fig. 4.2. The non-equal time correlation function

$$S^{zz}(t,0) = \langle\phi|\sigma^z(t)\sigma^z(0)|\phi\rangle = \cos(\Omega t) + i\sin(\Omega t)\cos\left[\frac{2A}{\omega}\sin(\omega t)\right],$$

can also be obtained and its imaginary part serves as a suitable measure for the quasi-periodicity.

The dominating peaks in the frequencies spectrum of the magnetisation S^z (blue line of Fig. 4.2) locate at $\frac{k\pm1}{2}\omega_1 + \frac{k\mp1}{2}\omega_2$ or equivalently $k\omega \pm \Omega$ for odd integer k. Therefore, only integer multiples of $\omega_{1/2}$ appear in the spectrum like the first two blue peaks at ω_1, ω_2, implying that the observable synchronises with the external driving field. The fact that the peaks of the Fourier spectrum of the observables coincide with the driving spectrum of the Hamiltonian, signifying that the resulting dynamics preserves the long-range quasi-periodic temporal order originated from the external drive. Such a phenomenon is analogous to observables of well known spatial quasi-crystals, where the translation symmetry is lacking while still remain long-range ordered [182]. In the following section, I will discuss the intriguing possibility to break such long-range quasi-periodic order, i.e. peaks at half integer multiples of the driving frequencies may appear in the Fourier decomposition.

4.3 Discrete-Time Quasicrystal

Here I generalize the idea of FTS to study QPD many-body systems, e.g. interacting spin chains. I will focus on a new type of DTQC and discuss its rigidity which shows that it is robust beyond my method of construction.

To formally define the meaning of the breaking of long-range quasi-periodic temporal order, let us first recall the usual definition of discrete time translational symmetry breaking (TTSB) [183]. For a PD system with period T, there exists an operator $\hat{O}$ signalling TTSB if $\langle \hat{O} \rangle_t$ is only invariant under time translation by nT for $n > 1$. As a comparison, QPD systems do not have a well defined period but, loosely speaking, one can still define quasi-periodic time translation symmetry breaking (QTTSB) via the frequency. For instance, consider a quasi-periodic driving defined by Eq. (1.48), QTTSB happens if there exists an operator $\langle \hat{O} \rangle_t$ with Fourier decomposition as

$$\langle \hat{O} \rangle_t = \sum_{\vec{n}} O_{\vec{n}} e^{i \sum_i n_i \omega_i / p_i t}, \tag{4.9}$$

with at least one of the non-negative integers p_i larger than 1. Similar definitions have also been proposed in [104, 105]. Strictly speaking, such phenomenon is not the breaking of a symmetry but rather the long-range quasi-periodic order in time imprinted by the Hamiltonian drive. However, in analogy with the widely used TTSB we use the term QTTSB. Basic TTSB in Floquet system is a special case of the definition, i.e. period doubling with only one ω_0 and $p_0 = 2$ [183]. There is no general agreement on the definition of QTTSB, and the behavior proposed here differs from the previous observation of the time quasi-crystals in bosonic systems [71, 184]. There, the frequencies of the time-dependent Hamiltonian and of the observable are not simply related, which is similar to other DTQCs identified before [185–187].

The combination of a standard Floquet DTC with the idea of FTS permits us to construct a QPD model realising QTTSB. The Hamiltonian is given by

$$\hat{H}(t) = \hat{H}_{MBL}(t) + \hat{H}_d(t) + \frac{\Omega}{2}\sum_j \sigma_j^x, \tag{4.10}$$

where the first term involves Ising interaction and local fields in the same direction as

$$\hat{H}_{MBL}(t) = h_1(t)\sum_{j=1}^{N}\left[J_j\sigma_j^x\sigma_{j+1}^x - h_j^x\sigma_j^x\right], \tag{4.11}$$

where the disordered prefactors J_j, h_j^x are selected from uniform distributions. A QPD field is introduced to each site as

$$\hat{H}_d(t) = h_2(t)\sum_j\left[\cos(\Omega t)\sigma_j^z - \sin(\Omega t)\sigma_j^y\right]. \tag{4.12}$$

The driving terms in the Hamiltonian are switched on and off periodically such that the stepwise functions within one period $t \in (-T/2, T/2)$ read

$$h_1(t) = \begin{cases} 1, & |t| \le \frac{T}{4} \\ 0, & |t| > \frac{T}{4} \end{cases}, \quad h_2(t) = \begin{cases} 0, & |t| \le \frac{T}{4} \\ g, & |t| > \frac{T}{4} \end{cases}, \tag{4.13}$$

ensuring that the time evolution governed by $\hat{H}_d, \hat{H}_{MBL}$ happens in two different time windows. According to the definition in Eq. (1.48), the combined driving in Eq. (4.12), $h_2(t)\cos(\Omega t)$ or $h_2(t)\sin(\Omega t)$ is quasi-periodic in time, which can be verified by using the Fourier expansion of the box function, e.g.

$$h_2(t)\cos(\Omega t) = \sum_{n_1=-\infty}^{+\infty}\sum_{n_2=\pm 1} c_{n_1} e^{i(n_1\omega + n_2\Omega)t}, \tag{4.14}$$

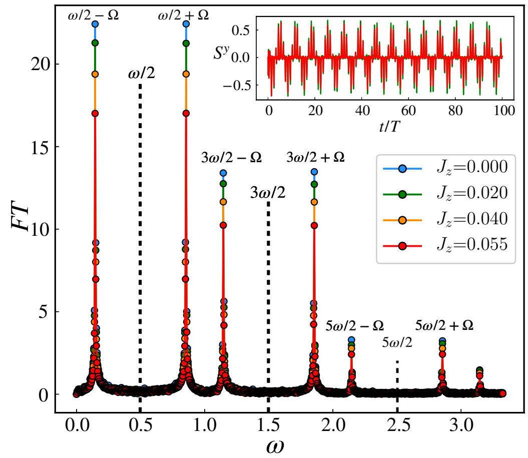

FIGURE 4.3: Fourier transformation (FT) of the average magnetization in y direction of the DTQC, simulated by exact diagonalization with 10 sites for different interaction perturbations J_z. 300 different disorder realizations are averaged over to get the real time dynamics as shown in the inset with $J_z = 0.02, 0.055$. FT is done in a window 200-400 T. At the fine-tuning point, in the rotating frame, subharmonic responses appear at $k\omega/2$ with an odd integer k labelled by the dashed line. In the original frame, peaks are fixed at $k\omega/2 \pm \Omega$ even when perturbations are present, indicating the existence of the robust time quasi-crystal.

with $\omega = 2\pi/T$ and coefficients $c_{n_1=0} = g/2$, and $-g\ \mathrm{sinc}(n_1/2)/2$ for non-zero n_1. By using the unitary transformation $\hat{U}(t) = e^{i\frac{\Omega}{2}t\sum_j^N \sigma_j^x}$, I can derive the new Hamiltonian $\tilde{H}(t) = \tilde{H}_{MBL}(t) + \tilde{H}_d(t)$ in the rotating frame as

$$\tilde{H}(t) = h_1(t)\sum_j^N \left[J_j\sigma_j^x\sigma_{j+1}^x - h_j^x\sigma_j^x\right] + h_2(t)\sum_j \sigma_j^z, \tag{4.15}$$

which reduces to a standard model of DTC with a well-defined period T. As introduced in Sec. 1.3.2, robust TTSB is predicted for $g \approx \omega/2$ in the rotating frame, which further translates into QTTSB in the original physical frame.

4.4 Signature of QTTSB, Rigidity, and Thermalization

I will detect QTTSB via measuring expectation values of the magnetization in y and z directions $S^{y,z}(t)$. However, such a behavior does not appear in $S^x(t)$ as it commutes with the unitary transformation. Hence, even in the physical frame, $S^x(t)$ only exhibits the same period-doubling behavior as in the rotating frame. In the following, exact diagonalization is used to simulate the dynamics for parameters $J_i \in [1/2, 3/2], h_j^x \in [0,1], \omega = 1, \Omega = \sqrt{2}/4$ with periodic boundary condition and trotter step $\Delta t = T/300$. Fig. 4.3 and Fig. 4.5 depict the real time dynamics of the

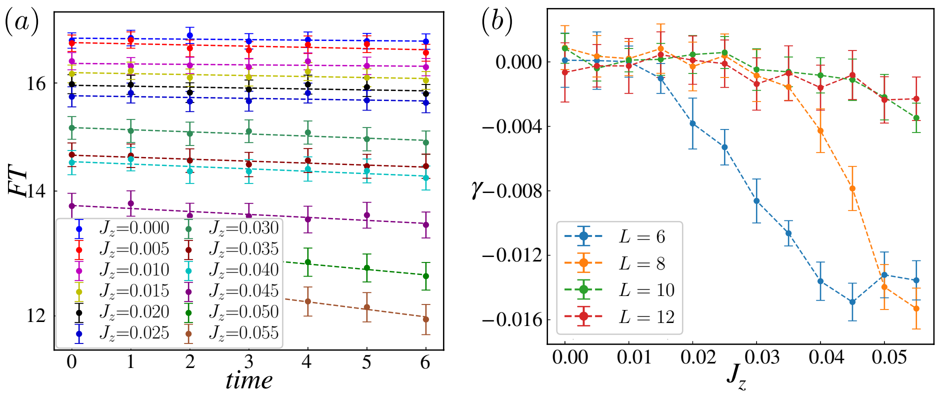

FIGURE 4.4: (a) Height of the first subharmonic peak of the Fourier spectrum of $S_y(t)$ for the DTQC on a log scale, as a function of increasing time windows (averaged over 300 disorder realizations) for different interaction perturbations with J_z and $L = 10$. Slope of the linear fit defines the decay rate γ. (b) Decay rate γ versus J_z for different system sizes.

magnetization $S^y(t)$ and its Fourier transformation. Clearly, the comparison between the subharmonic response of the dynamics (sharp peaks appear at $k\omega/2 \pm \Omega$ for odd integer k) and the Fourier spectrum of the drive [Eq. (4.14)] confirms the existence of QTTSB.

The observed DTQC trivially mains stable in the presence of small perturbations which does not break the mapping to the Floquet systems. In the rotating frame, these perturbations become periodic and the level statistics to examine whether they induces the Floquet MBL to thermalization phase transition [69]. However, it is highly non-trivial to rigorously argue the stableness of DTQC when generic perturbations are present which do not commute with the unitary transformation $\hat{U}(t)$. This question is also closely related to the stability of Anderson localization (or MBL) in QPD systems which have been recently investigated numerically [112] yet there is no rigorous theoretical proof. In the following, I will provide numerical evidences demonstrating that DTQC can still remain stable within the numerically accessible time for generic perturbations. It is then suggested DTQC is more fundamental than the fine-tuning FTS construction. For concreteness, the interaction perturbation $h_1(t)\sum_j J_z\sigma_j^z\sigma_{j+1}^z$ of uniform strength J_z, or rotation imperfection $-h_2(t)\epsilon_z\sum_j \cos(\Omega t)\sigma_j^z$ of uniform strength ϵ_z will be individually added to $\hat{H}_{MBL}$ [Eq. (4.11)] and $\hat{H}_d$ [Eq. (4.12)] respectively. They do not commute with the rotation, therefore even after the unitary transformation the driving remains quasi-periodic.

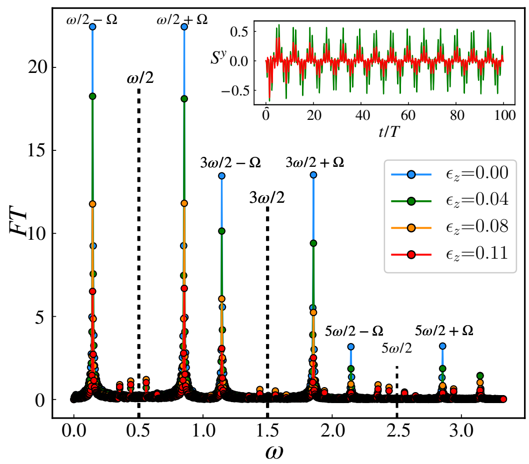

FIGURE 4.5: Fourier transformation of the average magnetization in y direction of DTQC, computed by ED with 10 sites (300 disorder configurations) for different ϵ_z. FT is done with 200-400 T. Peaks are locked at $k\omega/2 \pm \Omega$, indicating robustness of DTQC w.r.t. rotation imperfection. Inset is the dynamics for $\epsilon_z = 0.04, 0.11$.

4.4.1 Interaction Perturbation

First I analyse the effect induced by a perturbative interaction. The Fourier spectrum is shown in Fig. 4.3 for various values of J_z. Robust peaks are locked at $k\omega/2 \pm \Omega$ as in unperturbed case, but now with descending heights for increasing perturbations. The long time stability of the DTQC phase is examined in panel (a) of Fig. 4.4 by extracting the amplitude of the first subharmonic peak as a function of shifting time windows for different perturbation strength. The Fourier transformation is done within 7 equally divided time windows in the domain $[300T, 1000T]$. The error bars are determined via the standard deviation of mean, $\sigma/\sqrt{N}$ with N being the number of disorder realizations. Linear fits are plotted as dotted line, the slopes γ of which capture the decay rate of the signal, and a non-zero value suggests thermalization. In panel (b), the decay rate γ is depicted w.r.t. J_z for different system sizes to investigate the thermalisation transition induced by J_z. Each data point is obtained by averaging γ calculated with varying lengths of time window from $70T$ to $100T$. The standard deviation is presented as error bar. Importantly, there is a stable regime $J_z \leq 0.04$ for $L > 8$ where the decay rate γ remain zero, implying that the DTQC is robust w.r.t. small perturbative interaction. For perturbations larger than certain critical value, γ is non-zero indicating thermalization already occurs for $t < 1000T$. Note, the critical value of the phase transition is still size dependent, but interestingly it enlarges with increasing system size. A precise determination of the transition point is beyond the

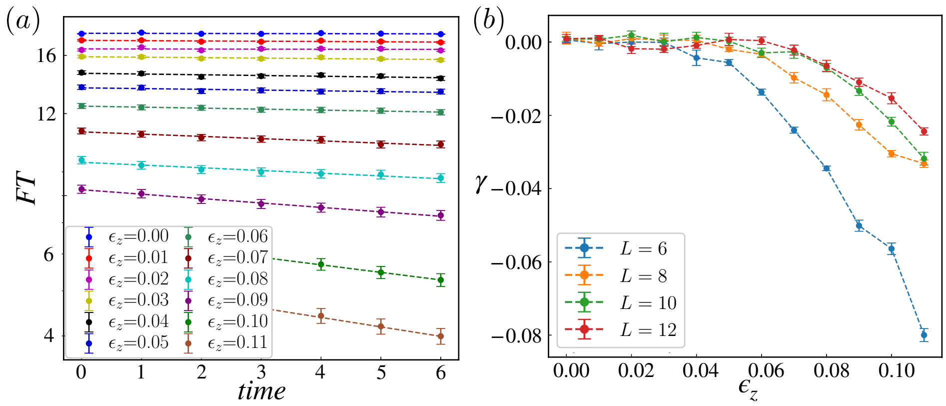

FIGURE 4.6: (a) Amplitudes of the first subharmonic peak of the Fourier spectrum of $S_y(t)$ for the DTQC on a log scale, as a function of increasing time windows (300 disorder configurations) for different rotation imperfections with ϵ_z. The linear fit gives the decay rate γ. (b) Decay rate γ versus ϵ_z for varying system sizes.

scope of this work.

4.4.2 Imperfect Rotation

Rotation imperfection induced effects can be analysed in the same way. In Fig. 4.5, the Fourier spectrum of $S^y(t)$ is presented for different ϵ_z. Similar as in previous case, subharmonic peaks are locked at $k\omega/2 \pm \Omega$ with descending heights for increasing ϵ_z. I confirm that the oscillation persists without thermalizing to at least $1000T$ for $\epsilon_z = 0.04$. As a comparison, it rapidly decays with $\epsilon_z = 0.11$ as depicted in the inset of Fig. 4.5 suggesting the deleterious thermalization.

Fig. 4.6 shows the long time behavior of the first subharmonic peak and the relation between the decay rate γ and ϵ_z. The same method to obtain average and error bar is applied here, and the stable regime with zero γ can be observed. The critical value of the thermal phase transition also tends to increase for larger system sizes and converge approximately at $\epsilon_z \sim 0.06$ for $L \geq 8$.

4.5 Discussion

Inspired by the co-planar spiral magnets, I have shown that certain QPD quantum systems can be transformed to Floquet systems via suitably chosen time-dependent unitary transformations. I generalized the definition of TTSB to QPD systems, and discovered DTQC as a new non-equilibrium phase of matter. The subharmonic response has also been verified to survive the presence of power-law decaying long-range interactions, suggesting that the DTQC should be implementable on current experimental setups of ion-trap quantum simulators [188–190].

The QPD Hamiltonian and the unitary transformation considered here are easiest obtained via backwards-engineering, namely one first starts from a periodic system of choice, then apply a time-dependent unitary and arrive at the QPD system. The inverse mapping ensures that it can be transformed back. As the soluble limit is arguably fine-tuned, it is important to show that the DTQC can persist in the presence of perturbations that do not permit a transformation to its Floquet counterpart. Therefore, the discovery of DTQC is more fundamental than the FTS construction. I admit that the stability of DTQC is currently examined via a small system and in a finite time window. Therefor, extensive numerical studies in the future would be worthwhile to check whether it is a prethermal phenomenon of exceptionally long lifetime [104] and to determine the phase diagram.

Examples discussed here are limited to unitary transformations of spin rotations changing linearly in time, but it would be interesting to consider QPD systems with more generic time- and site-dependent transformations. Furthermore, although the QTTSB is expected to happen with subharmonic responses associated with all primary incommensurate frequencies, e.g. ω and Ω in my case, here QTTSB only appears with $\omega/2$ but not Ω due to the special FTS construction. It will be fascinating to discover more general QTTSB and other DTQCs in the future.

A more ambitious goal would be to investigate the existence of possible mappings to Floquet systems for generic QPD systems. Establishing the connection between FTS of two-level systems and its topological classification via Floquet lattice might be insightful [107]. Moreover, it is also interesting to explore the fundamental idea of mapping between aperiodic and periodic systems in other contexts beyond the original spiral magnets or the FTS.

Although at the fine-tuned point the dynamics can be simulated efficiently due to the equivalence to Floquet systems, the computational cost quickly becomes unfeasible when generic perturbations are introduced. Alternatively, quasi-periodic driving can also be induced via discrete aperiodic sequences, e.g. Thue-Morse sequence where the TTS is also absent. The recursive structure of the sequence significantly facilitates the simulation. In the next chapter, I will show that a long-lived prethermal regime appears in the rapid driving regime similar to Floquet systems (see Sec. 1.4.2). More surprisingly, the randomized version of the Thue-Morse drive also yields slow heating, hence, prethermalization appears even when the driving is not deterministic.

Chapter 5

Prethermalization with Random-Multipolar Driving

The existence of a prethermal regime in Floquet systems is now well-established as a long-lived transient period before heating to infinite temperature as described in Sec. 1.4.2. In this chapter, I will show that prethermalization can also appear in driven systems without TTS. For continuous quasiperiodic drivings, slow heating has been suggested to exist in Ref. [104] but its numerical verification in many-body systems remains a challenging task.

The focus of this chapter is discrete drivings and I will demonstrate that prethermalization can occur for generic quantum many-body systems even when the drive is random. I introduce a new family of random but structured drives – *random multipolar drives* (RMD) – which interpolate between a deterministic quasiperiodic and a fully random drive. The temporal correlations of the protocol can be parameterized via a non-negative integer n: $n = 0$ corresponds to the uncorrelated random driving, while $n \to \infty$ corresponds to the quasi-periodic Thue-Morse driving. Fig. 5.1 compares different driving protocols and the precise definition of RMD will be given in Sec. 5.1.

The basic motivation for considering RMD is the observation that the bound of the suppressed heating rate underpinning Floquet perthermalization also applies for RMD without the need of perfect Floquet periodicity as discussed further in Sec. 5.2. As the central finding, I discover that energy absorption associated with RMD slows down *algebraically* with n, with the prethermal lifetime growing as $\tau \sim (1/T)^{2n+1}$ where T denotes the characteristic driving period. The quasiperiodic $n \to \infty$ limit leads

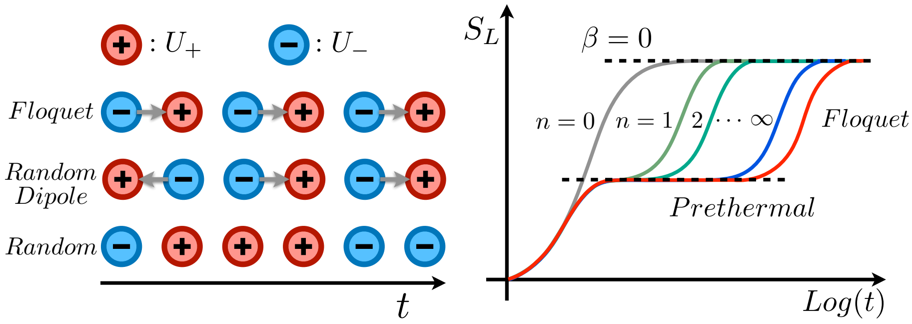

FIGURE 5.1: Left: schematic figure for different driving protocols. Two types of dipolar operators can be constructed from the unitaries $U_\pm = \exp(-iTH_\pm)$ as U_+U_- or U_-U_+. Floquet drivings are implemented by repeatedly using a single type of dipole whereas a uncorrelated random succession of both dipolar operators corresponds to a random dipolar drive (or 1-RMD). Right: Sketch of entanglement entropy dynamics. For a random drive ($n = 0$) the system heats rapidly to the featureless infinite temperature state with the inverse temperature $\beta = 0$, whereas for $n-$RMD ($n \geq 1$) a prethermal plateau emerges with a long lifetime.

to an scaling as $\tau \sim e^{C[\ln(T^{-1}/\lambda)]^2}$ with a constant C and a typical local energy scale λ. This unfamiliar scaling is faster than any power law but slower than exponential. Numerical verification of prethermalization will be presented in Sec. 5.3.

$n-$RMD represent a form of spectral engineering as the envelop of the Fourier coefficients of the correlated random time sequence vanishes algebraically as $(1/T)^n$ for decreasing frequency $1/T$, which effectively converts to a pseudogap in the limit $n \to \infty$. This characteristic frequency suppression justifies a simple Fermi's golden rule (FGR) calculation [89, 191, 192]. It further explains the observed slow heating behavior and the dependence on a finite n as detailed in Sec. 5.4. I will also comment on a rigorous and non-perturbative theory, which predicts the correct scaling for the $n \to \infty$ limit that is otherwise difficult to obtain via the linear response theory.

5.1 Driving Protocol

To start with, I first consider the two elementary time evolution operators as

$$U_+ = \exp(-iTH_+), \quad U_- = \exp(-iTH_-), \tag{5.1}$$

where $H_\pm$ is a time independent Hamiltonian and T defines the characteristic time scale. For periodic driving, the dynamics is governed by the Floquet operator $U_1 = U_-U_+$, and the Floquet Hamiltonian H_F is defined as $U_1 = e^{-i2TH_F}$. It is well established how to construct a perturbative Floquet-Magnus (FM) expansion for a small period T, $H_F = \sum_{n=0}^{\infty}(2T)^n H_F^n$ as seen in Eq. (1.23).

Random multipolar driving is performed via randomly driving the system with two multipolar operators U_n and $\tilde{U}_n$ parametrised by an integer n. As illustrated in Fig. 5.1, for $n = 0$, it involves a fully random sequence of operators

$$U_0 = U_+,\ \tilde{U}_0 = U_-, \tag{5.2}$$

while for $n = 1$ it is made up of 'dipoles', i.e. of terms

$$\begin{aligned} \tilde{U}_1 &= U_0\tilde{U}_0 = U_+U_-, \\ U_1 &= \tilde{U}_0U_0 = U_-U_+, \end{aligned} \tag{5.3}$$

and in turn $n = 2$, 'quadrupolar' sequences, are made up of antialigned dipoles as

$$\begin{aligned} \tilde{U}_2 &= U_1\tilde{U}_1 = U_-U_+U_+U_-, \\ U_2 &= \tilde{U}_1U_1 = U_+U_-U_-U_+, \end{aligned} \tag{5.4}$$

and so on for higher n as

$$\tilde{U}_{n+1} = U_n\tilde{U}_n, \quad U_{n+1} = \tilde{U}_nU_n. \tag{5.5}$$

The recursively defined limit $n \to \infty$ of such a driving thus corresponds to the Thue-Morse quasiperiodic drive as introduced in Sec. 1.5.2.

5.2 Rigorous Bound on Heating

Here I establish the rigorous bound on heating of RMD systems by generalizing the results of Floquet driving. The lowest order contribution to the Floquet Hamiltonian, $H_F^0 = (H_+ + H_-)/2$, is already insightful and most relevant for my purpose. The following rigorous bound for the difference between the dipolar operator U_-U_+ and the approximated time evolution operator for a single period has been obtained as

Corollary 1 in Ref. [19]:

$$\left\| U_- U_+ - e^{-iH_F^0 2T} \right\| \leqslant V_0 \left[6 \times 2^{-n_0} + \lambda T\right] 2T, \tag{5.6}$$

where V_0 is proportional to the driving amplitude, λ captures the local typical energy scale of the system, and $n_0 \sim \mathcal{O}(T^{-1})$ denotes the optimal order before the FM expansion diverges. Formal definitions of these quantities can be found in Sec. C.1 as well as in [19]. Crucially, I notice that the bound in Eq. (5.6) is independent of the order of U_+ and U_- as the dipolar operators U_+U_- and U_-U_+ have the same zeroth order contribution H_F^0. This observation further motivates me to use the triangle inequality

$$\left\| (U_-U_+)(U_+U_-) - e^{-iH_F^0 4T} \right\| \leq \left\| (U_-U_+) - e^{-iH_F^0 2T} \right\| + \left\| (U_+U_-) - e^{-iH_F^0 2T} \right\|, \tag{5.7}$$

and insert Eq. 5.6 to the right hand side. By repeating the above equation m times, the following bound can be obtained

$$\Big\| \underbrace{(U_-U_+)(U_+U_-)\dots}_{m \text{ dipoles}} - e^{-iH_F^0 t} \Big\| \leqslant V_0 \left[6 \times 2^{-n_0} + \lambda T\right] t. \tag{5.8}$$

with the time $t = 2mT$. This bound estimates the deviation which accumulates by a constant error after each application of the dipolar operator. Importantly, the bound is not limited to the periodic driving and, the dipolar operators can appear randomly.

For the quadrupolar operators U_2 and $\tilde{U}_2$, I realize that the first order contribution to their magnus expansion vanishes. Therefore, both the operators have the same effective Hamiltonian up to the order $\mathcal{O}(T)$ and, again by using Corollary.1 in Ref. [19], I improve the bound as

$$\left\| U_2/\tilde{U}_2 - e^{-iH_F^0 4T} \right\| \leqslant \left[6 \times 2^{-n_0'} + \frac{4}{9}(4T\lambda)^2\right] V_0 4T, \tag{5.9}$$

with the exponent $n_0' := \lfloor 1/16\lambda(4T) \rfloor = \mathcal{O}(T^{-1})$. At later times $t = 4mT$, the accumulated error can be estimated as

$$\Big\| \underbrace{U_2\, \tilde{U}_2 \ldots}_{m \text{ quadrupoles}} - e^{-iH_F^0 t} \Big\| \leqslant V_0 \left[6 \times 2^{-n_0'} + \frac{4}{9}(4T\lambda)^2 \right] t. \tag{5.10}$$

For $n > 2$, the bound has been rigorously analysed and significantly improved by Takashi et al. in Ref. [193], demonstrating that the multipolar operator U_n and $\tilde{U}_n$ have the same effective Hamiltonian up to the order $\mathcal{O}(T^{(n-1)})$.

Although the rigorous bound is not tight, Eq. (5.8) and Eq. (5.10) suggest that, in the fast driving regime, the error only becomes notable after a sufficiently long time. Therefore, similar to Floquet systems, a long-lived prethermal state should appear in the rapid driving regime and can be approximated by the micro-canonical ensemble of H_F^0. The mean energy of the effective system $\langle H_F^0 \rangle$ is thus also a quasi-conserved quantity.

In the following, by using exact diagonalization, I substantiate the existence of the prethermalization in the rapid driving regime. Surprisingly, I discover that the prethermal lifetime follows a simple algebraic scaling versus frequency, and such a relation can be explained via a simple Fermi's golden rule calculation.

5.3 Prethermalization

Let me focus on a generic spin model described by the Hamiltonian

$$H_{\pm} = \sum_i J_x \sigma_i^x \sigma_{i+1}^x + J_z \sigma_i^z \sigma_{i+1}^z + (B_0 \pm B_x)\sigma_i^x + B_z \sigma_i^z, \tag{5.11}$$

where J_x, J_z are the nearest-neighbor exchange interactions, B_0, B_z are static fields, and B_x denotes the driving amplitude. Periodic boundary condition is used such that translation invariance of the Hamiltonian permits us to access the longer time simulation for larger system sizes. Although not shown here, I also verify that the following numerical observations maintain qualitatively the same in other systems, e.g. Bose-Hubbard model or Anderson localized system.

I use the mean energy of the effective system $\langle H_F^0 \rangle$ a measure for thermalization, which should remain constant during prethermalization before dropping to zero once

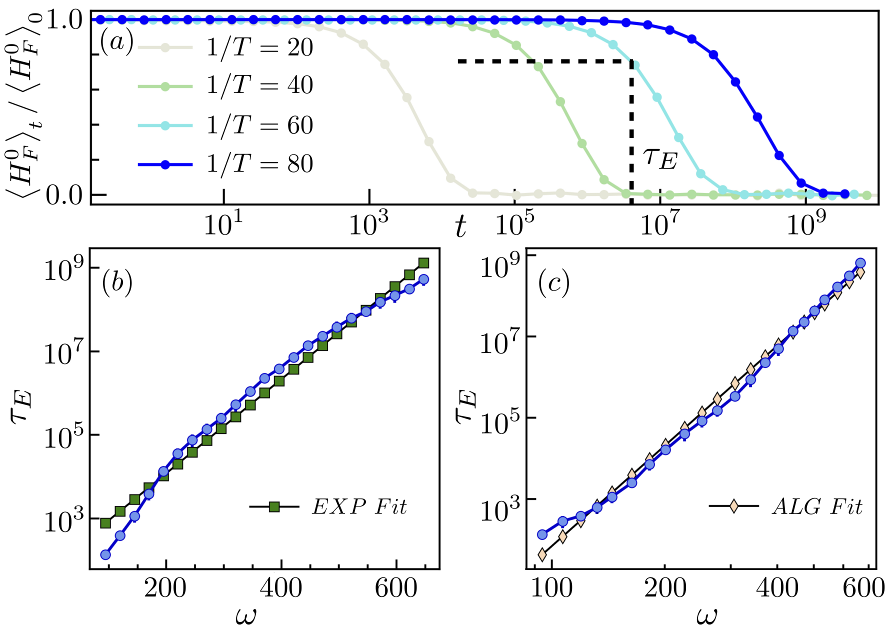

FIGURE 5.2: (a) Dynamics of mean energy with Thue-Morse driving as a function of characteristic time T, using parameters $\{J_z, J_x, B_x, B_z, B_0\} = \{1, 0.72, 0.61, 0.49, 0.21\}$ and system size $L = 20$. Prethermalization appears and the energy absorption is significantly suppressed. Panel (b) and (c) show the semi-log and log-log plot respectively of the thermalization time versus driving rate (blue circles). Straight lines in panel (b) (green squares) and (c) (pink diamonds) are obtained by an exponential fit and an algebraic fit, respectively. The numerical data (blue circles) curves down from an exponential fit as shown in panel (b) whereas in panel (c), it curves up from an algebraic fit.

the system heats up to infinite temperature. The quasiperiodic Thue-Morse driving is first studied. According to Eq. (5.1) and Eq. (5.5), I can recursively obtain the time evolution operator $U_n, \tilde{U}_n$ of time length 2^nT. This recursive construction enables the simulation of the dynamics for an exponentially long time by only computing a linearly increasing number of matrix multiplications, i.e. $|\psi(2^nT)\rangle = U_n\,|\psi(0)\rangle$.

Fig. 5.2 panel (a) depicts the dynamics of the mean energy density for different driving rates $1/T$ at stroboscopic time 2^nT. The initial state is taken with all spins pointing up. The mean energy remains constant over a large time window indicating the existence of prethermalization. In between stroboscopic times, I also verify that the mean energy remains quasi-conserved. After a long time scale τ_E, the system finally evolves to the thermal death and the mean energy drops to zero.

Next, I analyse the scaling of the thermalization times as a function of frequency. Numerically, the heating time τ_E is extracted by averaging the times such that $\langle H_F^0\rangle_t \,/\, \langle H_F^0\rangle_0 = 0.75, 0.75 \pm 0.03, 0.75 \pm 0.06$, see details in Appendix C.3. Figure 5.2 (b) and (c) show a semi-log plot and a log-log plot of the heating time τ_E,

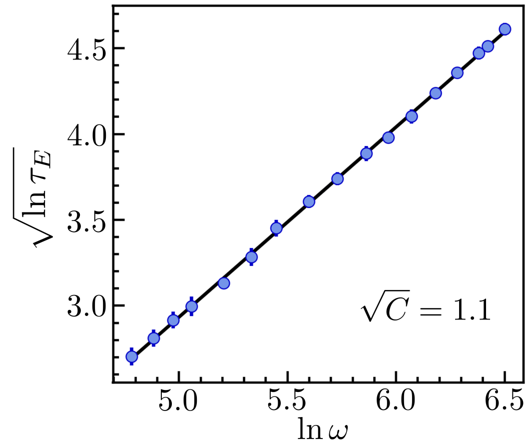

FIGURE 5.3: Dependence of the modified thermalization time $\sqrt{\ln \tau_E}$ against frequency $\ln \omega$. Numerical data (blue circles) fits well with a straight line of slope $\sqrt{C} = 1.1$, which implies that the heating time behaves like $\tau_E \sim e^{C[\ln(\omega/\lambda)]^2}$ as suggested in [193].

respectively. In the semi-log (log-log) plot, numerical data curves down (up) from a straight line, which indicates that the heating time is shorter than exponential but longer than algebraic in $\omega = 2\pi/T$. This is consistent with the prediction of the heating time for TMS driving proposed in Ref. [193] [1],

$$\tau_E \approx e^{C[\ln(\omega/\lambda)]^2}. \tag{5.12}$$

In Fig. 5.3, I plot the function $\sqrt{\ln \tau_E}$ against $\ln \omega$. A straight line of slope $\sqrt{C}$ would appear if Eq. (5.12) predicts the correct dependence on the driving frequency. Numerical data fits well with a straight line of slope $\sqrt{C} = 1.1$, which does not depend on initial state and converges for $L = 20$ as shown in the Appendix C.3.

I verified that the prethermal regime also exists for RMD with finite n and not only for the Thue-Morse limit but with a different scaling behaviour. Panel (a) of Fig. 5.4 depict the dynamics of mean energy for a random quadrupolar drive with all initial spins pointing down, where a similar lack of energy absorption can be observed. In Fig. 5.4 (b), the dynamics of entanglement entropy S_L is plotted for different frequencies. It first saturates to a prethermal plateau which is well captured by the zeroth order effective Hamiltonian. The entropy grows rapidly to the final value S_∞ as introduced in Eq. (1.26), confirming that the system heats up to infinite temperature.

[1] I contributed to the conceptual ideas for the derivation of Eq. (5.12) in Ref. [193] but did not derive this analytical form. The numerical verification presented in Figs. 5.2 and 5.3 are my own work.

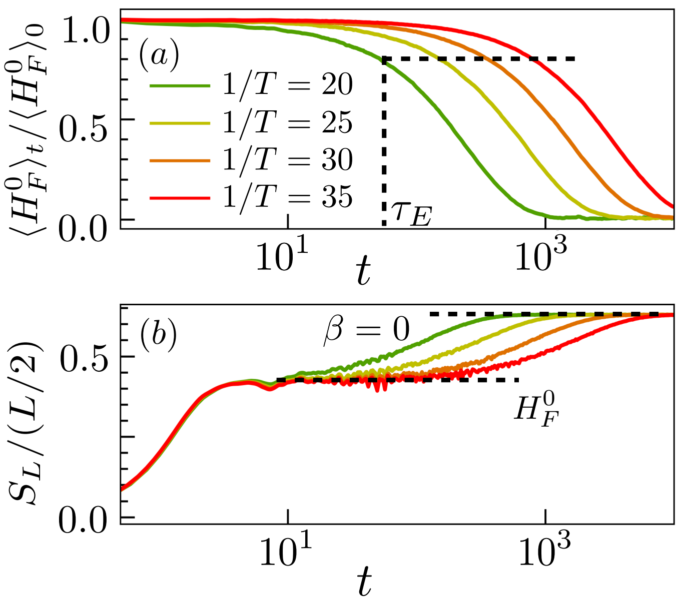

FIGURE 5.4: Evolution of (a) mean energy and (b) entanglement entropy with quadrupolar random driving, with parameters $\{J_z, J_x, B_x, B_z, B_0\} = \{1, 0.71, 3.2, 0.25, 0.21\}$, $L = 16$. Prethermal plateau of entanglement entropy appears for $1/T \geq 20$.

As before, I determine thermalization time by the thresholds $\langle H_F^0\rangle_t/\langle H_F^0\rangle_0 \sim 0.96 \pm 0.01$. In Fig. 5.5 (a), I show the scaling of τ_E on a double log plot for different RMD structures with $n = 0, 1, 2, 3$. In contrast to the scaling observed for the Thue-Morse driving, I identify an algebraic dependence

$$\tau_E \propto (1/T)^\alpha \quad \text{with} \quad \alpha \approx 2n + 1, \tag{5.13}$$

for $n \geq 1$. Interestingly, the fitted exponent strongly depends on the multipolar order and is to a good accuracy a simple function of n. I have verified that the scaling exponent is robust to change of parameters. In Fig. 5.5 (b), as a comparison, I also plot the same result on a log scale showing a clear deviation from an exponential fit towards larger $1/T$, especially for $n \geq 2$.

The thermalization time of the $n = 0$ RMD is short ($\tau_E < 1$ as seen in Fig. 5.5) and independent on the driving rate, suggesting a qualitative improvement for heating suppression by the multipolar structure. Indeed, I identify that Eq. (5.13) may also work for $n = 0$ with exponent $\alpha = 1$. However, the crucial difference to the case of $n > 0$ is that such scaling is only observed in the perturbative regime for small driving amplitudes.

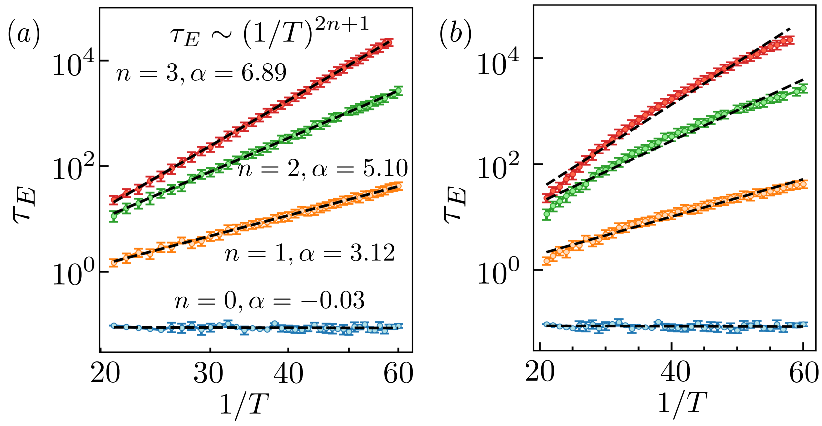

FIGURE 5.5: Thermalization time dependence on $1/T$ in log-log (c) and log scale (d) for $n-$multipolar drivings which confirms the algebraic dependence $(1/T)^\alpha$ with $\alpha \approx 2n+1$ for $n \geq 1$
.

5.4 Linear Response Theory

Although the bound in Eq. (5.8) implies the existence of a prethermal regime, it is not tight and insufficient to predict the $n-$dependent scaling behavior of the thermalization time. As an alternative, in the following, I show that the characteristic scaling can be understood via a simple generalization of Fermi's golden rule (FGR) as applied to Floquet systems [191, 192, 194–196].

I first follow Ref. [191] to review the FGR for Floquet systems described by the Hamiltonian $\hat{H}(t) = \hat{H}_0 + g(t)\hat{K}$, where $g(t)\hat{K}$ denotes a weak periodic driving with

$$g(t) = \sum_m g_m \sin(m\Omega t) \tag{5.14}$$

with $\Omega = 2\pi/T$ and g_m the strength of the Fourier components. In the linear response regime, after the short transient period, the system starts absorbing energy quanta independently from each Fourier mode m as illustrated in Fig. 5.6. The average rate of energy absorption over a driving period reads

$$\dot{E}(t) = \sum_{m>0} \dot{E}_m(t), \tag{5.15}$$

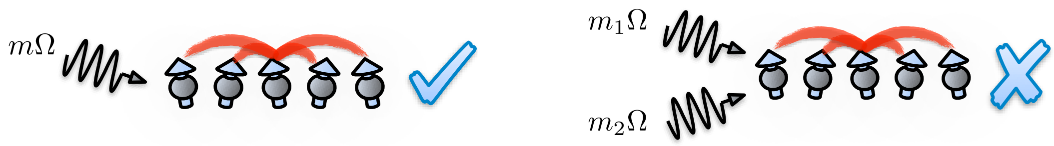

FIGURE 5.6: In the linear response regime, the dominant heating resource is the single-photon absorption. Multi-photon events rarely happen hence are neglected in the FGR calculation.

where $\dot{E}_m(t)$ is expected from Fermi's golden rule [191]

$$\begin{aligned}\dot{E}_m(t) = 2\pi g_m^2 \textstyle\sum_{i,f} \left|\left\langle E_f^0|\hat{K}|E_i^0\right\rangle\right|^2 \left(E_f^0 - E_i^0\right) P_i^0(t) \\ \times\delta\left(E_f^0 - E_i^0 \pm m\Omega\right),\end{aligned} \tag{5.16}$$

where $|E_i^0\rangle$ are the eigenstates of the static Hamiltonian $\hat{H}_0$ and, the probability of finding the eigenstate $|E_i^0\rangle$ in the density matrix $\hat{\rho}(t)$ at time t is defined as $P_i^0(t) = \left\langle E_i^0|\hat{\rho}(t)|E_i^0\right\rangle$. The thermalization rate can be written as

$$\Gamma(t) = \sum_m \dot{E}_m(t)/\left[E_\infty - E(t)\right], \tag{5.17}$$

where E_∞ represents the energy of the system at infinite temperature which turns to be zero in our case. It has been shown in Ref. [191] that this rate remains almost constant in the linear response regime. For fast drivings, extensive numerical evidence [191, 197] and theoretical analysis [13, 198–202] indicates that the thermalization rate is exponentially suppressed

$$\Gamma = \sum_m g_m^2 A e^{-m\Omega/\epsilon}, \tag{5.18}$$

where A, ϵ are both model dependent parameters. Accordingly, the inverse of the heating rate permits us to approximately estimate the prethermal life-time as $\tau \propto 1/\Gamma \sim e^{\Omega}$ for Floquet systems.

To extend the FGR to the $n-$RMD, the first task is analyzing the Fourier spectrum of the random multipolar sequence to generalize Eq. (5.14). Due to the temporal randomness of the driving, the frequency spectrum now becomes continuous and I approximate RMD by a continuous function as $g(t) = \int dx g_x \sin(x\Omega t)$. In Appendix C.2, by establishing the connection between the auto-correlation relation of the multipolar sequence and its Fourier decomposition, I obtain the following

$$g_x \propto x^n, \tag{5.19}$$

suggesting an algebraic suppression at low frequencies.

Similar to the Floquet case, in the linear response regime it is assumed that the system absorbs energy from each frequency mode independently. As such, Eq. (5.18) needs to be modified as a continuous integral as

$$\begin{aligned}\Gamma &\propto \int_0^\infty dx x^{2n} e^{-x\Omega} = \int_0^\infty d(x\Omega)(x\Omega)^{2n} e^{-x\Omega}\Omega^{-2n-1} \\ &= \Omega^{-2n-1}\int_0^\infty dy y^{2n} e^{-y} = \Omega^{-2n-1}(2n)!,\end{aligned} \tag{5.20}$$

where I use the formula

$$\int y^n e^{cy} dy = e^{cy}\sum_{i=0}^{n}(-1)^{n-i}\frac{n!}{i!c^{n-i+1}}y^i. \tag{5.21}$$

Correspondingly, the thermalization time scales as $(1/T)^{2n+1}$ in accordance with the numerical results as presented in Fig. 5.5 (a).

The Fourier spectrum of the quasiperiodic TMS driving vanishes as $x^{(n\to\infty)}$ for $x \to 0$, therefore I expect the scaling behavior will be faster than any algebraic function. One can also approximate such low frequency suppression as a pseudogap in the Fourier spectrum, the size of which is proportional to Ω, see details in Appendix C.2. Therefore, the most dominating heating rate is given by the smallest allowed frequency and I can simply model $g_x \propto \delta(x - x_0)$ to obtain

$$\Gamma_{TMS} \propto \int_0^\infty \mathrm{d}x\delta(x-x_0)Ae^{-x\Omega/\epsilon} \propto e^{-x_0\Omega/\epsilon}, \tag{5.22}$$

with $x_0\Omega$ the gap size. Therefore, an exponential scaling of the thermalization time $\mathcal{O}(e^{1/T})$ is expected similar to Floquet systems. However, such an approximation overestimates the suppression of energy absorption hence heating happens at an earlier time. Therefore, based on the linear response theory, the heating time should be shorter than exponential but longer than algebraic in accordance of the numerical results in Fig. 5.2 [2].

Overall, the fact that FGR rate Eq. (5.20) agrees with numerical results implies a surprisingly simple picture, that the heating is dominantly induced by the independent absorption of modes at low energies even for the continuous spectrum. Higher order effects deserves more investigation as the typical algebraic scaling persists even in the non-perturbative regime for which FGR is not expected to work generically. It implies that the multipolar structure also suppresses multi-modes heating channels which can be potentially analysed via the 2nd order time-dependent perturbation theory.

5.5 Random Multipolar Discrete Time Crystal

Finally, I provide a concrete example of a prethermal non-equilibrium phase for the family of RMDs. I extend the idea of Floquet DTCs to a situation where the drive contains *temporally random* components between the spin flips. To be precise, I introduce the global spin flipping operators, $X = \exp\left(i\frac{\pi}{2}\sum_i \sigma_i^x\right) \sim \prod_i \sigma_i^x$ in between the dipolar operators as

$$U_1' = e^{-iH_-T}e^{-iH_+T}X,\ \tilde{U}_1' = e^{-iH_+T}e^{-iH_-T}X. \tag{5.23}$$

According to Eq. (5.6), both dipolar operators can be approximated by the effective Hamiltonian as

$$U_1',\ \tilde{U}_1' \approx e^{-i(H_++H_-)T}X. \tag{5.24}$$

Ideally, if the effective Hamiltonian, $H_F^0 = (H_+ + H_-)/2$, preserves the $\mathbb{Z}_2$ Ising symmetry, products of $U_1', \tilde{U}_1'$ can be approximated as $(e^{-iH_F^0 2T}X)^2 = e^{-iH_F^0 4T}$ analogous to the Floquet DTC [see Eq. (1.37)]. As a consequence in the prethermal regime, the time evolution at stroboscopic times $4T$ can be well-captured by the effective Hamitonian H_F^0. Therefore, for a $\mathbb{Z}_2$ symmetry broken initial state, the local magnetization will persistently oscillate between ± 1 with period $4T$, doubling the period $2T$ of spin flips. Such a random prethermal DTC should still persist if the $\mathbb{Z}_2$ symmetry of H_F^0

[2] A non-perturbative calculation based on Magnus expansion and the self-similarity of Thue-Morse sequence was performed in Ref. [193], where the rigorous bound for heating was obtained as Eq. (5.12) for TMS driving.

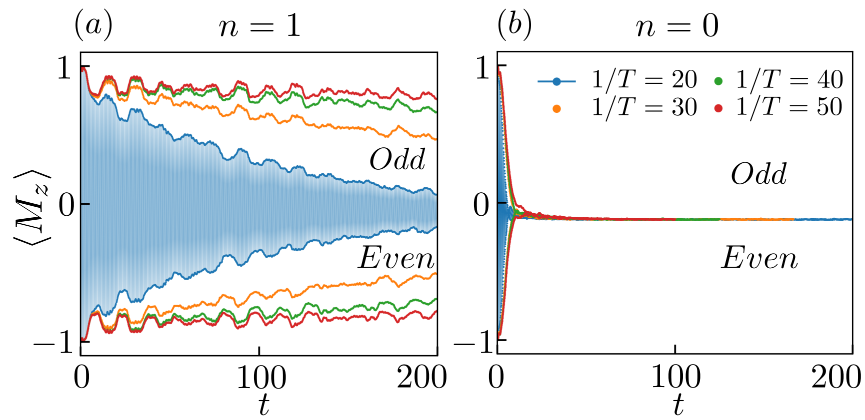

FIGURE 5.7: Dynamics of the magnetization of the central spin induced by a random dipolar drive with additional spin flips, using parameters $\{J_z, J_x, B_z, B_0, B_x\} = \{1, 0.315, 0.21, -0.05, 0.75\}, L = 18$. A long-lived prethermal DTC exists with $n = 1$ RMD driving (a), while heating is inevitably fast for the $n = 0$ random case (b).

is weakly broken, the lifetime of which will nevertheless decrease depending on the perturbation.

In Fig. 5.7 (a), I have numerically verified the existence of a prethermal DTC with 1−RMD starting from a fully polarized initial state [3]. The lifetime significantly increases for larger driving frequency, in particular for $T^{-1} = 50$ the amplitude of the period-doubling magnetization does not decrease appreciatively up to $t = 200$. I also verify the robustnes of the prethermal DTC for weak imperfect spin flip operations. Fig. 5.7 also contrasts the prethermal nature of RMD to the one of a purely random drive (shown in panel (b)) built from

$$U'_+ = e^{-iH_+T}X, \; U'_- = e^{-iH_-T}X. \tag{5.25}$$

As U'_+, U'_- also perform perfect spin flips, period-doubling oscillations appear but only for a short transient period ($t \lesssim 10$). Thermalization is inevitably fast and prethermal DTC does not exist.

Beyond Floquet DTC or discrete time quasi-crystals, the random drives completely break discrete time translation symmetry, thus enriching the growing zoo of non-equilibrium phases of matter.

[3] Strictly speaking, uniform nearest-neighbour interaction is insufficient to stablize ferromagnetism in 1D at finite temperature. The presence of disorders or long-range interactions is necessary for DTC for generic symmetry-broken initial states. The persist period-doubling behaviour observed here is mainly because of the special fully polarized initial state. See more discussions in Ref. [73, 203].

5.6 Discussion

RMD present an elementary and controlled way to introduce temporal randomness to driven systems. The resulting tunable algebraic prethermalisation adds a new aspect to our understanding of paths towards thermalization. There are some direct extensions of the current RMD protocol. First, instead of considering the elementary operators constructed via static Hamiltonians as in Eq. (5.1), one can consider the time-dependent Hamiltonian $H_{\pm}(t)$ and the operator $U_{\pm} = \mathcal{T} e^{-i\int_0^T dt H_{\pm}(t)}$. The additional time dependence permits us to engineer the prethermal non-equilibrium phases with rich properties, for instance the anomalous Floquet-Anderson insulator with quantized charge pumping [18].

Second, RMD and the Thue-Morse driving can be generalized to involve more elementary unitaries. For example, one can start from three distinct unitaries $U_0 = e^{-iH_0T}$, $U_1 = e^{-iH_1T}$, and $U_2 = e^{-iH_2T}$ constructed from local Hamiltonians H_σ ($\sigma = 0, 1, 2$). Similar as Eq. (5.5), U_n^σ are defined cyclically as $U_n^\sigma = U_{n-1}^{\sigma+2} U_{n-1}^{\sigma+1} U_{n-1}^{\sigma}$, where the sums $\sigma+1$ and $\sigma+2$ are defined modulo 3. Fourier spectrum of the driving sequence might exhibit different types of frequency suppression, hence, leading to other interesting scaling behavior of the thermalization time.

RMD represents a simple form of spectral engineering in driven systems and it is worth to explore more general method to design the spectrum of driving protocols. For instance, one possible approach would be first to sample a pre-defined frequency spectrum with desired properties, then convert it back to a correlated sequence in time via the inverse Fourier transformation [204]. It would be interesting to establish connections between dynamical response of quantum many-body systems and the engineered temporal correlation.

Chapter 6

Conclusion and Outlook

This thesis explored several new forms of ergodicity-breaking phenomena, with a particular focus on QMBS in both static and Floquet systems with TTS, as well as prethermalization in aperiodically driven systems when TTS is absent.

In Chapter 2, I introduced an experimentally feasible proposal for the realization of QMBS via Floquet engineering in optical lattices. Hopping channels between particular Fock states can be suppressed to zero and HSF naturally appears. Compared with Rydberg atomic arrays where QMBS were first discovered, bosonic systems have a much larger local Hilbert space and substantially more initial states accessible in optical lattice experiments. For example, systems with different fillings, which can be easily controlled physically, feature a great variety of scars. One can exploit such freedom to explore versatile paths towards thermalization by suppressing different hopping channels in a controllable manner.

In Chapter 3, I addressed the intriguing question of whether there are non-ergodic QMBS with volume-law entanglement in an interacting many-body system. Or from the perspective of dynamics, can coherent oscillations of local observables in many-body systems coexist with volume-law entanglement in a standard quench setting? All previously discovered QMBS can only establish sub-extensive entanglement, which has also been regarded as a clear indicator of QMBS in the spectrum. I confirm the existence of this counter-intuitive phenomenon via a minimally coupled multi-component system — the kinetically constrained orthogonal metal — which naturally hosts two dynamical fractionalized d.o.f. The emergent $\tilde{\tau}-$spin are thermal and rapidly generate extensive entanglement, while the other $f-$fermion exhibit persistent oscillations as a result of Hilbert space fragmentation. As the orthogonal metal is itself constructed from a slave-particle description of strongly correlated phases, the orthogonal QMBS can potentially exist in non fine-tuned settings.

Kinetically constrained multi-component systems are a largely unexplored but experimentally relevant field. It is instructive to compare our model to the alternative Z_2 lattice gauge model of Ref. [150] which also hosts two emergent d.o.f., the matter fermions and gauge charges. However, the gauge d.o.f. are static, hence, cannot generate extensive entanglement if the fermion is constrained. The separability of the emergent dynamical d.o.f. in my model is also linked to recent works on the disordered Hubbard model where disorder may appear only for one type of excitation [205, 206]. There, although the disorder only appears for charge d.o.f., the spin transport is significantly influenced and becomes subdiffusive. On the contrary, in our model, kinetic constraints only locally enter the emergent fermionic d.o.f. while the $\tilde{\tau}$-spin dynamics remains ergodic. In the future, a systematic comparison between different kinetically constrained multi-component systems would be worthwhile.

The discovery of QMBS has significantly enriched our fundamental understanding of ergodicity-breaking phenomena. On the application side, it is also of great interest to explore whether they can be helpful for the development of new quantum technologies. For instance, instead of simply isolating a quantum system as much as possible to avoid thermalization, one can potentially exploit fragmented Hilbert subspaces, which can itself be engineered via suitable driving protocols. As such, a quantum state can naturally evolve to a coherent superposition of Fock states by choice [144], which are potentially beneficial for precision sensing.

Then I explored possible mechanisms leading to ergodicity-breaking dynamics when many-body systems are modulated by quasi-periodical drives where TTS of the driving is explicitly broken. Up to now, there is no universal theoretical framework, e.g. Floquet theory for TTS-preserving systems, and the numerical simulation of their time evolution is computationally expensive. In Chapter 4, inspired by spiral magnets, I proposed the idea of FTS which can be mapped to usual Floquet systems via time-dependent unitary transformations.

As a fine-tuned toy model, a FTS is first demonstrated in a two-level system where an exact solution of the time evolution can be obtained. Then I generalize the idea to many-body systems with disorder, which has further been shown to host a DTQC which breaks the quasi-periodic TTS. Crucially, this intriguing phenomenon persists up to the longest numerically accessible time scale when generic perturbations are present which breaks the equivalence between FTS and Floquet systems. Therefore, I argue that the DTQC is a stable non-equilibrium phase of matter more fundamental than the fine-tuned FTS construction.

To investigate more generic dynamical properties of driven systems without TTS, I study the so-called RMD systems in Chapter 5. An integer n parametrizes the temporal correlation of the random sequence, $n = 0$ and $n \to \infty$ limit correspond to the purely random and quasi-periodic Thue-Morse sequence respectively. A long-lived prethermal regime appears for $n \geq 1$, the lifetime of which scales algebraically for larger driving frequencies as $T^{-(2n+1)}$ which converts to the scaling $e^{C[\ln(1/T)]^2}$ for the Thue-Morse driving, in agreement with the numerical simulations.

RMD provides a simple example of spectral engineering as the Fourier decomposition of the correlated sequences of multipoles decreases as a power law T^{-n} with an integer n, which becomes a pseudogap in the $n \to \infty$ Thue-Morse limit. Such suppression of low frequency property underpins a simple theory of FGR explaining the observed slow heating and the dependence on the multipolar order n. Remarkably, the prethermalization also occurs in the strong driving regime for which FGR is not expected to work. It indicates that not only the single-photon absorption but also the multi-photon processes which cannot be simply captured by the linear response theory are also suppressed. Although the subsequent rigorous results obtained by generalizing Floquet-Magnus expansion [193] also imply the suppression of higher order processes, a direction calculation via the higher order FGR [207], which could in principle provide more physical intuition regarding the heating, would be worthwhile.

The idea of spectral engineering can indeed be generalized to other types of random sequences. Besides the Thue-Morse sequence, one might search for other aperiodic sequences whose randomized version can also lead to prethermalization. Another broad class of random sequences with hyperuniform correlations [204, 208] would be of great interest to study. Their fluctuations at large scales are sufficiently reduced resulting in a suppressed frequency behavior reminiscent of RMD but with a continuously tunable scaling exponent [204].

A different interesting question regarding RMD concerns what types of non-trivial prethermal states can be achieved apart from the random multipolar discrete time crystalline behavior presented in this thesis. It is naturally expected that (many-body) localization will not be stable with random driving [209], but how does the additional multipolar structure protect the localization? Can localization further stabilize the prethermal topologically protected phases [18] and result in a new scaling of prethermal lifetime better than $T^{-(2n+1)}$? Another intriguing direction would be searching for fundamentally different prethermal phases beyond Floquet, which emerges particularly because of the temporally correlated randomness.

There are countless ways to drive a system in the absence of TTS. However, identifying protocols that lead to novel universal phenomena and are theoretically tractable remains a big challenge. Based on the current exploration of FTS and RMD systems, the present work shows that aperiodically driven systems are expected to exhibit a much lower degree of universality compared with Floquet systems. To analyze aperiodically driven systems, one cannot rely on the theoretical tools of Floquet theory and it is fair to say that we are lacking similarly powerful tools for aperiodic systems. However, the specific examples of this thesis show that many techniques developed for Floquet systems can still be surprisingly helpful even if TTS is absent. Naturally, beyond the discrete RMD drive protocols one can expect that there are plenty of other types which go beyond the scope of the Floquet framework. Therefore, I expect that formulating new methods and unifying our understanding of aperiodically driven systems remains a formidable challenge for the future.

With this thesis, I addressed several crucial problems and opened new avenues in quantum many-body systems. Particularly, I proposed a few simple yet insightful models demonstrating conceptually new non-ergodic phenomena which substantially deepen our understanding of quantum thermalization and lack thereof. Most of these models can already be experimentally implementable. I believe these works will be of broad interest and can shed further light on the future exploration of quantum many-body phenomena.

Appendix A

Derivation of Effective Hamiltonian

A.1 Rotating Frame

Here we explain the details for deriving the effective Hamiltonian of the doubly modulated Bose-Hubbard model. In the physical frame, the Hamiltonian reads

$$\hat{H}(t) = \sum_{\langle pq \rangle} \hat{c}_p^\dagger J_{pq} \hat{c}_q + \frac{U(t)}{2} \sum_p \hat{n}_p(\hat{n}_p - 1) + F(t) \sum_p \epsilon_p \hat{n}_p. \tag{A.1}$$

We can only perform high frequency expansion if the driving frequency of $U(t), F(t)$ is the dominating energy scale, hence, we want to transform to the rotating frame via the unitary transformation

$$R(t) = \exp\left[i \left(\sum_p \theta_p(t) \hat{n}_p + \frac{\Gamma(t)}{2} \sum_p \hat{n}_p \left(\hat{n}_p - 1 \right) \right) \right], \tag{A.2}$$

where $\Gamma(t) = \int_0^t d\tau U(\tau)$ and $\theta_p(t) = \epsilon_p \int_0^t d\tau F(\tau)$. In the rotating frame, the Hamiltonian transforms as $\tilde{H}(t) = R\hat{H}(t)R^\dagger - iR\dot{R}^\dagger$, where the second terms cancels the time-dependent modulation of energy and interaction. Therefore we obtain

$$\tilde{H}(t) = R(t) \sum_{\langle pq \rangle} \hat{c}_p^\dagger J_{pq} \hat{c}_q R^\dagger(t). \tag{A.3}$$

The above unitary $R(t)$ can be decomposed as $R(t) = R_1(t)R_2(t)$ where

$$R_1(t) = \exp\left[i \sum_p \theta_p(t) \hat{n}_p \right], R_2(t) = \exp\left[i \frac{\Gamma(t)}{2} \sum_p \hat{n}_p \left(\hat{n}_p - 1 \right) \right], \tag{A.4}$$

and $[R_1, R_2] = 0$. We first perform the rotation $R_1(t)$ as

$$\tilde{H}(t) = \sum_{\langle pq \rangle} J_{pq} R_1(t) \hat{c}_p^\dagger \hat{c}_q R_1^\dagger(t). \tag{A.5}$$

The following formula is particularly useful to compute the unitary transformation

$$e^X Y e^{-X} = \sum_{n=0}^{\infty} \frac{[(X)^n, Y]}{n!}, \tag{A.6}$$

where $[(X)^n, Y] \equiv \underbrace{[X, \cdots [X, [X, Y]] \cdots]}_{n \text{ times}}, [(X)^0, Y] \equiv Y$. In our case, we choose $X = i \sum_k \theta_k n_k$ and $Y = c_p^\dagger c_q$, we obtain

$$R_1(t) \hat{c}_p^\dagger \hat{c}_q R_1^\dagger(t) = \sum_{n=0}^{\infty} \frac{[(X)^n, Y]}{n!} = c_p^\dagger c_q \sum_{n=0}^{\infty} \frac{[i(\theta_p(t) - \theta_q(t))]^n}{n!} = c_p^\dagger c_q e^{i(\theta_p(t) - \theta_q(t))}. \tag{A.7}$$

Similarly one can carry out the second rotation $R_2(t)$, but the algebra can be simplified by noting that the hopping term $\hat{c}_p^\dagger \hat{c}_q$ preserves the total particle number $\sum_p \hat{n}_p$. Therefore, the unitary transformation of $R_2(t)$ reduces to

$$\begin{aligned} R_2(t) \hat{c}_p^\dagger \hat{c}_q R_2^\dagger(t) &= \exp\left[i \frac{\Gamma(t)}{2} \sum_p \hat{n}_p^2 \right] \hat{c}_p^\dagger \hat{c}_q \exp\left[-i \frac{\Gamma(t)}{2} \sum_p \hat{n}_p^2 \right] \\ &= c_p^\dagger \sum_{n=0}^{\infty} \frac{[i\Gamma(t)(n_p - n_q)]^n}{n!} c_q = c_p^\dagger e^{i\Gamma(t)(n_p - n_q)} c_q. \end{aligned} \tag{A.8}$$

In the end, in the rotating frame, the Hamiltonian reads

$$\tilde{H}(t) = \sum_{\langle pq \rangle} \hat{c}_p^\dagger \hat{A}_{pq}(t) \hat{c}_q, \tag{A.9}$$

where the hopping term modifies to

$$\hat{A}_{pq}(t) = J_{pq} e^{i(\theta_p(t) - \theta_q(t))} e^{i\Gamma(t)(\hat{n}_p - \hat{n}_q)}, \tag{A.10}$$

the time average of which will give the lowest order contribution to the effective Hamiltonian. It is worth noting that the derivation above can be modified to fermionic system as well. Moreover, Eq. (A.8) can be generalized to other density-density interactions which do not need to be short-ranged. It will be interesting to explore other emergent processes by driving longer-ranged interaction.

A.2 Driving Profile

The following driving profile is used in Chapter 2, $U(t) = U_d \cos(\omega t)$, $F(t) = F_2 \cos(2\omega t) + F_4 \cos(4\omega t)$, therefore we have

$$\begin{aligned} \Gamma(t) &= \int_0^t d\tau U(\tau) = \tilde{U}_d \sin(\omega t), \\ \theta_p(t) &= \epsilon_p \int_0^t d\tau F(\tau) = \epsilon_p \left[\tilde{F}_2 \sin(2\omega t) + \tilde{F}_4 \sin(4\omega t) \right], \end{aligned} \tag{A.11}$$

where $\tilde{U}_d = U_d/\omega$, $\tilde{F}_2 = F_2/2\omega$ and $\tilde{F}_4 = F_4/4\omega$ for simplification. The modified time-dependent hopping in the rotating frame reduces to

$$\hat{A}_{pq}(t) = J_{pq} \exp\left[i(q-p)\left(\tilde{F}_2 \sin(2\omega t) + \tilde{F}_4 \sin(4\omega t) \right) + i\tilde{U}_d \sin(\omega t)\left(\hat{n}_p - \hat{n}_q \right) \right]. \tag{A.12}$$

Its time average over one period reproduces the modified hopping rate in Eq. (2.6)

$$\hat{A}^0_{pq}(\hat{n}_p, \hat{n}_q) = -J\mathcal{J}_0\Big(\tilde{U}_d(\hat{n}_p - \hat{n}_q), \tilde{F}_2(p-q), \tilde{F}_4(p-q) \Big), \tag{A.13}$$

where $\mathcal{J}_0$ denotes the zeroth order three dimensional Bessel function defined via nth order one dimensional Bessel function $\mathcal{B}_n$ as [210]

$$\mathcal{J}_0(x, y, z) = \sum_{s_2, s_4 = -\infty}^{+\infty} \mathcal{B}_{-2s_2 - 4s_4}(x) \mathcal{B}_{s_2}(y) \mathcal{B}_{s_4}(z). \tag{A.14}$$

$\mathcal{J}_0$ has the symmetry $\mathcal{J}_0(x, y, z) = \mathcal{J}_0(-x, y, z) = \mathcal{J}_0(x, -y, -z)$ which can be proved by using the symmetry property $\mathcal{B}_{-n}(x) = (-1)^n \mathcal{B}_n(x)$.

A.3 Numerical Implementation

For numerical calculation with exact digonalization, normally only single operators or simple products of them can be easily converted into matrix form [135], whereas the above density-assisted tunneling [Eq. (A.13)] in a highly-nonlinear form is difficult to implement. However, one can instead use Taylor expansion to approximate the Bessel function, and for instance the nearest-neighbor hopping reads

$$\hat{A}^{0}_{p,p+1} = -j_0 \sum_{\nu=0}^{\infty} \frac{\tilde{U}_d^{\nu} \left(\hat{n}_p - \hat{n}_{p+1}\right)^{\nu}}{\nu!} \left. \frac{\partial^{\nu}}{\partial \tilde{F}_1^{\nu}} \mathcal{J}_0 \left(\tilde{F}_1, \tilde{F}_2, \tilde{F}_4\right) \right|_{\tilde{F}_1 = 0}, \tag{A.15}$$

with

$$\frac{\partial^{\nu}}{\partial \tilde{F}_1^{\nu}} \mathcal{J}_0 \left(\tilde{F}_1, \tilde{F}_2, \tilde{F}_4\right) = \sum_{s_2, s_4 = -\infty}^{+\infty} 2^{-\nu} \sum_{k=0}^{\nu} C_n^k \mathcal{B}_{2k-\nu-2s_2-4s_4} \left(\tilde{F}_1\right) \mathcal{B}_{s_2} \left(\tilde{F}_2\right) \mathcal{B}_{s_4} \left(\tilde{F}_4\right), \tag{A.16}$$

where $\tilde{F}_1$ is introduced for the calculation of derivative. It is worth noting that Eq. (A.15) converges badly when the density difference between adjacent sites is large. Therefore, the maximum bosonic particle filling should be relatively low, e.g. below 12 in our simulation, which physically corresponds to a system with relatively large static onsite energy penalty either induced by potential or contact interaction.

Appendix B

Fermionic Dynamics with Density-Density Interaction

B.1 Non-Thermal Dynamics

The persistent oscillation in fermionic sector is robust in the presence of any perturbations which preserves the structure of Hilbert space fragmentation and fractionalization. For example, here we consider fermionic density-density interaction $\delta V = \delta \sum_i n_i n_{i+1} + 0.3 n_i n_{i+2} + 0.55 n_i n_{i+3}$ and plot the dynamics of the initial state $|01110110\rangle$. Compared with the case in Sec. 3.2.2, here the middle four sites are all active, hence, spanning an isolated subspace of dimension larger than 2. Therefore the dynamics becomes quasi-periodic as seen in Fig. B.1. We also depicted the dynamics in the presence of additional fermionic interaction $\delta = 0.3$ (orange), which deviates from the blue one but maintains the persistent oscillation.

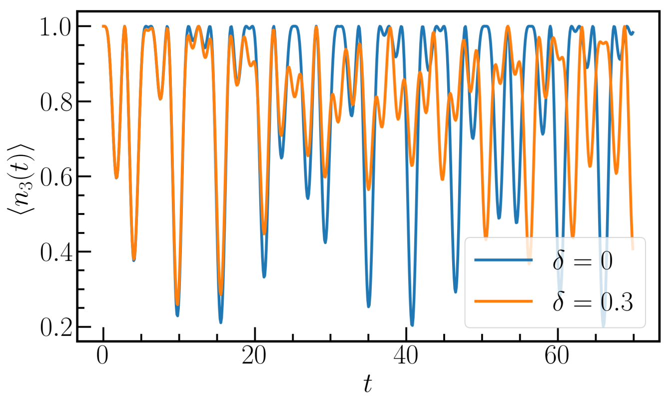

FIGURE B.1: Comparison between the dynamics with or without fermionic density-density interaction. Coherent oscillation survives although the oscillating patterns are different. Parameters are the same as in Fig. 3.3.

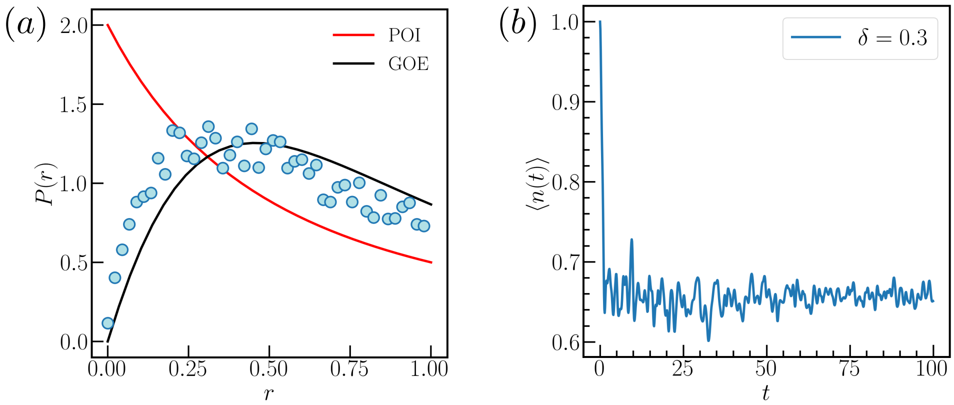

FIGURE B.2: (a)Level statistics of a thermal fermionic sector. (b) Local particle number quickly thermalizes.

B.2 Non-Integrable Fermionic Sector

There are also initial states that thermalize because the dimension of the corresponding fermonic fragmented subspace grows exponentially with system size. For instance, we consider a fermionic state $|111011101101110111011011100\rangle$ containing 27 sites and 19 fermions, the fragmented subspace involves 9240 fermonic Fock states in the momentum and positive parity sector. The level statistics (see details in Sec. 1.2.2) in the subspace is plotted in Fig. B.2 exhibiting Wigner-Dyson (non-integrable) statistics and clearly shows level repulsion. The quench dynamics of the particle number on the middle site is illustrated in the right panel for $\delta = 0.3$, which equilibrates rapidly without any coherent oscillations.

Appendix C

Appendix for RMD and TMS Driving

C.1 Proof of the Bound Eq. (5.8)

Here closely following Ref. [19] we derive the bound for the time evolution operators of the random dipolar drives, which is made up of random sequences of dipoles $U_1 = U_-U_+$ or $\tilde{U}_1 = U_+U_-$ with

$$U_+ = \exp(-iTH_+), U_- = \exp(-iTH_-). \tag{C.1}$$

The time-dependent Hamiltonian for each dipole can be written respectively as

$$\begin{aligned} H^A(t) &= H_-(0<t<T), H_+(T<t<2T), & \text{(C.2)} \\ H^B(t) &= H_+(0<t<T), H_-(T<t<2T), & \text{(C.3)} \end{aligned}$$

which can also be rewritten as $H^{A/B}(t) = H_{\text{static}} + V^{A/B}(t)$, with H_{static} being the time-independent part. We consider a general few body Hamiltonian involving at most k-body interactions with finite k:

$$H_{\text{static}} = \sum_{|X|\le k} h_X, \quad V^{A/B}(t) = \sum_{|X|\le k} v_X^{A/B}(t), \tag{C.4}$$

where X labels the set of interacting sites and $|X|$ is the size of the set. Note, we also have the property

$$v_X^{A/B}(0 < t < T) = v_X^{B/A}(T < t < 2T), \tag{C.5}$$

which will be used later.

We use the parameter $J^{B/A}$ to denote the local interaction strength (or single particle energy) of the system:

$$\sum_{X:X\ni i} \left(\|h_X\| + \|v_X^{A/B}(t)\|\right) \leq J^{A/B}, \tag{C.6}$$

where $||\ldots||$ is the operator norm, and $\sum_{X:X\ni i}$ denotes the summation w.r.t. the supports containing the spin i. Based on Eq. (C.5), we can easily see $J^A = J^B := J$ and define $\lambda := 2kJ$ as the typical local energies of the system. We introduce the average driving norm as

$$V_0^{A/B} := \sum_{|X|\leq k} \frac{1}{2T} \int_0^{2T} \left\|v_X^{A/B}(t)\right\| dt, \tag{C.7}$$

where $2T$ is used because each dipole takes time $2T$. Moreover by separating the time integral and using Eq. (C.5), one arrives at

$$\begin{aligned} V_0^{A/B} &= \sum_{|X|\leq k} \frac{1}{2T} \Big[\int_0^T \left\|v_X^{A/B}(t)\right\| dt + \int_T^{2T} \left\|v_X^{A/B}(t)\right\| dt \Big] \\ &= \sum_{|X|\leq k} \frac{1}{2T} \int_0^T \Big[\left\|v_X^{B/A}(t)\right\| + \left\|v_X^{A/B}(t)\right\| \Big] dt. \end{aligned} \tag{C.8}$$

One can realize that $V_0^A = V_0^B$, which will be denoted as V_0 in the following.

According to Ref. [19], both of the dipole operators, U_1 and $\tilde{U}_1$, can be approximated by the same zeroth order effective Hamiltonian $H_F^0 = (H_+ + H_-)/2$, and the error is bounded as

$$\left\|U_1/\tilde{U}_1 - e^{-iH_F^0 2T}\right\| \leqslant [6 \cdot 2^{-n_0} + \lambda T]V_0 2T. \tag{C.9}$$

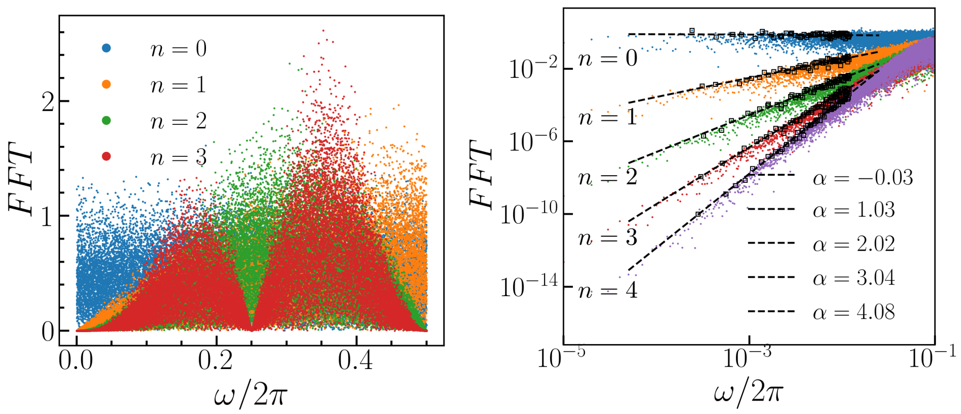

FIGURE C.1: Left: Fourier spectrum of random multipolar sequences for different n. Right: Log-Log plot for the spectrum. Suppression at low frequencies scales algebraically as ω^n.

The exponent

$$n_0 := \left\lfloor \frac{1}{16\lambda(2T)} \right\rfloor = \mathcal{O}(T^{-1}), \tag{C.10}$$

with the floor function $\lfloor . \rfloor$, denotes the optimal order of the Floquet-Magnus expansion before it diverges [19]. The error accumulates during the time evolution hence the dynamics deviate from the one H_F^0 predicts. The rigorous bound in Eq. (5.8) can be obtained by using Eq. (C.9) and the triangle inequality for arbitrary unitaries

$$\begin{aligned} &\|W_1W_2 - V_1V_2\| = \|(W_1 - V_1)W_2 + V_1(W_2 - V_2)\| \\ &\leq \|(W_1 - V_1)W_2\| + \|V_1(W_2 - V_2)\| \\ &= \|W_1 - V_1\| + \|W_2 - V_2\|, \end{aligned} \tag{C.11}$$

where we used that unitary operators do not change the norm in the last equality.

C.2 Algebraic Suppression of Spectrum at Low Frequency

We now can compare the real part of the discrete Fourier transformation of sequences for different n. As seen in the left panel of Fig. C.1, for a random sequence (blue, $n = 0$), the spectrum fluctuates randomly over all frequencies with a flat envelop. Once imposing the multipolar structure, several suppression of frequencies appears at different positions, for example at $\omega = 0$ for $n \geq 1$, and ar $\omega = \pi$ for $n \geq 2$. By plotting the spectrum on a Log-Log scale in the right panel, we can fit the envelope of the spectrum and identify the scaling of suppression at low frequencies as ω^n.

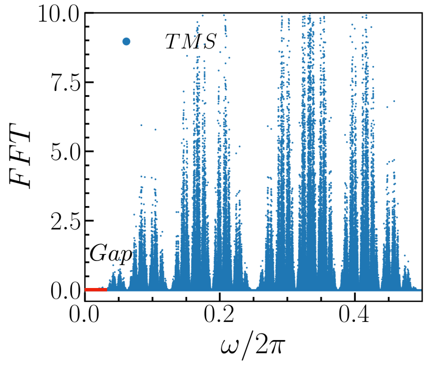

FIGURE C.2: Frequency spectrum for the TMS.

The quasiperiodic Thue-Morse sequence (TMS) corresponds to the random multipolar sequence in the $n \to \infty$ limit, and practically we use $n = 18$ to approximate it. In this limit, the low frequency spectrum scales as $\omega^{n\to\infty}$ thus fast approaching zero for $\omega \to 0$. Hence, the algebraic scaling converts to a gap at low frequency as observed in Fig. C.2.

Analytical Derivation of the Low Frequency Behavior.– The low frequency scaling can be rationalized by the autocorrelation function of the sequence. The autocorrelation function for the $n-$multipolar sequence $x^{(n)}(t)$ is defined as

$$R^{(n)}(t,\tau) = \langle x^{(n)}(t)x^{(n)}(t+\tau)\rangle, \tag{C.12}$$

where $\langle \dots \rangle$ denotes the average over both different random realization and t. In this case, $R^{(n)}(t,\tau)$ becomes translation invariant in t. For the fully random sequence $n = 0$, one obtains the standard white noise form $R^{(0)}(\tau) = \delta_{\tau,0}$; for the dipolar sequence $n = 1$, $R^{(1)}(\tau) = \delta_{\tau,0} + \delta_{\tau,0} - \delta_{\tau,1} - \delta_{\tau,-1}$ in each dipolar unit cell; etc. The Fourier transformation $\hat{R}^{(n)}(\omega)$, which is also known as the spectral density, can be defined as

$$\hat{R}^{(n)}(\omega) = \int_{-\infty}^{\infty} d\tau R^{(n)}(\tau)e^{i\omega\tau}. \tag{C.13}$$

The dipolar sequence has $\hat{R}^{(1)}(\omega) = 2 - 2\cos(\omega)$, exhibiting the scaling ω^2 at low frequencies.

For $n > 1$, one can derive the scaling in the following way. First, we know the $n-$multipolar unit cells are formed by two anti-aligned $(n-1)-$multipoles of size 2^{n-1}.

Accordingly, each $(n-1)-$multipole contributes $R^{(n-1)}(\tau)$ to the anticorrelation, and the interplay between different types of $(n-1)-$multipoles gives the negative contribution $-R^{(n-1)}(\tau \pm 2^{n-1})$, where $\pm 2^{n-1}$ is introduced due to the relative displacement of the two $(n-1)-$multipoles. Therefore we arrive at the following iterative relation

$$\begin{aligned} R^{(n)}(\tau) = 2R^{(n-1)}(\tau) \\ - R^{(n-1)}(\tau - 2^{n-1}) - R^{(n-1)}(\tau + 2^{n-1}), \end{aligned} \tag{C.14}$$

corresponding to the following relation for the spectral density

$$\hat{R}^{(n)}(\omega) = \hat{R}^{(n-1)}(\omega)\left[2 - 2\cos(2^{n-1}\omega)\right], \tag{C.15}$$

with the initial condition $\hat{R}^{(0)}(\omega) = 1$. In the end, we arrive at

$$\hat{R}^{(n)}(\omega) = 2^n \prod_{j=1}^{n} \left[1 - \cos(2^{j-1}\omega)\right], \tag{C.16}$$

which has multiple zero points depending on the tunable order n. In particular, one zero point locates at $\omega = 0$, and the nearby suppression scales as ω^{2n}. The following relation [38]

$$\hat{R}^{(n)}(\omega) = \lim_{T\to\infty} \left\langle |\hat{x}^{(n)}(\omega)|^2 \right\rangle, \tag{C.17}$$

now helps us to identify the scaling behavior of the Fourier transformation of $x^{(n)}(t)$ defined as

$$\hat{x}^{(n)}(\omega) = \frac{1}{\sqrt{T}} \int_0^T x^{(n)}(t) e^{-i\omega t} dt. \tag{C.18}$$

From Cauchy-Schwarz inequality, we have

$$\left\langle |\hat{x}^{(n)}(\omega)| \right\rangle \leq \sqrt{\langle |\hat{x}^{(n)}(\omega)|^2 \rangle}, \tag{C.19}$$

suggesting that $\langle |\hat{x}^{(n)}(\omega)| \rangle$ is upper bounded by $\sqrt{\hat{R}^{(n)}(\omega)} \propto \omega^n$ for a $n-$multipolar sequence given a long enough time window of integration $T \to \infty$. Although Eq. (C.19) is valid for the average of the Fourier spectrum, we also expect it to impose the same bound ω^n for a single sequence realization in accordance with the numerical results of Fig. C.1.

C.3 Additional Numerical Results for TMS Driving

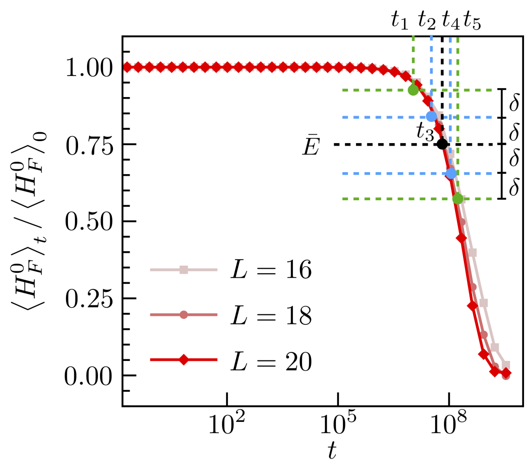

FIGURE C.3

C.3.1 Determination of the Heating Time

As show in Fig. C.3, to determine the thermalization time for $L = 20$, we first use five different mean energies, $\bar{E}+2\delta$, $\bar{E}+\delta$, $\bar{E}$, $\bar{E}-\delta$, $\bar{E}-2\delta$, and extract the corresponding time t_1, t_2, t_3, t_4, t_5. In the manuscript we use $\bar{E} = 0.75$ and $\delta = 0.03$ in Fig. 5.2. The thermalization time is defined as their average, and the standard deviation defines the error bar, which is only visible at low frequencies.

C.3.2 Finite Size Effect

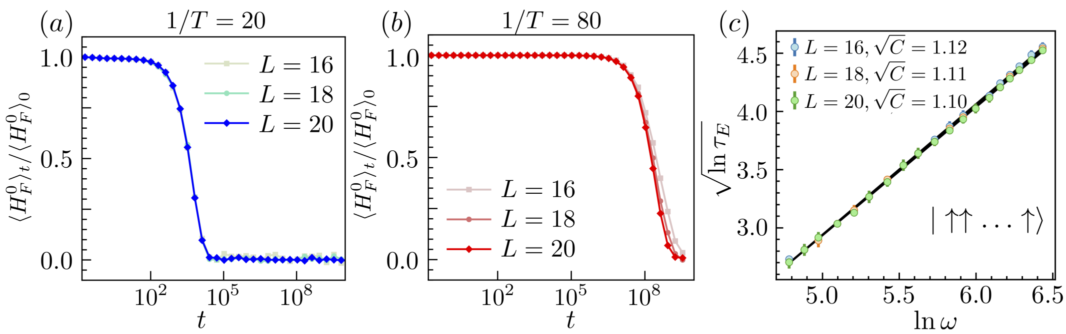

FIGURE C.4

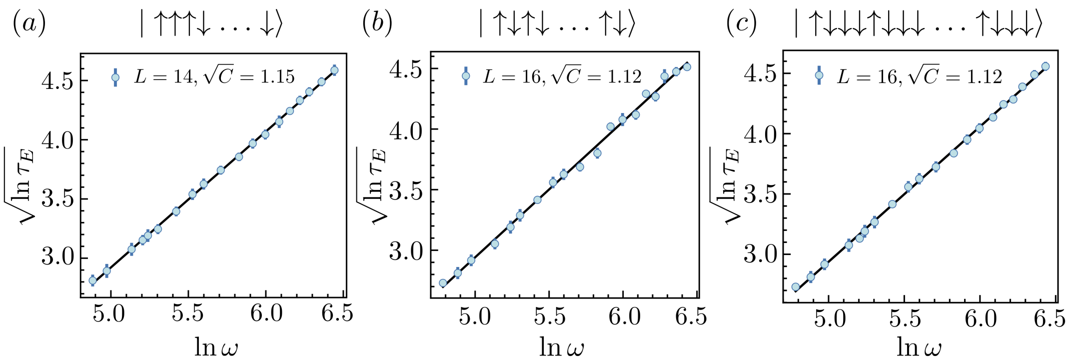

FIGURE C.5

In Fig. C.4, we depict the dynamics of the normalized energy for three different system sizes, and parameters of the Hamiltonian are the same as in Fig. 5.2. In panel (a) with $1/T = 20$, three curves do not exhibit differences until $t = 10^5$ where the system already heats to infinite temperature. As a comparison, in the panel (b) with $1/T = 80$, finite size effect can be observed for $t > 10^9$ before the system completely heats up. However, at the mean energy(around 0.75) used to determine the thermalization time, the dynamics clearly converges for $L \geq 18$. In panel (c), the scaling of thermalization time versus frequency is illustrated for different sizes, and all three results lead to almost the same slope. Therefore, within the time window that we are interested in, for instance $t < 10^9$, finite size effect is negligible.

C.3.3 Initial State Dependence

The heating rate is a general feature of the Hamiltonian therefore the thermalization time should be independent of the initial state. To verify this, in Fig. C.5, we test different initial states either with or without translation symmetry for the same parameters of the Hamiltonian used in Fig. 5.2. All of the dynamics thermalize roughly at the same time and lead to a similar fitted slope.

Bibliography

[1] Philip W Anderson. "More is different". In: *Science* 177.4047 (1972), pp. 393–396.

[2] Luca D'Alessio et al. "From quantum chaos and eigenstate thermalization to statistical mechanics and thermodynamics". In: *Advances in Physics* 65.3 (2016), pp. 239–362.

[3] Martin C Gutzwiller. *Chaos in classical and quantum mechanics.* Vol. 1. Springer Science & Business Media, 2013.

[4] Edwin T Jaynes. "Information theory and statistical mechanics". In: *Physical review* 106.4 (1957), p. 620.

[5] Werner Heisenberg. "Über den anschaulichen Inhalt der quantentheoretischen Kinematik und Mechanik". In: *Original Scientific Papers Wissenschaftliche Originalarbeiten.* Springer, 1985, pp. 478–504.

[6] Mark Srednicki. "Chaos and quantum thermalization". In: *Physical Review E* 50.2 (1994), p. 888.

[7] Josh M Deutsch. "Quantum statistical mechanics in a closed system". In: *Physical Review A* 43.4 (1991), p. 2046.

[8] Christian Schweizer et al. "Floquet approach to Z2 lattice gauge theories with ultracold atoms in optical lattices". In: *Nature Physics* 15.11 (2019), pp. 1168–1173.

[9] Michael Messer et al. "Floquet dynamics in driven Fermi-Hubbard systems". In: *Physical review letters* 121.23 (2018), p. 233603.

[10] Gaston Floquet. "Sur les équations différentielles linéaires à coefficients périodiques". In: *Annales scientifiques de l'École normale supérieure.* Vol. 12. 1883, pp. 47–88.

[11] Eugene Cosserat and François Cosserat. *Theorie des corps dédormables.* A. Hermann et fils, 1909.

[12] Yvette Kosmann-Schwarzbach. "The Noether Theorems". In: *The Noether Theorems*. Springer, 2011, pp. 55–64.

[13] Tomotaka Kuwahara, Takashi Mori, and Keiji Saito. "Floquet–Magnus theory and generic transient dynamics in periodically driven many-body quantum systems". In: *Annals of Physics* 367 (2016), pp. 96–124.

[14] Frank Arute et al. "Quantum supremacy using a programmable superconducting processor". In: *Nature* 574.7779 (2019), pp. 505–510.

[15] Christian Gross and Immanuel Bloch. "Quantum simulations with ultracold atoms in optical lattices". In: *Science* 357.6355 (2017), pp. 995–1001.

[16] Esteban A Martinez et al. "Real-time dynamics of lattice gauge theories with a few-qubit quantum computer". In: *Nature* 534.7608 (2016), pp. 516–519.

[17] Vedika Khemani, Roderich Moessner, and S. L. Sondhi. "A Brief History of Time Crystals". In: *arXiv preprint arXiv:1910.10745* (2019).

[18] Paraj Titum et al. "Anomalous Floquet-Anderson insulator as a nonadiabatic quantized charge pump". In: *Physical Review X* 6.2 (2016), p. 021013.

[19] Tomotaka Kuwahara, Takashi Mori, and Keiji Saito. "Floquet–Magnus theory and generic transient dynamics in periodically driven many-body quantum systems". In: *Annals of Physics* 367 (2016), pp. 96–124.

[20] Marcos Rigol, Vanja Dunjko, and Maxim Olshanii. "Thermalization and its mechanism for generic isolated quantum systems". In: *Nature* 452.7189 (2008), pp. 854–858.

[21] Mark Srednicki. "The approach to thermal equilibrium in quantized chaotic systems". In: *Journal of Physics A: Mathematical and General* 32.7 (1999), p. 1163.

[22] Michael A Nielsen and Isaac Chuang. *Quantum computation and quantum information.* 2002.

[23] Ryszard Horodecki et al. "Quantum entanglement". In: *Reviews of modern physics* 81.2 (2009), p. 865.

[24] Jens Eisert, Marcus Cramer, and Martin B Plenio. “Colloquium: Area laws for the entanglement entropy”. In: *Reviews of modern physics* 82.1 (2010), p. 277.

[25] Matthew B Hastings. “An area law for one-dimensional quantum systems”. In: *Journal of statistical mechanics: theory and experiment* 2007.08 (2007), P08024.

[26] Dmitry A Abanin et al. “Colloquium: Many-body localization, thermalization, and entanglement”. In: *Reviews of Modern Physics* 91.2 (2019), p. 021001.

[27] Wen Wei Ho and Dmitry A Abanin. “Entanglement dynamics in quantum many-body systems”. In: *Physical Review B* 95.9 (2017), p. 094302.

[28] Patrycja Łydżba, Marcos Rigol, and Lev Vidmar. “Eigenstate entanglement entropy in random quadratic hamiltonians”. In: *Physical review letters* 125.18 (2020), p. 180604.

[29] Hongzheng Zhao et al. “Orthogonal quantum many-body scars”. In: *arXiv preprint arXiv:2102.07672* (2021).

[30] Eugene P Wigner. “On the distribution of the roots of certain symmetric matrices”. In: *Annals of Mathematics* (1958), pp. 325–327.

[31] Freeman J Dyson. “Statistical theory of the energy levels of complex systems. I”. In: *Journal of Mathematical Physics* 3.1 (1962), pp. 140–156.

[32] Thomas Guhr, Axel Müller-Groeling, and Hans A Weidenmüller. “Random-matrix theories in quantum physics: common concepts”. In: *Physics Reports* 299.4-6 (1998), pp. 189–425.

[33] Didier Poilblanc et al. “Poisson vs. goe statistics in integrable and non-integrable quantum hamiltonians”. In: *Europhysics Letters* 22.7 (1993), p. 537.

[34] Vadim Oganesyan and David A Huse. “Localization of interacting fermions at high temperature”. In: *Physical review b* 75.15 (2007), p. 155111.

[35] YY Atas et al. “Distribution of the ratio of consecutive level spacings in random matrix ensembles”. In: *Physical review letters* 110.8 (2013), p. 084101.

[36] Luca D’Alessio and Marcos Rigol. “Long-time behavior of isolated periodically driven interacting lattice systems”. In: *Physical Review X* 4.4 (2014), p. 041048.

[37] Roderich Moessner and Shivaji Lal Sondhi. “Equilibration and order in quantum Floquet matter”. In: *Nature Physics* 13.5 (2017), pp. 424–428.

[38] Takashi Oka and Sota Kitamura. "Floquet engineering of quantum materials". In: *Annual Review of Condensed Matter Physics* 10 (2019), pp. 387–408.

[39] Sang-Kil Son, Siyuan Han, Shih-I Chu, et al. "Floquet formulation for the investigation of multiphoton quantum interference in a superconducting qubit driven by a strong ac field". In: *Physical Review A* 79.3 (2009), p. 032301.

[40] Anirban Gangopadhyay, Maxim Dzero, and Victor Galitski. "Exact solution for quantum dynamics of a periodically driven two-level system". In: *Physical Review B* 82.2 (2010), p. 024303.

[41] Takashi Mori et al. "Thermalization and prethermalization in isolated quantum systems: a theoretical overview". In: *Journal of Physics B: Atomic, Molecular and Optical Physics* 51.11 (2018), p. 112001.

[42] Takashi Mori. "Heating rates under fast periodic driving beyond linear response". In: *arXiv preprint arXiv:2107.12587* (2021).

[43] Szabolcs Vajna et al. "Replica resummation of the Baker-Campbell-Hausdorff series". In: *Physical review letters* 120.20 (2018), p. 200607.

[44] André Eckardt and Egidijus Anisimovas. "High-frequency approximation for periodically driven quantum systems from a Floquet-space perspective". In: *New journal of physics* 17.9 (2015), p. 093039.

[45] Albert Verdeny, Andreas Mielke, and Florian Mintert. "Accurate effective Hamiltonians via unitary flow in Floquet space". In: *Physical review letters* 111.17 (2013), p. 175301.

[46] Achilleas Lazarides, Arnab Das, and Roderich Moessner. "Equilibrium states of generic quantum systems subject to periodic driving". In: *Physical Review E* 90.1 (2014), p. 012110.

[47] Antonio Rubio-Abadal et al. "Floquet prethermalization in a Bose-Hubbard system". In: *Physical Review X* 10.2 (2020), p. 021044.

[48] Don N Page. "Average entropy of a subsystem". In: *Physical review letters* 71.9 (1993), p. 1291.

[49] Marcos Rigol et al. “Relaxation in a completely integrable many-body quantum system: an ab initio study of the dynamics of the highly excited states of 1D lattice hard-core bosons”. In: *Physical review letters* 98.5 (2007), p. 050405.

[50] Amy C Cassidy, Charles W Clark, and Marcos Rigol. “Generalized thermalization in an integrable lattice system”. In: *Physical review letters* 106.14 (2011), p. 140405.

[51] Lev Vidmar and Marcos Rigol. “Generalized Gibbs ensemble in integrable lattice models”. In: *Journal of Statistical Mechanics: Theory and Experiment* 2016.6 (2016), p. 064007.

[52] Achilleas Lazarides, Arnab Das, and Roderich Moessner. “Periodic thermodynamics of isolated quantum systems”. In: *Physical review letters* 112.15 (2014), p. 150401.

[53] Rahul Nandkishore and David A Huse. “Many-body localization and thermalization in quantum statistical mechanics”. In: *Annu. Rev. Condens. Matter Phys.* 6.1 (2015), pp. 15–38.

[54] Dmitry A Abanin and Zlatko Papić. “Recent progress in many-body localization”. In: *Annalen der Physik* 529.7 (2017), p. 1700169.

[55] SA Parameswaran and Romain Vasseur. “Many-body localization, symmetry and topology”. In: *Reports on Progress in Physics* 81.8 (2018), p. 082501.

[56] Philip W Anderson. “Absence of diffusion in certain random lattices”. In: *Physical review* 109.5 (1958), p. 1492.

[57] Marko Žnidarič, Tomaž Prosen, and Peter Prelovšek. “Many-body localization in the heisenberg x x z magnet in a random field”. In: *Physical Review B* 77.6 (2008), p. 064426.

[58] Arijeet Pal and David A Huse. “Many-body localization phase transition”. In: *Physical review b* 82.17 (2010), p. 174411.

[59] Glen Bigan Mbeng, Angelo Russomanno, and Giuseppe E Santoro. “The quantum Ising chain for beginners”. In: *arXiv preprint arXiv:2009.09208* (2020).

[60] David A Huse, Rahul Nandkishore, and Vadim Oganesyan. "Phenomenology of fully many-body-localized systems". In: *Physical Review B* 90.17 (2014), p. 174202.

[61] Maksym Serbyn, Zlatko Papić, and Dmitry A Abanin. "Local conservation laws and the structure of the many-body localized states". In: *Physical review letters* 111.12 (2013), p. 127201.

[62] Pedro Ponte et al. "Many-body localization in periodically driven systems". In: *Physical review letters* 114.14 (2015), p. 140401.

[63] Yevgeny Bar Lev and David R Reichman. "Dynamics of many-body localization". In: *Physical Review B* 89.22 (2014), p. 220201.

[64] Michael Schreiber et al. "Observation of many-body localization of interacting fermions in a quasirandom optical lattice". In: *Science* 349.6250 (2015), pp. 842–845.

[65] Jae-yoon Choi et al. "Exploring the many-body localization transition in two dimensions". In: *Science* 352.6293 (2016), pp. 1547–1552.

[66] Dmitry A Abanin, Wojciech De Roeck, and François Huveneers. "Theory of many-body localization in periodically driven systems". In: *Annals of Physics* 372 (2016), pp. 1–11.

[67] Marin Bukov, Luca D'Alessio, and Anatoli Polkovnikov. "Universal high-frequency behavior of periodically driven systems: from dynamical stabilization to Floquet engineering". In: *Advances in Physics* 64.2 (2015), pp. 139–226.

[68] Krzysztof Sacha and Jakub Zakrzewski. "Time crystals: a review". In: *Reports on Progress in Physics* 81.1 (2017), p. 016401.

[69] Vedika Khemani et al. "Phase structure of driven quantum systems". In: *Physical review letters* 116.25 (2016), p. 250401.

[70] Norman Y Yao et al. "Discrete time crystals: Rigidity, criticality, and realizations". In: *Physical review letters* 118.3 (2017), p. 030401.

[71] Andrea Pizzi, Johannes Knolle, and Andreas Nunnenkamp. "Period-n discrete time crystals and quasicrystals with ultracold bosons". In: *Physical review letters* 123.15 (2019), p. 150601.

[72] Andrea Pizzi, Johannes Knolle, and Andreas Nunnenkamp. "Higher-order and fractional discrete time crystals in clean long-range interacting systems". In: *Nature communications* 12.1 (2021), pp. 1–7.

[73] Andrea Pizzi, Andreas Nunnenkamp, and Johannes Knolle. "(Classical) Prethermal phases of matter". In: *arXiv preprint arXiv:2104.13928* (2021).

[74] Hannes Bernien et al. "Probing many-body dynamics on a 51-atom quantum simulator". In: *Nature* 551.7682 (2017), pp. 579–584.

[75] Soonwon Choi et al. "Emergent SU (2) dynamics and perfect quantum many-body scars". In: *Physical review letters* 122.22 (2019), p. 220603.

[76] Christopher J Turner et al. "Weak ergodicity breaking from quantum many-body scars". In: *Nature Physics* 14.7 (2018), pp. 745–749.

[77] Pablo Sala et al. "Ergodicity breaking arising from hilbert space fragmentation in dipole-conserving hamiltonians". In: *Physical Review X* 10.1 (2020), p. 011047.

[78] Sanjay Moudgalya, Nicolas Regnault, and B. Andrei Bernevig. "Entanglement of exact excited states of Affleck-Kennedy-Lieb-Tasaki models: Exact results, many-body scars, and violation of the strong eigenstate thermalization hypothesis". In: *Phys. Rev. B* 98 (23 2018), p. 235156.

[79] Ana Hudomal et al. "Quantum scars of bosons with correlated hopping". In: *arXiv preprint arXiv:1910.09526* (2019).

[80] Hongzheng Zhao et al. "Quantum many-body scars in optical lattices". In: *Physical Review Letters* 124.16 (2020), p. 160604.

[81] Thomas Iadecola and Michael Schecter. "Quantum many-body scar states with emergent kinetic constraints and finite-entanglement revivals". In: *Physical Review B* 101.2 (2020), p. 024306.

[82] Maksym Serbyn, Dmitry A Abanin, and Zlatko Papić. "Quantum many-body scars and weak breaking of ergodicity". In: *Nature Physics* (2021), pp. 1–11.

[83] Sanjay Moudgalya, Nicolas Regnault, and B Andrei Bernevig. "Entanglement of exact excited states of Affleck-Kennedy-Lieb-Tasaki models: Exact results, many-body scars, and violation of the strong eigenstate thermalization hypothesis". In: *Physical Review B* 98.23 (2018), p. 235156.

[84] Naoto Shiraishi and Takashi Mori. "Systematic construction of counterexamples to the eigenstate thermalization hypothesis". In: *Physical review letters* 119.3 (2017), p. 030601.

[85] Vedika Khemani, Michael Hermele, and Rahul Nandkishore. "Localization from Hilbert space shattering: From theory to physical realizations". In: *Physical Review B* 101.17 (2020), p. 174204.

[86] Kieran Bull, Ivar Martin, and Z Papić. "Systematic construction of scarred many-body dynamics in 1D lattice models". In: *Physical review letters* 123.3 (2019), p. 030601.

[87] Shriya Pai and Michael Pretko. "Dynamical scar states in driven fracton systems". In: *Physical review letters* 123.13 (2019), p. 136401.

[88] Sebastian Scherg et al. "Observing non-ergodicity due to kinetic constraints in tilted Fermi-Hubbard chains". In: *arXiv preprint arXiv:2010.12965* (2020).

[89] Krishnanand Mallayya, Marcos Rigol, and Wojciech De Roeck. "Prethermalization and Thermalization in Isolated Quantum Systems". In: *Phys. Rev. X* 9 (2 2019), p. 021027.

[90] Matteo Marcuzzi et al. "Prethermalization in a nonintegrable quantum spin chain after a quench". In: *Physical review letters* 111.19 (2013), p. 197203.

[91] N Nessi, A Iucci, and MA Cazalilla. "Quantum quench and prethermalization dynamics in a two-dimensional fermi gas with long-range interactions". In: *Physical review letters* 113.21 (2014), p. 210402.

[92] Krishnanand Mallayya and Marcos Rigol. "Heating rates in periodically driven strongly interacting quantum many-body systems". In: *Physical review letters* 123.24 (2019), p. 240603.

[93] William Beatrez et al. "Floquet prethermalization with lifetime exceeding 90s in a bulk hyperpolarized solid". In: *arXiv preprint arXiv:2104.01988* (2021).

[94] Dmitry Abanin et al. "A rigorous theory of many-body prethermalization for periodically driven and closed quantum systems". In: *Communications in Mathematical Physics* 354.3 (2017), pp. 809–827.

[95] Monika Aidelsburger et al. "Measuring the Chern number of Hofstadter bands with ultracold bosonic atoms". In: *Nature Physics* 11.2 (2015), pp. 162–166.

[96] Gregor Jotzu et al. "Experimental realization of the topological Haldane model with ultracold fermions". In: *Nature* 515.7526 (2014), pp. 237–240.

[97] Francesco Petiziol et al. "Quantum simulation of three-body interactions in weakly driven quantum systems". In: *Physical Review Letters* 126.25 (2021), p. 250504.

[98] André Eckardt, Christoph Weiss, and Martin Holthaus. "Superfluid-insulator transition in a periodically driven optical lattice". In: *Physical review letters* 95.26 (2005), p. 260404.

[99] Cheng Chin et al. "Feshbach resonances in ultracold gases". In: *Rev. Mod. Phys.* 82 (2 2010), pp. 1225–1286.

[100] Hans Lignier et al. "Dynamical control of matter-wave tunneling in periodic potentials". In: *Physical review letters* 99.22 (2007), p. 220403.

[101] JK Freericks and H Monien. "Phase diagram of the Bose-Hubbard model". In: *EPL (Europhysics Letters)* 26.7 (1994), p. 545.

[102] Markus Greiner et al. "Quantum phase transition from a superfluid to a Mott insulator in a gas of ultracold atoms". In: *nature* 415.6867 (2002), pp. 39–44.

[103] Thilo Stöferle et al. "Transition from a strongly interacting 1D superfluid to a Mott insulator". In: *Physical review letters* 92.13 (2004), p. 130403.

[104] Dominic V Else, Wen Wei Ho, and Philipp T Dumitrescu. "Long-lived interacting phases of matter protected by multiple time-translation symmetries in quasiperiodically driven systems". In: *Physical Review X* 10.2 (2020), p. 021032.

[105] Philipp T Dumitrescu, Romain Vasseur, and Andrew C Potter. "Logarithmically slow relaxation in quasiperiodically driven random spin chains". In: *Physical review letters* 120.7 (2018), p. 070602.

[106] Yang Peng and Gil Refael. "Time-quasiperiodic topological superconductors with Majorana multiplexing". In: *Physical Review B* 98.22 (2018), p. 220509.

[107] Philip JD Crowley, Ivar Martin, and Anushya Chandran. "Topological classification of quasiperiodically driven quantum systems". In: *Physical Review B* 99.6 (2019), p. 064306.

[108] Ivar Martin, Gil Refael, and Bertrand Halperin. "Topological frequency conversion in strongly driven quantum systems". In: *Physical Review X* 7.4 (2017), p. 041008.

[109] Albert Verdeny, Joaquim Puig, and Florian Mintert. "Quasi-Periodically Driven Quantum Systems". In: *Zeitschrift für Naturforschung A* 71 (10 2016), pp. 897–907.

[110] Y Pomeau, B Dorizzi, and B Grammaticos. "Chaotic Rabi oscillations under quasiperiodic perturbation". In: *Physical review letters* 56.7 (1986), p. 681.

[111] Giulio Casati, Italo Guarneri, and DL Shepelyansky. "Anderson transition in a one-dimensional system with three incommensurate frequencies". In: *Physical review letters* 62.4 (1989), p. 345.

[112] David M Long, Philip JD Crowley, and Anushya Chandran. "Nonadiabatic Topological Energy Pumps with Quasiperiodic Driving". In: *Physical Review Letters* 126.10 (2021), p. 106805.

[113] Frederik Nathan et al. "Quasiperiodic Floquet-Thouless energy pump". In: *arXiv preprint arXiv:2010.11485* (2020).

[114] Eric Boyers et al. "Exploring 2D Synthetic Quantum Hall Physics with a Quasiperiodically Driven Qubit". In: *Physical Review Letters* 125.16 (2020), p. 160505.

[115] Daniel Malz and Adam Smith. "Topological two-dimensional Floquet lattice on a single superconducting qubit". In: *Physical Review Letters* 126.16 (2021), p. 163602.

[116] Mahito Kohmoto, Leo P Kadanoff, and Chao Tang. "Localization problem in one dimension: Mapping and escape". In: *Physical Review Letters* 50.23 (1983), p. 1870.

[117] Sourav Nandy, Arnab Sen, and Diptiman Sen. "Aperiodically driven integrable systems and their emergent steady states". In: *Physical Review X* 7.3 (2017), p. 031034.

[118] Xueda Wen et al. "Periodically, quasiperiodically, and randomly driven conformal field theories". In: *Physical Review Research* 3.2 (2021), p. 023044.

[119] Bastien Lapierre et al. "Fine structure of heating in a quasiperiodically driven critical quantum system". In: *Physical Review Research* 2.3 (2020), p. 033461.

[120] Enrique Maciá. "On the nature of electronic wave functions in one-dimensional self-similar and quasiperiodic systems". In: *International Scholarly Research Notices* 2014 (2014).

[121] Somnath Maity et al. "Fibonacci steady states in a driven integrable quantum system". In: *Phys. Rev. B* 99 (2 2019), p. 020306.

[122] Wen Wei Ho et al. "Periodic orbits, entanglement, and quantum many-body scars in constrained models: Matrix product state approach". In: *Physical review letters* 122.4 (2019), p. 040603.

[123] Shriya Pai, Michael Pretko, and Rahul M Nandkishore. "Robust quantum many-body scars in fracton systems". In: *arXiv preprint arXiv:1903.06173* (2019).

[124] Bhaskar Mukherjee et al. "Collapse and revival of quantum many-body scars via Floquet engineering". In: *arXiv preprint arXiv:1907.08212* (2019).

[125] Michael Schecter and Thomas Iadecola. "Weak Ergodicity Breaking and Quantum Many-Body Scars in Spin-1 X Y Magnets". In: *Physical review letters* 123.14 (2019), p. 147201.

[126] AA Michailidis et al. "Slow quantum thermalization and many-body revivals from mixed phase space". In: *arXiv preprint arXiv:1905.08564* (2019).

[127] Sho Sugiura, Tomotaka Kuwahara, and Keiji Saito. "Many-body scar state intrinsic to periodically driven system: Rigorous results". In: *arXiv preprint arXiv:1911.06092* (2019).

[128] Asmi Haldar et al. "Scars in strongly driven Floquet matter: resonance vs emergent conservation laws". In: *arXiv preprint arXiv:1909.04064* (2019).

[129] Thomas Iadecola, Michael Schecter, and Shenglong Xu. "Quantum many-body scars from magnon condensation". In: *Phys. Rev. B* 100 (18 2019), p. 184312.

[130] Thomas Iadecola and Michael Schecter. "Quantum many-body scar states with emergent kinetic constraints and finite-entanglement revivals". In: *Phys. Rev. B* 101 (2 2020), p. 024306.

[131] Sanjay Moudgalya, B Andrei Bernevig, and Nicolas Regnault. "Quantum many-body scars in a Landau level on a thin torus". In: *Physical Review B* 102.19 (2020), p. 195150.

[132] Ph. Courteille et al. "Observation of a Feshbach Resonance in Cold Atom Scattering". In: *Phys. Rev. Lett.* 81 (1 1998), pp. 69–72.

[133] Hongzheng Zhao, Johannes Knolle, and Florian Mintert. "Engineered nearest-neighbor interactions with doubly modulated optical lattices". In: *Phys. Rev. A* 100 (5 2019), p. 053610.

[134] Sebastian Greschner, Luis Santos, and Dario Poletti. "Exploring Unconventional Hubbard Models with Doubly Modulated Lattice Gases". In: *Phys. Rev. Lett.* 113 (18 2014), p. 183002.

[135] Phillip Weinberg and Marin Bukov. "QuSpin: a Python package for dynamics and exact diagonalisation of quantum many body systems part I: spin chains". In: *SciPost Phys* (2017).

[136] Zachary A. Geiger et al. "Observation and Uses of Position-Space Bloch Oscillations in an Ultracold Gas". In: *Phys. Rev. Lett.* 120 (21 2018), p. 213201.

[137] Andreas Buchleitner and Andrey R Kolovsky. "Interaction-induced decoherence of atomic Bloch oscillations". In: *Physical review letters* 91.25 (2003), p. 253002.

[138] Pranjal Bordia et al. "Periodically driving a many-body localized quantum system". In: *Nature Physics* 13.5 (2017), pp. 460–464.

[139] Florian Meinert et al. "Floquet engineering of correlated tunneling in the Bose-Hubbard model with ultracold atoms". In: *Physical review letters* 116.20 (2016), p. 205301.

[140] Konrad Viebahn et al. “Suppressing dissipation in a Floquet-Hubbard system”. In: *Physical Review X* 11.1 (2021), p. 011057.

[141] Jacob F. Sherson et al. “Single-atom-resolved fluorescence imaging of an atomic Mott insulator”. In: *Nature* 467.7311 (2010), pp. 68–72.

[142] Christof Weitenberg et al. “Single-spin addressing in an atomic Mott insulator”. In: *Nature* 471.7338 (2011), pp. 319–324.

[143] Seulgi Ok et al. “Topological many-body scar states in dimensions 1, 2, and 3”. In: *arXiv preprint arXiv:1901.01260* (2019).

[144] Christie S. Chiu et al. “Quantum State Engineering of a Hubbard System with Ultracold Fermions”. In: *Phys. Rev. Lett.* 120 (24 2018), p. 243201.

[145] Yu Kagan and LA Maksimov. “Localization in a system of interacting particles diffusing in a regular crystal”. In: *Zhurnal Eksperimental'noi i Teoreticheskoi Fiziki* 87 (1984), pp. 348–365.

[146] Z Papić, E Miles Stoudenmire, and Dmitry A Abanin. “Many-body localization in disorder-free systems: The importance of finite-size constraints”. In: *Annals of Physics* 362 (2015), pp. 714–725.

[147] NY Yao et al. “Quasi-many-body localization in translation-invariant systems”. In: *Physical review letters* 117.24 (2016), p. 240601.

[148] Tarun Grover and Matthew PA Fisher. “Quantum disentangled liquids”. In: *Journal of Statistical Mechanics: Theory and Experiment* 2014.10 (2014), P10010.

[149] Thomas Veness, Fabian HL Essler, and Matthew PA Fisher. “Quantum disentangled liquid in the half-filled Hubbard model”. In: *Physical Review B* 96.19 (2017), p. 195153.

[150] Adam Smith et al. “Disorder-free localization”. In: *Physical review letters* 118.26 (2017), p. 266601.

[151] Adam Smith et al. “Dynamical localization in Z 2 lattice gauge theories”. In: *Physical Review B* 97.24 (2018), p. 245137.

[152] Marlon Brenes et al. “Many-body localization dynamics from gauge invariance”. In: *Physical review letters* 120.3 (2018), p. 030601.

[153] P Karpov et al. “Disorder-free localization in an interacting two-dimensional lattice gauge theory”. In: *arXiv preprint arXiv:2003.04901* (2020).

[154] Danny Paulson et al. “Towards simulating 2D effects in lattice gauge theories on a quantum computer”. In: *arXiv preprint arXiv:2008.09252* (2020).

[155] Irene Papaefstathiou, Adam Smith, and Johannes Knolle. “Disorder-free localization in a simple U (1) lattice gauge theory”. In: *Physical Review B* 102.16 (2020), p. 165132.

[156] Paul A McClarty et al. “Disorder-free localization and many-body quantum scars from magnetic frustration”. In: *Physical Review B* 102.22 (2020), p. 224303.

[157] Guo-Yi Zhu and Markus Heyl. “Subdiffusive dynamics and critical quantum correlations in a disorder-free localized Kitaev honeycomb model out of equilibrium”. In: *arXiv preprint arXiv:2012.05753* (2020).

[158] Rahul Nandkishore, Max A Metlitski, and T Senthil. “Orthogonal metals: The simplest non-Fermi liquids”. In: *Physical Review B* 86.4 (2012), p. 045128.

[159] Hendrik A Kramers and Gregory H Wannier. “Statistics of the two-dimensional ferromagnet. Part I”. In: *Physical Review* 60.3 (1941), p. 252.

[160] Franz J Wegner. “Duality in generalized Ising models and phase transitions without local order parameters”. In: *Journal of Mathematical Physics* 12.10 (1971), pp. 2259–2272.

[161] Pierre Pfeuty. “The one-dimensional Ising model with a transverse field”. In: *ANNALS of Physics* 57.1 (1970), pp. 79–90.

[162] A Yu Kitaev. “Fault-tolerant quantum computation by anyons”. In: *Annals of Physics* 303.1 (2003), pp. 2–30.

[163] Charles Kittel. “Introduction to solid state physics”. In: (1976).

[164] Elliott Lieb, Theodore Schultz, and Daniel Mattis. “Two soluble models of an antiferromagnetic chain”. In: *Annals of Physics* 16.3 (1961), pp. 407–466.

[165] Pasquale Calabrese, Fabian HL Essler, and Maurizio Fagotti. “Quantum quench in the transverse-field Ising chain”. In: *Physical review letters* 106.22 (2011), p. 227203.

[166] Angelo Russomanno, Alessandro Silva, and Giuseppe E Santoro. "Periodic steady regime and interference in a periodically driven quantum system". In: *Physical review letters* 109.25 (2012), p. 257201.

[167] Sung-Sik Lee. "Recent developments in non-fermi liquid theory". In: *Annual Review of Condensed Matter Physics* 9 (2018), pp. 227–244.

[168] Robin Steinigeweg, Jacek Herbrych, and Peter Prelovšek. "Eigenstate thermalization within isolated spin-chain systems". In: *Physical Review E* 87.1 (2013), p. 012118.

[169] Hyungwon Kim and David A Huse. "Ballistic spreading of entanglement in a diffusive nonintegrable system". In: *Physical review letters* 111.12 (2013), p. 127205.

[170] Ana Hudomal et al. "Quantum scars of bosons with correlated hopping". In: *Communications Physics* 3.1 (2020), pp. 1–12.

[171] Pasquale Calabrese and John Cardy. "Evolution of entanglement entropy in one-dimensional systems". In: *Journal of Statistical Mechanics: Theory and Experiment* 2005.04 (2005), P04010.

[172] Philip JD Crowley and Anushya Chandran. "Partial thermalisation of a two-state system coupled to a finite quantum bath". In: *arXiv preprint arXiv: 2104.03312* (2021).

[173] Cheng-Ju Lin, Vladimir Calvera, and Timothy H Hsieh. "Quantum many-body scar states in two-dimensional Rydberg atom arrays". In: *Physical Review B* 101.22 (2020), p. 220304.

[174] Mari Carmen Banuls et al. "Simulating lattice gauge theories within quantum technologies". In: *The European physical journal D* 74.8 (2020), pp. 1–42.

[175] Bing Yang et al. "Observation of gauge invariance in a 71-site Bose–Hubbard quantum simulator". In: *Nature* 587.7834 (2020), pp. 392–396.

[176] Giuseppe De Tomasi et al. "Dynamics of strongly interacting systems: From Fock-space fragmentation to many-body localization". In: *Physical Review B* 100.21 (2019), p. 214313.

[177] H. J. Schulz. "Effective action for strongly correlated fermions from functional integrals". In: *Phys. Rev. Lett.* 65 (19 1990), pp. 2462–2465.

[178] E. Arrigoni and G. C. Strinati. "Doping-induced incommensurate antiferromagnetism in a Mott-Hubbard insulator". In: *Phys. Rev. B* 44 (14 1991), pp. 7455–7465.

[179] A. P. Kampf. "Collective excitations in itinerant spiral magnets". In: *Phys. Rev. B* 53 (2 1996), pp. 747–757.

[180] Guillaume Salomon et al. "Direct observation of incommensurate magnetism in Hubbard chains". In: *Nature* 565.7737 (2019), pp. 56–60.

[181] André Eckardt et al. "Exploring dynamic localization with a Bose-Einstein condensate". In: *Phys. Rev. A* 79 (1 2009), p. 013611.

[182] Marjorie Senechal. *Quasicrystals and geometry.* CUP Archive, 1996.

[183] Dominic V. Else, Bela Bauer, and Chetan Nayak. "Floquet Time Crystals". In: *Phys. Rev. Lett.* 117 (9 2016), p. 090402.

[184] Krzysztof Giergiel, Arkadiusz Kuroś, and Krzysztof Sacha. "Discrete Time Quasi-Crystals". In: *arXiv preprint arXiv:1807.02105* (2018).

[185] Tongcang Li et al. "Space-Time Crystals of Trapped Ions". In: *Phys. Rev. Lett.* 109 (16 2012), p. 163001.

[186] Yi Huang, Tongcang Li, and Zhang-qi Yin. "Symmetry-breaking dynamics of the finite-size Lipkin-Meshkov-Glick model near ground state". In: *Phys. Rev. A* 97 (1 2018), p. 012115.

[187] S. Autti, V. B. Eltsov, and G. E. Volovik. "Observation of a Time Quasicrystal and Its Transition to a Superfluid Time Crystal". In: *Phys. Rev. Lett.* 120 (21 2018), p. 215301.

[188] Jiehang Zhang et al. "Observation of a discrete time crystal". In: *Nature* 543.7644 (2017), pp. 217–220.

[189] Jared Rovny, Robert L. Blum, and Sean E. Barrett. "Observation of Discrete-Time-Crystal Signatures in an Ordered Dipolar Many-Body System". In: *Phys. Rev. Lett.* 120 (18 2018), p. 180603.

[190] Soonwon Choi et al. “Observation of discrete time-crystalline order in a disordered dipolar many-body system”. In: *Nature* 543 (Mar. 2017), 221 EP –.

[191] Krishnanand Mallayya and Marcos Rigol. “Heating rates in periodically driven strongly interacting quantum many-body systems”. In: *Physical Review Letters* 123.24 (2019), p. 240603.

[192] Thomas Bilitewski and Nigel R Cooper. “Scattering theory for Floquet-Bloch states”. In: *Physical Review A* 91.3 (2015), p. 033601.

[193] Takashi Mori et al. “Rigorous Bounds on the Heating Rate in Thue-Morse Quasiperiodically and Randomly Driven Quantum Many-Body Systems”. In: *arXiv preprint arXiv:2101.07065* (2021).

[194] Thomas Bilitewski and Nigel R. Cooper. “Population dynamics in a Floquet realization of the Harper-Hofstadter Hamiltonian”. In: *Phys. Rev. A* 91 (6 2015), p. 063611.

[195] Simon A Weidinger and Michael Knap. “Floquet prethermalization and regimes of heating in a periodically driven, interacting quantum system”. In: *Scientific reports* 7 (2017), p. 45382.

[196] Samuel Lellouch et al. “Parametric instability rates in periodically driven band systems”. In: *Physical Review X* 7.2 (2017), p. 021015.

[197] Francisco Machado et al. “Exponentially slow heating in short and long-range interacting Floquet systems”. In: *Physical Review Research* 1.3 (2019), p. 033202.

[198] Dmitry A Abanin, Wojciech De Roeck, and François Huveneers. “Exponentially slow heating in periodically driven many-body systems”. In: *Physical review letters* 115.25 (2015), p. 256803.

[199] Wen Wei Ho, Ivan Protopopov, and Dmitry A Abanin. “Bounds on energy absorption and prethermalization in quantum systems with long-range interactions”. In: *Physical review letters* 120.20 (2018), p. 200601.

[200] Takashi Mori, Tomotaka Kuwahara, and Keiji Saito. “Rigorous Bound on Energy Absorption and Generic Relaxation in Periodically Driven Quantum Systems”. In: *Phys. Rev. Lett.* 116 (12 2016), p. 120401.

[201] Dmitry A. Abanin et al. "Effective Hamiltonians, prethermalization, and slow energy absorption in periodically driven many-body systems". In: *Phys. Rev. B* 95 (1 2017), p. 014112.

[202] Minh C. Tran et al. "Locality and heating in periodically driven, power-law-interacting systems". In: *Phys. Rev. A* 100 (5 2019), p. 052103.

[203] Andrea Pizzi et al. "Time crystallinity and finite-size effects in clean Floquet systems". In: *Physical Review B* 102.21 (2020), p. 214207.

[204] Philip JD Crowley, CR Laumann, and Sarang Gopalakrishnan. "Quantum criticality in Ising chains with random hyperuniform couplings". In: *Physical Review B* 100.13 (2019), p. 134206.

[205] Maciej Kozarzewski, Peter Prelovšek, and Marcin Mierzejewski. "Spin subdiffusion in the disordered Hubbard chain". In: *Physical review letters* 120.24 (2018), p. 246602.

[206] Peter Prelovšek, Osor Slaven Barišić, and Marko Žnidarič. "Absence of full many-body localization in the disordered Hubbard chain". In: *Physical Review B* 94.24 (2016), p. 241104.

[207] PW Langhoff, ST Epstein, and M Karplus. "Aspects of time-dependent perturbation theory". In: *Reviews of Modern Physics* 44.3 (1972), p. 602.

[208] Salvatore Torquato. "Hyperuniform states of matter". In: *Physics Reports* 745 (2018), pp. 1–95.

[209] Sarang Gopalakrishnan, K Ranjibul Islam, and Michael Knap. "Noise-induced subdiffusion in strongly localized quantum systems". In: *Physical review letters* 119.4 (2017), p. 046601.

[210] Albert Verdeny and Florian Mintert. "Tunable Chern insulator with optimally shaken lattices". In: *Phys. Rev. A* 92 (6 2015), p. 063615.